

AD-A035 138

ROCK ISLAND ARSENAL ILL GENERAL THOMAS J RODMAN LAB
THE INVESTIGATION OF DYNAMIC GUN POINTING ERRORS FOR HELICOPTER--ETC(U)
NOV 76 T D HUTCHINGS, A R ZAK

F/G 1/3

UNCLASSIFIED

RIA-R-TR-76-042

NL

1 OF 2
AD-A
035 138



U.S. DEPARTMENT OF COMMERCE
National Technical Information Service

AD-A035 138

THE INVESTIGATION OF DYNAMIC GUN POINTING ERRORS
FOR HELICOPTER MOUNTED AUTOMATIC CANNON SYSTEMS

Rock Island Arsenal
Rock Island, ILLINOIS

2 NOVEMBER 1976

ADA035138

AD

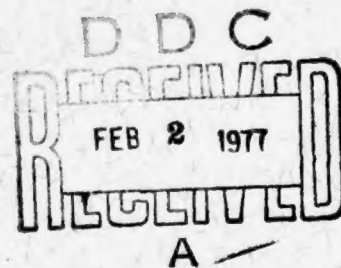
THE INVESTIGATION OF DYNAMIC GUN POINTING ERRORS FOR HELICOPTER MOUNTED AUTOMATIC CANNON SYSTEMS

BY

THOMAS D. HUTCHINGS

ADAM R. ZAK

2 NOVEMBER 1976



FINAL REPORT



RESEARCH DIRECTORATE

DISTRIBUTION STATEMENT

APPROVED FOR PUBLIC RELEASE; DISTRIBUTION UNLIMITED.

REPRODUCED BY
NATIONAL TECHNICAL
INFORMATION SERVICE
U. S. DEPARTMENT OF COMMERCE
SPRINGFIELD, VA. 22161

**GENERAL THOMAS J. RODMAN LABORATORY
ROCK ISLAND ARSENAL
ROCK ISLAND, ILLINOIS 61201**

DISCLAIMER

The findings in this report are not to be construed as an official Department of the Army position, unless so designated by other authorized documents.

DISPOSITION INSTRUCTIONS

Destroy this report when it is no longer needed.

UNCLASSIFIED

SECURITY CLASSIFICATION OF THIS PAGE (When Data Entered)

REPORT DOCUMENTATION PAGE		READ INSTRUCTIONS BEFORE COMPLETING FORM
1. REPORT NUMBER R-TR-76-042	2. JOINT ACCESSION NO.	3. RECIPIENT'S CATALOG NUMBER
4. TITLE (and Subtitle) The Investigation of Dynamic Gun Pointing Errors for Helicopter Mounted Automatic Cannon Systems		5. TYPE OF REPORT & PERIOD COVERED Final Report July 1975 - June 1976
7. AUTHOR(s) Thomas D. Hutchings Adam R. Zak		6. PERFORMING ORG. REPORT NUMBER
9. PERFORMING ORGANIZATION NAME AND ADDRESS Research Directorate GEN Thomas J. Rodman Laboratory SARRI-RLR-S RIA Rock Island, IL 61201		8. CONTRACT OR GRANT NUMBER(s)
11. CONTROLLING OFFICE NAME AND ADDRESS Research Directorate GEN Thomas J. Rodman Laboratory SARRI-RLR-S RIA Rock Island, IL 61201		10. PROGRAM ELEMENT, PROJECT, TASK AREA & WORK UNIT NUMBERS IF2622201.DH96 TA01/WA03
14. MONITORING AGENCY NAME & ADDRESS (if different from Controlling Office)		12. REPORT DATE 2 NOV 76
		13. NUMBER OF PAGES 100 143
		15. SECURITY CLASS. (of this report) Unclassified
		15a. DECLASSIFICATION/DOWNGRADING SCHEDULE
16. DISTRIBUTION STATEMENT (of this Report) Approved for public release, distribution unlimited.		
17. DISTRIBUTION STATEMENT (of the abstract entered in Block 20, if different from Report)		
18. SUPPLEMENTARY NOTES		
19. KEY WORDS (Continue on reverse side if necessary and identify by block number)		
1. Error Analysis	5. Dynamic	9. Mathematical Model
2. Helicopter	6. Vibrations	10. Simulation
3. Turret	7. Servocontrol	11. Weapon System
4. Automatic Cannons	8. Recoil	12. Computer
20. ABSTRACT (Continue on reverse side if necessary and identify by block number) In a helicopter-weapon-system, the dynamic gun-pointing errors, caused by the application of weapon recoil forces, are the helicopter airframe vibrations and the relative turret servocontrol oscillations between the interconnected rigid body segments (i.e., motions of the azimuth and the elevation drive systems). A two-step analytical procedure has been developed to quantify these errors for different weapon systems and for different operating conditions. In this analysis, the airframe dynamics are first determined with a finite-element		

DD FORM 1 JAN 73 1473 EDITION OF 1 NOV 65 IS OBSOLETE

UNCLASSIFIED

1 SECURITY CLASSIFICATION OF THIS PAGE (When Data Entered)

UNCLASSIFIED

SECURITY CLASSIFICATION OF THIS PAGE(When Data Entered)

structural vibration model; the dynamics of the turret servocontrol system are then determined with a model of the gun and turret.

The results of the two models are combined to obtain the dynamic motions of the gun about the initial aim-position. Finally, the statistical mean and the standard deviation errors in gun pointing are derived from the dynamic gun vibration patterns.

These analytical techniques have been used to predict the gun-pointing errors for several types of weapons and to investigate the dynamic effects of certain proposed modifications of the servocontrols. Some specific weapons that have been investigated include the 20mm XM197 gun, the Bushmaster 25mm gun, and the AMCAWS 30mm gun. Both the standard spring adapter mounts and the constant recoil mounts were considered in the analysis; the weapons were mounted on a modified version of the XM97 turret that was attached to the Bell AH-1 helicopter airframe. The analysis of each weapon system is performed for several initial orientations of the turret to determine the sensitivity of the error to the gun-pointing direction.

The major findings from these investigations are that the constant recoil device improves the gun-pointing accuracy; that a simple rate-gyro-feedback in the turret servocontrols does not significantly improve the dynamic response of the weapon; and, finally, that the dynamic response of the weapon is rather sensitive to the initial turret orientation and to the weapon firing rate.

UNCLASSIFIED

SECURITY CLASSIFICATION OF THIS PAGE(When Data Entered)

ACKNOWLEDGMENTS

The authors wish to express their appreciation of Mr. Robert Radkiewicz and the test crew at the GEN Keith L. Ware Simulation Center for their efforts to record and reduce the 20mm XM197 weapon recoil test data that were used extensively in support of this study. Also, the authors wish to acknowledge the help of Mr. Robert Kasten and Mr. Joseph Murdock of the Research Directorate, of Mr. Phillip Townsend and Mr. Timothy Flynn of the Aircraft Weapons Directorate, and of the Honeywell Corporation for their assistance in providing valuable data for the analysis.

Special thanks are due to Miss Louise Vaughn for her expert advice in the technical editing of this report, and to Mrs. Jan Keller, for her professional job of typing and assembling this manuscript.

APPROVED BY	
DATE	WITH SIGNATURE
DATE	DATE
BY	
EXEMPTION/AVAILABILITY CODES	
DATE	AVAIL. AND/OR SPECIAL
A	

CONTENTS

	<u>Page</u>
I. INTRODUCTION	1
II. ANALYTICAL PROCEDURE	5
A. Factors Affecting the Gun-Pointing Error Analysis	5
B. Finite-Element Structural Models	6
C. Helicopter Vibration Model Description	8
D. Gun-Turret Dynamic Model	12
E. Evaluation of the Gun-Pointing Errors	23
F. Recoil Forces	25
III. ANALYSIS OF THE 20mm XM197 WEAPON	34
A. Weapon Description	34
B. Analysis of the AH-1J Helicopter	34
C. Analysis of the AH-1G Helicopter	38
D. The XM97 Turret Servocontrol Modifications	55
IV. ANALYSIS OF THE 25mm WEAPON	64
A. Weapon Description	64
B. Recoil Force	64
C. Turret Controls	65
D. Mass and Inertia Properties	65
E. Results	66
V. ANALYSIS OF THE 30mm WEAPON	74
A. Weapon Description	74
B. Recoil Force	74
C. Turret Controls	75
D. Mass and Inertia Properties	75
E. Results	76
VI. EXTRAPOLATION MODEL	78

CONTENTS (cont'd)

	<u>Page</u>
VII. SUMMARY AND CONCLUSIONS	79
APPENDIX	
A. FORTRAN IV Source Listing of the Helicopter Vibration Model	A-1
B. FORTRAN IV Source Listing of the Gun-Turret Dynamic Model	B-1

ILLUSTRATIONS

<u>Figure</u>	<u>Title</u>	<u>Page</u>
1	AH-1J NASTRAN Elastic Axis ("Stick") Model	3
2	AH-1G NASTRAN Built-up Dynamic Model	4
3	Helicopter Weapon System Model Block Diagram	7
4	Schematic Diagram of the Turret and Gun Configuration	13
5	Coordinate Systems Used in the Analysis	14
6	Schematic Diagram of the Moving Parts in the Turret-Gun Dynamic Analysis	16
7	AH-1J Turret Servosystem Diagram	20
8	Recoil Force for the 20mm XM197 Gun; Test 2, 26 Mar 74; 20 Rounds; 670 spm	26
9	Recoil Force for the 20mm XM197 Gun; Test 2, 28 Mar 74; 20 Rounds; 817 spm	27
10	Recoil Force for the 20mm XM197 Gun; Test 3, 28 Mar 74; 20 Rounds; 500 spm	28
11	Honeywell Constant Recoil Force for the 20mm XM197 Gun; Code RAANM; 34.56 lb-sec Impulse; 25 Rounds; 750 spm; Mechanism Model Data	30
12	Honeywell Constant Recoil Force for the 20mm XM197 Gun; Code RAAM2; 34.56 lb-sec Impulse; 25 Rounds; 750 spm; Misfires: RDS 2 and 4; Mechanism Model Data	31
13	Honeywell Constant Recoil Force for the 20mm XM197 Gun; Code DDFFTA; 10 Rounds; 750 spm; Experimental Test Data	32
14	Dynamic Azimuth Response to the 670 spm Standard 20mm XM197 Recoil Force at the 45° Azimuth and -5° Elevation Position	40
15	Dynamic Elevation Response to the 670 spm Standard 20mm XM197 Recoil Force at the 45° Azimuth and -5° Elevation Position	41
16	Dynamic Azimuth Response to the Honeywell Constant Recoil Force (Code DDFFTA) at the 45° Azimuth and -5° Elevation Position	43
17	Dynamic Elevation Response to the Honeywell Constant Recoil Force (Code DDFFTA) at the 45° Azimuth and -5° Elevation Position	44
18	Statistical Gun Vibration Errors vs. Turret Azimuth Angle for the Test 2-3/28/74 Recoil Force, -25° Turret Elevation Angle	45

<u>Figure</u>	<u>Title</u>	<u>Page</u>
19	Statistical Gun Vibration Errors vs. Turret Azimuth Angle for the Honeywell Constant Recoil Mechanism Model Data (Code RAANM), -25° Turret Elevation Angle	46
20	Statistical Gun Vibration Errors vs. Turret Azimuth Angle for the Honeywell Constant Recoil Test Data (Code DDFFTA), -25° Turret Elevation Angle	47
21	Comparison of the Standard Deviation Elevation Error at -25° Elevation Angle vs. Turret Azimuth Angle, Standard Recoil Test 2-3/26/74 and Constant Recoil Codes RAANM and DDFFTA	49
22	Comparison of the Standard Deviation Elevation Error at -25° Elevation Angle vs. Turret Azimuth Angle for Different Standard Recoil Firing Rates	50
23	Modified AH-1J Turret Servosystem Diagram	56
24	Transfer Function Q(S) for the Modified Turret Servocontrol System	58
25	Standard Deviation Elevation Error at -25° Turret Elevation Angle vs. Turret Azimuth Angle for the Bushmaster 25mm Gun at Three Different Gun CG Positions	73

TABULAR DATA

<u>Table</u>	<u>Title</u>	<u>Page</u>
1	List of Experimentally Measured XM197 20mm Standard Recoil Data	25
2	List of Honeywell XM197 20mm Constant Recoil Data	29
3	AH-1J Analysis Results for Test 1-3/28/74 (669 spm) Standard Recoil	36
4	AH-1J Analysis Results for Test 2-3/28/74 (817 spm) Standard Recoil	36
5	AH-1J Analysis Results for Test 3-3/28/74 (500 spm) Standard Recoil	37
6	AH-1J Analysis Results for Honeywell Constant Recoil Force (Code RAANM)	37
7	AH-1J Analysis Results for Honeywell Constant Recoil Force (Code RAAM2)	38
8	AH-1G Analysis Results for Test 2-3/26/74 (670 spm) Standard Recoil	52
9	AH-1G Analysis Results for Test 2-3/28/74 (817 spm) Standard Recoil	52
10	AH-1G Analysis Results For Test 3-3/28/74 (500 spm) Standard Recoil	53
11	AH-1G Analysis Results for Honeywell Constant Recoil Force (Code RAANM)	53
12	AH-1G Analysis Results for Honeywell Constant Recoil Force (Code DDFFTA)	54
13	Effect on Dynamic Response Due to Servocontrol Modifications	60
14	Position of Gun Center of Gravity for the 25mm Analysis	66
15	Statistical Error Parameters for the Standard 25mm Recoil Force and Gun CG Position No. 1	67
16	Statistical Error Parameters for the Standard 25mm Recoil Force and Gun CG Position No. 2	68
17	Statistical Error Parameters for the Standard 25mm Recoil Force and Gun CG Position No. 3	68
18	Statistical Error Parameters for the Standard 25mm Recoil Force and Gun CG Position No. 4	69
19	Statistical Error Parameters for the 25mm Constant Recoil Force and Gun CG Position No. 1	69

<u>Table</u>	<u>Title</u>	<u>Page</u>
20	Statistical Error Parameters for the 25mm Constant Recoil Force and Gun CG Position No. 2	70
21	Statistical Error Parameters for the 25mm Constant Recoil Force and Gun CG Position No. 3	70
22	Statistical Error Parameters for the 25mm Constant Recoil Force and Gun CG Position No.4	71
23	Dynamic Response of AH-1G Model to 30mm Constant Recoil Force (Transmission Stiffness $k = 10 \times 10^5$ lb-ft/rad)	77
24	Dynamic Response of AH-1G Model to 30mm Constant Recoil Force (Transmission Stiffness $k = 15 \times 10^5$ lb-ft/rad)	77

I. INTRODUCTION

One of the factors that contributes to the gun-pointing errors of the helicopter automatic cannon system is the dynamic vibration of the system components. The vibrating components of the automatic cannon system consist of the helicopter structure, the gun turret, and the gun itself. When this system is excited by a dynamic force, the resulting motion will alter the gun orientation, which in turn will affect the accuracy of the weapon system.

To analyze and predict the gun errors due to this effect necessitated extensive analytical and computer studies. The purpose of the present report is to describe these studies and present results that have been obtained in the course of this investigation.

For the dynamic analysis, the helicopter-weapon system was divided into two parts. The first part of the system, called the helicopter model, is a detailed representation of the helicopter mass and structural components, with the turret and the gun represented by a concentrated mass. The second part of the system, called the gun-turret model, is a dynamic model used to describe the moving components of the turret and the gun. The dynamic motion of the helicopter is analyzed by use of a finite-element model of the Bell AH-1 structural airframe. A prescribed forcing function is applied to induce the structural vibrations. Since this model contains a relatively large number of degrees of freedom (approximately 1800), a considerable reduction in the order of the system is first achieved by a matrix condensation procedure. Then the characteristic frequencies and the mode shapes of the structure are determined, and the governing dynamic equations of motion are reformulated in terms of a set of uncoupled modal equations. The modal equations are solved numerically to obtain the translational and the angular accelerations of the concentrated mass, representing the turret and the gun. These accelerations are then used as an input into the gun-turret dynamic model, which is a two-degree-of-freedom model representing the azimuth and the elevation motions of the turret.

The response of the turret is affected by the inertial properties of the turret and the gun, the characteristics of the servocontrols, and the stiffness of the drive systems used for the azimuth and elevation controls.

The dynamic equations for this system are solved by numerical methods, and the solutions for the azimuth and elevation dynamic motions are presented in a form which is useful for the statistical analysis of gun errors. In particular, the mean and the standard deviation errors of the azimuth and the elevation motions are determined from the vibrations about the initial aim-position. These statistical parameters are evaluated for the time interval during which the gun is firing.

Two different finite-element structural models are used to represent the AH-1J and AH-1G helicopter structures. These two models differ primarily in the way that the structure of the helicopter is modeled. The AH-1J model, described in Reference 1, is an elastic axis NASTRAN representation of the structural airframe. The AH-1G NASTRAN model, described in Reference 2, contains a much more detailed representation of the fuselage and wingstub structures. Both models have been validated by comparisons of model predictions with results from static deflection tests and dynamic shake tests. Structural plots of the AH-1J and AH-1G models are shown in Figures 1 and 2, respectively.

A number of different forcing functions can initiate the dynamic vibration of the total system. The main unsteady forces are the main rotor loads and the recoil force of the gun. Experimental data from a recent series of flight tests of the AH-1G helicopter show that the recoil forces are, by far, the most predominant in producing airframe and turret vibrations. Consequently, numerical results are obtained and presented for the recoil force excitation only. Weapons of different caliber have been examined, including 20, 25, and 30 mm automatic cannons. Different recoil forces for each of these weapons were obtained from experimental tests and from computer simulations of the assembled weapon-and-mount mechanisms.

¹Cronkhite, J.D. and Wilson, W.F., "Dynamic Analysis of Two-Per-Rev Vibrations in the Model AH-1J Helicopter", Report No. 299-100-021, Bell Helicopter Company, Fort Worth, Texas (Feb 1972)

²Cronkhite, J.D., and Berry, V.L. and Brunken, J.E., "A NASTRAN Vibration Model of the AH-1G Helicopter Airframe", Volumes I and II, Bell Helicopter Company, AD R-TR-74-045, Fort Worth, Texas (April 1974)

The simulated data are used to examine the effect of the constant recoil mechanism. The use of this mechanism is necessary to reduce the peak-to-peak variation in the transmitted recoil load, and hence, the dynamic vibration of the weapon, to accepted levels.

AH-1J NASTRAN ELASTIC AXIS ("STICK") MODEL

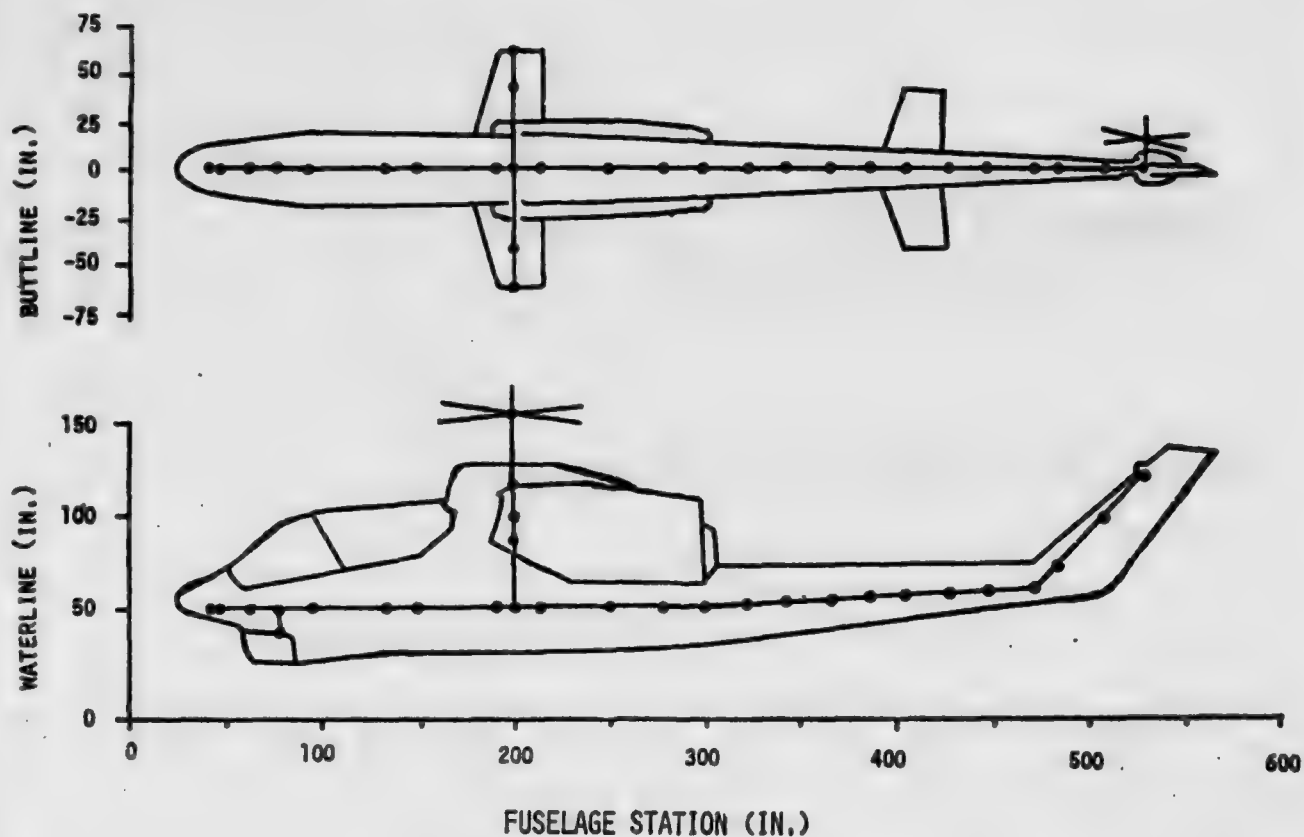


Figure 1. AH-1J NASTRAN Elastic Axis ("Stick") Model

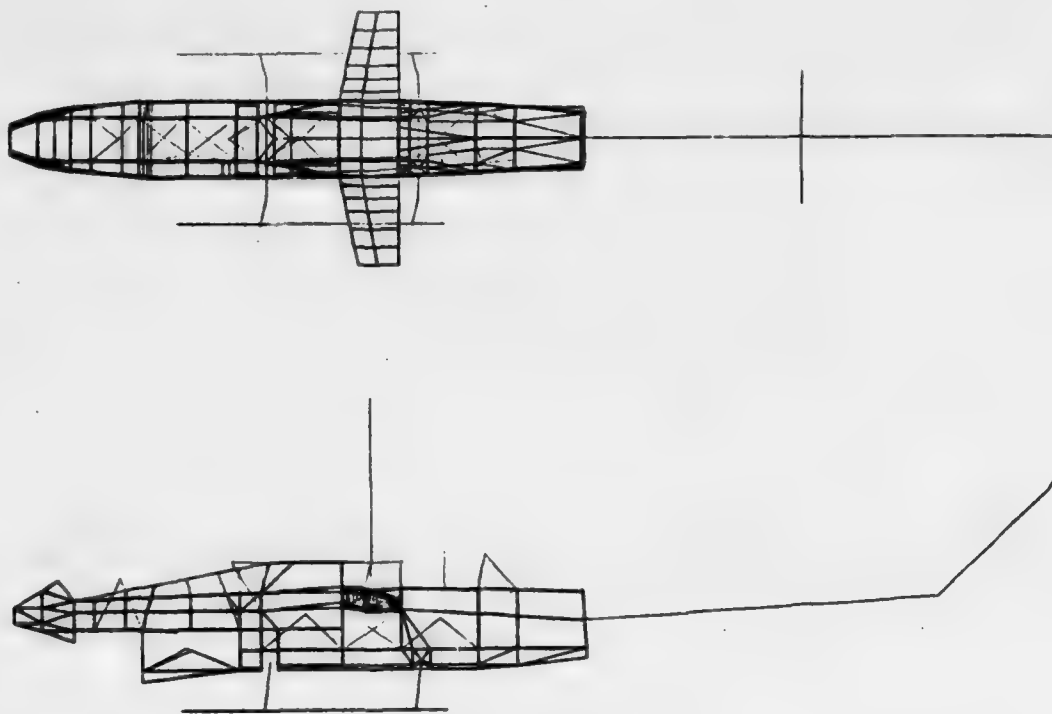


Figure 2. AH-1G NASTRAN Built-up Dynamic Model

II. ANALYTICAL PROCEDURE

A. Factors Affecting the Gun-Pointing Error Analysis

Dynamic gun-pointing errors, in a turreted attack-helicopter, are caused by the dynamic effects of weapon recoil. Essentially, two primary errors are attributed to the weapon recoil loads - namely, the helicopter airframe vibrations and the turret servocontrol oscillations. The airframe vibrations that affect the gun-pointing accuracy are the three angular vibration components at the turret attachment platform. Since the turret consists of a stiff linkage of rigid body segments, the oscillations of the turret platform are a direct source of gun-pointing error. In addition, the relative oscillations between the interconnected rigid body segments of the turret (i.e. motions of the azimuth and elevation drive systems) constitute a second source of gun-pointing error. The turret servocontrol system responds dynamically to the applied recoil torques and also to the accelerations of the turret attachment platform.

A two-step analytical procedure has been developed to determine the cumulative gun-pointing error due to weapon recoil loads. First, the airframe flexural vibrations are determined with a structural vibration model. The location of the gun-barrel axis is defined in the model by azimuth and elevation angles, and the predicted turret platform vibrations are resolved in terms of the azimuth and elevation gun-line components. Furthermore, the accelerations of the turret attachment platform are determined by the structural vibration model. The dynamics of the turret servocontrol system are then predicted with a model that utilizes the platform accelerations and recoil data generated by the structural vibration model. In the turret model, the turret servocontrol oscillations are calculated and the resulting gun-line turret vibrations are combined with the platform vibrations.

This procedure leads to predictions of the time variations in the gun-line azimuth and elevation angles about the initial aim-position. Statistical error parameters are then calculated for the burst interval. In particular, the means and the standard deviations of the dynamic azimuth and elevation angle errors are determined, and these parameters are used to represent the gun-pointing error components statistically.

Since the magnitude of each statistical error parameter is dependent on the initial aim-position, a matrix of statistical error parameters is

calculated for several discrete turret orientations. In this manner, the sensitivity of the gun-pointing error to the initial aim-position is determined over the normal operating range of the turret. The turret considered in this analysis operates approximately between 0° and $\pm 110^\circ$ in azimuth, and between 0° and -50° in elevation. However, in practical applications, the azimuth angle position normally does not exceed $\pm 70^\circ$.

To show how the present investigation fits into the overall error analysis of a helicopter mounted automatic cannon, a schematic diagram of the Helicopter Weapon System Model is presented in Figure 3. This figure shows the flow chart representing the order of the various calculations, which are performed to determine the hit probability for a specified set of input parameters.

With reference to Figure 3, note that, with this model, four different types of input parameters are used for the evaluation of the final hit probability. The four inputs, shown on the left side of the flow chart, consist of the line of sight and aircraft sensor data, the weapon recoil force, wind and ballistic data, and the target data. The present investigation is designed to develop a portion of this system model that comprises the Turret Servocontrol Model, the Turret Dynamic Model, and the Helicopter Vibration Model. This portion of the system model responds to two different input functions: the first is the gun aim angle commands passed from the fire control computer model and the second is the weapon recoil force. During the target tracking process, the command aim-angles produced by the fire control computer are relatively slowly varying input signals into the turret control system and, therefore, do not, in general, significantly affect the dynamic vibration of the system. Consequently, the main excitation for the dynamic motion is the recoil force of the weapon.

B. Finite-Element Structural Models

The helicopter vibration analysis, to be described in the following section of this report, is used to predict the dynamic structural response to a general, time-dependent recoil force. In this analysis, the natural frequencies, the generalized masses, and the free-vibration modes shapes of the helicopter structure are used in the governing dynamic equations to represent the dynamic characteristics of the airframe. Before a

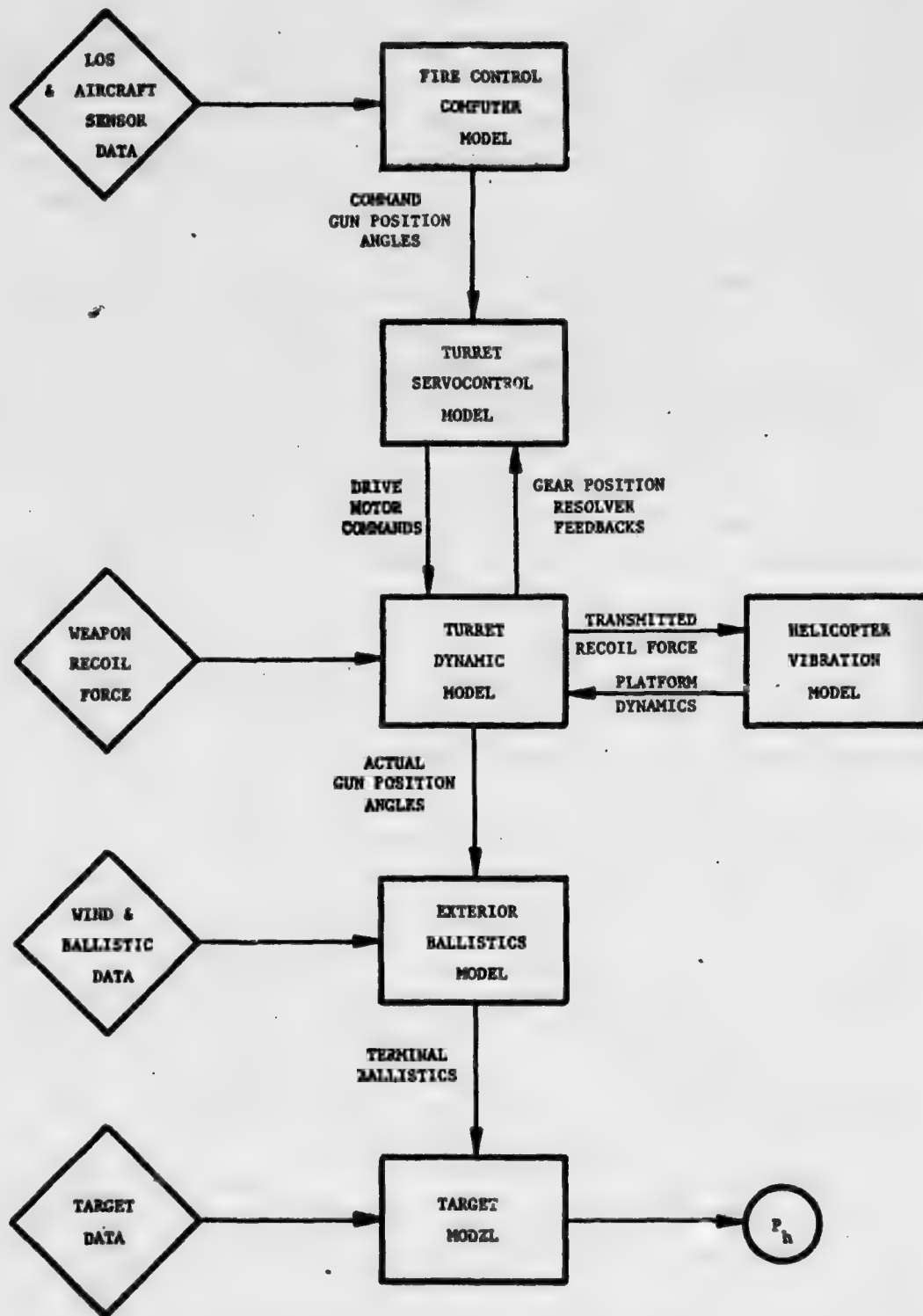


Figure 3. Helicopter Weapon System Model Block Diagram

forced-vibration problem can be solved, the free-vibration properties of the structure have to be obtained. In the present investigation, these properties were supplied from the finite-element NASTRAN computer program. This program is a general-purpose structural analysis program developed by NASA and by several aerospace companies. One of the capabilities of the NASTRAN program is to solve for the natural frequencies and mode shapes of the multi-degree-of-freedom systems.

In the modeling of the AH-1 helicopter structure in terms of finite-elements, two different structural models were used. These two models correspond to the AH-1J and the AH-1G helicopter structures. Structural plots of the AH-1J and the AH-1G models are shown in Figures 1 and 2, respectively. In spite of the minor structural differences in the AH-1J and in the AH-1G helicopter configurations, the two models differ substantially in the detail of the structural representations. In the case of the AH-1J model, the helicopter structure was represented by the so-called "elastic axis" configuration. In this approach, the structure is modeled entirely by beam finite elements that can carry axial tension, bending, and torsion. The mass of the system was lumped at the nodes. This is a relatively simple representation, as is evident from the structural plot of the AH-1J model in Figure 1. For example, the main fuselage of the helicopter is modeled by a row of elements in series. In the case of the AH-1G structure, a more detailed finite-element model representation was developed. In this case, the total structure was modeled by many different types of elements including beams, rods, plates, and shear panels. Consequently, this led to a larger degree-of-freedom system. As in the first model, the mass of the helicopter was lumped at the nodes of the finite elements. Both in the AH-1J and in the AH-1G models, one concentrated mass was chosen to represent the mass of the gun-turret system. This mass was placed as close as possible to the center of gravity of the turret and weapon.

C. Helicopter Vibration Model Description

In the finite-element NASTRAN formulation of the structural model, the helicopter structure is idealized by a set of discrete structural elements connected at suitable nodal or grid points. For this type of model, the dynamic equations for the forced vibration of the helicopter can be written

in the matrix form

$$[m] \{\ddot{x}\} + [k] \{x\} = \{F\} \quad (1)$$

where

$[m]$ is the mass matrix,

$[k]$ is the stiffness matrix,

$\{F\}$ is the force matrix,

and $\{x\}$ is the vector of the grid point displacements.

Note that equation (1) does not contain any damping terms. With respect to the present problem, the incorporation of terms to represent structural damping is desirable; but, because of its frictional nature, damping can only be represented empirically. Such a correction can be done most conveniently after the modal formulation has been introduced and the equations (1) have been decoupled.

To transform the matrix equation (1) to the modal formulation necessitated the examination of the free-vibration characteristics of the homogeneous problem corresponding to equation (1),

$$[m] \{\ddot{x}\} + [k] \{x\} = 0. \quad (2)$$

The eigenvalues for equation (2) will be denoted by ω^2 , and these are obtained from a characteristic equation

$$\begin{vmatrix} -\omega^2 [m] + [k] \end{vmatrix} = 0 \quad (3)$$

where the vertical bars indicate a determinant. This procedure results in the determination of the characteristic frequencies, ω_i , where i varies over the number of degrees of freedom of the system. Once the frequencies ω_i are known, the corresponding eigenvectors or mode-shape vectors $\{\phi\}_i$ are determined by a standard procedure. Both of these steps were carried out by the NASTRAN computer program. The modal transformation matrix is defined by the relation

$$[\phi] \triangleq [\phi_1, \phi_2, \dots, \phi_N] \quad (4)$$

where N is the number of degrees of freedom. In the definition (4), the modal matrix consists of column vectors of the mode shapes.

Consider now a modal coordinate transformation

$$\{x\} = [\phi] \{q\}. \quad (5)$$

By the substitution of equation (5) in equation (1) and the multiplication of both sides by the transposed matrix $[\phi]^T$, the dynamic equations can be written in the new form

$$[\phi]^T [m] [\phi] \{\ddot{q}\} + [\phi]^T [k] [\phi] \{q\} = [\phi]^T \{F\}. \quad (6)$$

The normalization of the modal matrix $[\phi]$ and the use of the orthogonal properties of the natural modes lead to the following simplifications:

$$[\phi]^T [m] [\phi] = [I] \quad (7)$$

$$\text{and } [\phi]^T [k] [\phi] = [\omega^2] \quad (8)$$

where $[I]$ is a unit diagonal matrix and $[\omega^2]$ is a diagonal matrix containing the squares of the natural frequencies. From equations (6), (7), and (8) a set of uncoupled, second-order differential equations is obtained in the variables q_i ,

$$\ddot{q}_i + \omega_i^2 q_i = Q_i \quad (i = 1, 2, 3, \dots, N) \quad (9)$$

where no summation on i is implied and Q_i is a generalized force defined by

$$Q_i = \{\phi\}_i^T \{F\}.$$

The consequence of equations (9) is that the helicopter vibration problem has been reduced to a solution of a large number of uncoupled differential equations.

Normally, however, an accurate solution to the forced-vibration problem can be obtained by the solution to only those equations for which ω_i is below some cutoff frequency. For the helicopter vibration problem, only the first 30 of equations (9) are solved and the higher frequency equations are neglected. In general, the number of equations that need to be retained to obtain an accurate solution is dependent upon the nature of the excitation force vector $\{F\}$.

Before the equations (9) are solved, they are modified to include structural damping effects. Any correction for this type of damping has to satisfy the experimental observations that the damping force is in phase with velocity and is independent of frequency. When the structure is subject to sinusoidal vibration, these facts can be represented mathematically by the introduction of the complex stiffness and the replacement of the frequency term ω_i^2 in equations (9) by the complex quantity $\omega_i^2 (1 + j\gamma)$, where j rep-

resents the pure imaginary number $\sqrt{-1}$ and γ is defined as the damping coefficient. The complex representation for the structural damping is not convenient when it is applied to general time-dependent problems. Consequently, in this case, a more general correction is applied that include the first time-derivative. In this approach, the ω_1^2 term in equations (9) is replaced by $\omega_1^2(1 + \gamma/\omega_1 \frac{d}{dt})$; this substitution leads to the modified dynamic equations

$$\ddot{q}_i + \gamma \omega_1 \dot{q}_i + \omega_1^2 q_i = Q_i \quad (i = 1, 2, 3, \dots, N). \quad (10)$$

Note that the behavior of the damping term in these equations reduces to the desired form when the system is excited with a sinusoidal force with frequency ω_1 . In general, the value of the damping coefficient γ has to be obtained experimentally; however, for the present analysis, a value of 0.02 was used because this value has been found by previous investigators to be quite representative of airframe construction.

Before the solutions to equations (10) are obtained for general forcing functions, these equations are first solved for impulsive loading. Dropping the subscript i for convenience results in the following equation for the impulsive load problem:

$$\ddot{q} + \gamma \omega \dot{q} + \omega^2 q = \delta(t) \quad (11)$$

where $\delta(t)$ is a unit delta function. The solution to equation (11) is denoted by q_δ and can be obtained by the expression of equation (11) as a homogeneous equation with a nonzero initial velocity condition. This solution is given by

$$q_\delta = \frac{1}{\beta} e^{-\alpha t} \sin \beta t \quad (12)$$

$$\text{where } \alpha = \gamma\omega/2 \quad (13a)$$

$$\text{and } \beta = \omega \sqrt{1 - (\gamma/2)^2} \quad (13b)$$

The solution for the general forcing function $Q(t)$ can be obtained by use of equation (12) and the superposition integral. The general solution to equation (10) is then given by

$$q(t) = \int_0^t Q(\tau) q_\delta(t - \tau) d\tau. \quad (14)$$

By the substitution of equation (12) in (14), the solution for $q(t)$ is then

given in the following form:

$$q(t) = \frac{1}{\beta} e^{at} \left\{ \sin \beta t \int_0^t Q(\tau) e^{-a\tau} \cos \beta \tau d\tau - \cos \beta t \int_0^t Q(\tau) e^{-a\tau} \sin \beta \tau d\tau \right\}. \quad (15)$$

In the present analysis, equation (15) was used for the solution to each modal equation, and the integration with respect to time was carried out numerically. Altogether, 30 modal equations were used in the analysis for both the AH-1J and the AH-1G helicopter models.

After the set of modal equations is solved to obtain the modal coordinate vector $\{q\}$, the grid-point displacement vector $\{x\}$ is determined from equation (5). The results of this analysis are used as the input to the Gun-Turret Dynamic Model, which is described in the next section of this report. This input comprises the angular displacements, velocities, and accelerations, and the linear accelerations of the grid point corresponding to the turret attachment platform. Therefore, only the six displacement terms that correspond to the turret attachment grid point in the vector $\{x\}$ need to be evaluated. The velocities and accelerations of the turret attachment grid point are then calculated by differentiation.

The FORTRAN IV source program for the Helicopter Vibration Model is listed in the Appendix A. The output data that is required, in the analysis, by the Gun-Turret Dynamic Model is written on a sequential data set (file 12). Two temporary I/O files (files 13 and 14) are also used in the program, for the storage of the intermediate results. These temporary files are provided primarily to reduce the central core storage requirements and to increase the execution efficiency.

D. Gun-Turret Dynamic Model

In this section, the dynamic model for the gun-turret configuration, including the effects of the servocontrols in the turret, is described. The forcing function for the dynamic motion is provided by the gun recoil force and by the accelerations of the helicopter structure to which the turret is attached. The dynamic motion of the turret can be described by two rotational equations of motion: one for the azimuth motion, and the other for the elevation motion. The three main components of the turret

system, shown in Figure 4, consist of the stationary ring, the rotating ring, and the gun. The stationary ring is attached to the helicopter platform and will therefore move with the vibration of the helicopter structure. The azimuth motion will involve the rotation of the rotating ring, the saddle mechanism, and the gun about the turret azimuth axis. The elevation motion will involve the rotation of the gun and saddle mechanism about the elevation trunnion axis.

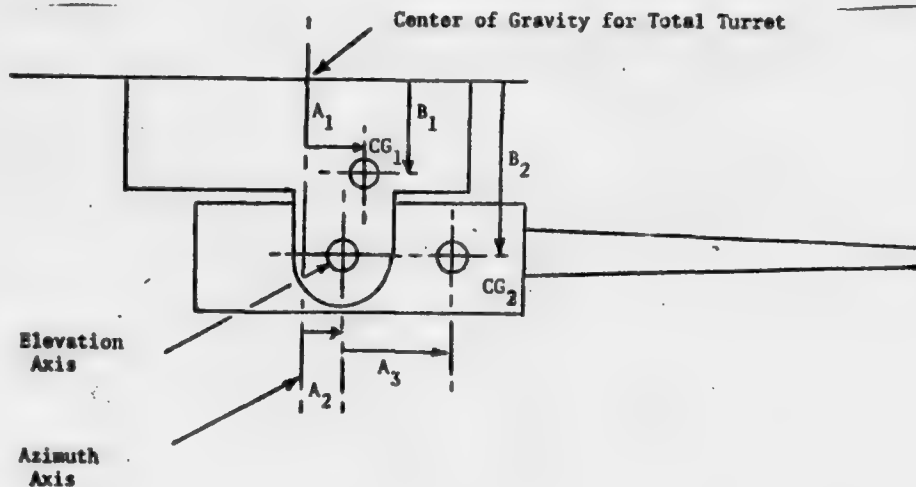


Figure 4. Schematic Diagram of the Turret and Gun Configuration

In the derivation of the dynamic equations, various coordinate systems are used. The three different coordinates systems ξ_i , x_i , and z_i ($i = 1, 2, 3$) used in the analysis are shown in Figure 5. The coordinates ξ_i are the inertial coordinates, and the coordinates x_i are moving coordinates that rotate with the helicopter vibration and, therefore, differ from ξ_i by small angular deflections. The coordinates z_i are oriented with respect to the coordinates x_i by the initial azimuth and elevation angles that are denoted by ϕ and α , respectively. The azimuth dynamic equation refers to the rotation about the axis x_2 , and the elevation dynamic equation refers to the

rotation about the axis z_3 . The origin of the ξ_1 coordinates is assumed to be situated at the concentrated mass corresponding to the gun-turret configuration in the NASTRAN finite-element model.

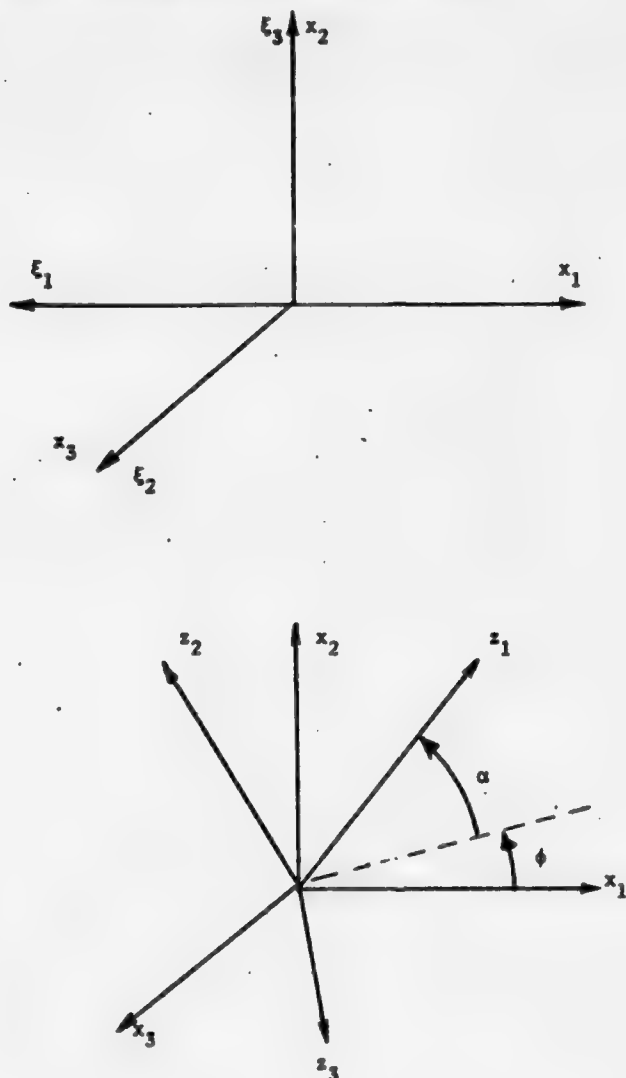


Figure 5. Coordinate Systems Used in the Analysis

To obtain the rotational equations of motion about the axes x_2 and z_3 involves the use of the general vector dynamic equations for a moving coordinate system. The moment vector equation is expressed as

$$\bar{M} = m \bar{\rho}_c \times \bar{a} + \dot{\bar{H}}_p \quad (16)$$

where

\bar{M} is the vector moment,

$\bar{\rho}_c$ is the vector position of the center of gravity of the rotating mass relative to the ξ_1 origin,

\bar{a} is the linear acceleration of the x_1 origin,

m is the mass of the rotating parts,

and

$\dot{\bar{H}}_p$ is the portion of the rate of change of angular momentum that is dependent upon the moments of inertia and the angular accelerations of the rotating parts.

The relative positions of the various pivot points and centers of mass are defined in Figure 4 by the parameters A_1 , A_2 , A_3 , B_1 , and B_2 . The center of gravity CG_1 is denoted by the length parameters A_1 and B_1 defined with reference to zero azimuth and elevation angles. The center of gravity CG_1 applies to the total mass involved in the azimuth vibration, which includes the rotating ring and the saddle-gun combination. The center of gravity CG_2 applies to the saddle-gun combination only, and it is defined by the lengths A_2 , A_3 , and B_2 . The parameter A_2 defines the pivot position, and A_3 and B_2 define the position of CG_2 .

Since the dynamic equations for the azimuth and the elevation motions are similar in form, a general set of equations can be derived that are valid for either of these motions. Consider the schematic representation in Figure 6 in which the three components involved in the vibration are shown. This schematic applies both to the azimuth and to the elevation motions. The three components in Figure 6 are the drive motor, the gear transmission system, and the turret mass. For convenience, the moments of inertia of the motor and the turret are referred to the turret coordinates. The moment of inertia of the gear box and the drive can be included in the motor and the turret inertias. The torques transmitted through the total system are also shown in Figure 6. The torque T_m is the torque applied electrically to the motor, and T_t is the torque transmitted to the turret.

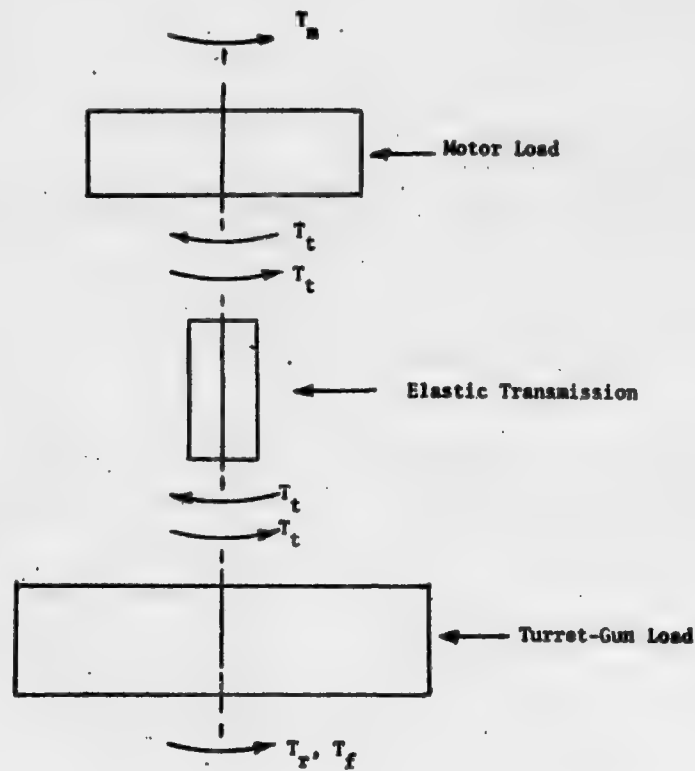


Figure 6. Schematic Diagram of the Moving Parts in the Turret-Gun Dynamic Analysis

The effect of friction in the system is represented by the torque T_f acting on the turret. The torque T_r represents the contribution of the recoil force. The rates of change of the angular momentum for the motor and for the turret are denoted by \dot{H}_m and \dot{H}_t , respectively. With the use of the torques shown in Figure 6, the dynamic equations of equilibrium are written as follows:

$$\dot{H}_m = T_m - T_t \quad (17)$$

$$\dot{H}_t = T_r + T_t + T_f \quad (18)$$

The transmitted torque T_t is related to the elastic deformation of the system. To express equations (17) and (18) in terms of angular displacements, let $\Delta\phi$ and $\Delta\alpha$ define dynamic rotations in the azimuth and

elevation mechanisms, respectively; and furthermore let

$$\Delta\phi \triangleq \phi_o + \phi_m + \phi_e, \quad (19)$$

and

$$\Delta\alpha \triangleq \alpha_o + \alpha_m + \alpha_e, \quad (20)$$

where ϕ_o and α_o are the dynamic components due to helicopter vibration, ϕ_m and α_m are the dynamic motions for rigid gear system drives, and ϕ_e and α_e are the contributions from the elastic effects in the system. For convenience, let ϕ_r and α_r define the relative displacements given by the expressions

$$\phi_r \triangleq \phi_m + \phi_e, \quad (21)$$

and

$$\alpha_r \triangleq \alpha_m + \alpha_e. \quad (22)$$

The angles ϕ_r and α_r are relative angles between various parts of the turret and are detected by the angular position resolvers in the servocontrol system. The motor torque T_t in equations (17) and (18) can be expressed in terms of the elastic displacements. For the azimuth motion:

$$T_t = -k\phi_e \quad (23)$$

and for the elevation motion:

$$T_t = -k\alpha_e \quad (24)$$

where k represents the elastic stiffness of the gear box and the transmission.

Consider now the torque T_f produced by the friction in the system. Since this term represents a combination of all frictional forces in the system, an exact analysis of this term is extremely difficult, and an empirical relation has to be used. In this analysis, the assumption is that this torque acts to oppose the relative motion of the various parts of the turret; but since it is a frictional force, it is independent of the magnitude of the angular velocities. Consequently, for the azimuth motion, this torque is represented by:

$$T_f = -kg(\dot{\phi}_r)/|\dot{\phi}_r| \quad (25)$$

and for the elevation motion

$$T_f = -kg(\dot{\alpha}_r)/|\dot{\alpha}_r| \quad (26)$$

where g is the damping coefficient.

Consider now the rates of change of angular momentum \dot{H}_m and \dot{H}_t in equations (17) and (18). Before writing the expression for \dot{H}_t , let a_1 , a_2 , and a_3 denote the linear acceleration components of the turret attachment platform in the ξ_1 axis system and let $\ddot{\theta}_1$, $\ddot{\theta}_2$, and $\ddot{\theta}_3$ denote the angular acceleration components. These are the hull accelerations that are calculated by the Helicopter Vibration Model. With the use of the azimuth and elevation angles ϕ and α , and the geometrical parameters shown in Figure 4, the component of the rate of change of angular momentum for the turret about the axis of rotation is given by

$$\dot{H}_t = -m_1 A_1 (-a_1 \sin \phi + a_2 \cos \phi) + I_t \Delta \ddot{\phi} \quad (27)$$

where m_1 is the turret mass involved in the azimuth motion and I_t is the turret moment of inertia about the turret azimuth axis. Consider now the angular acceleration term in equation (27). Differentiating equations (19) and (21) twice result in the expression

$$\Delta \ddot{\phi} = \ddot{\phi}_o + \ddot{\phi}_r \quad (28)$$

But $\ddot{\phi}_o$ is related to the hull vibration in the azimuth direction by

$$\ddot{\phi}_o = \ddot{\theta}_3 \quad (29)$$

For the motor, the predominant contribution to the angular momentum rate is from the relative motor rotations and, therefore, to a good approximation

$$\dot{H}_m = I_m \ddot{\phi}_m \quad (30)$$

where I_m is the moment of inertia of the motor referred to the turret coordinates.

For the case of the elevation vibration, the rotational equilibrium equations are referred to the saddle pivot axis. The rate of change of the angular momentum can be shown to be

$$\begin{aligned} \dot{H}_t = m_2 [(A_2 + A_3 \cos \alpha) a_3 + (a_1 \cos \phi + a_2 \sin \phi) (-B_2 + A_3 \sin \alpha)] \\ + I_t \Delta \ddot{\alpha} \end{aligned} \quad (31)$$

where m_2 is the mass of the saddle-gun combination and I_t is the moment of inertia about the saddle pivot axis. For the elevation motor, all terms

except the motor rotational effects can be neglected and therefore,

$$\dot{H}_m = I_m \ddot{\alpha}_m. \quad (32)$$

Equations (20) and (22) can be differentiated to get

$$\Delta \ddot{\alpha} = \ddot{\alpha}_0 + \ddot{\alpha}_r \quad (33)$$

and, as is shown in the next section, the acceleration $\ddot{\alpha}_0$ is related to the hull accelerations by

$$\ddot{\alpha}_0 = -\ddot{\theta}_1 \sin \phi + \ddot{\theta}_2 \cos \phi. \quad (34)$$

Consider now the azimuth vibration. By use of equations (17) and (18) and substitution from equations (23), (25), (27), (28), (29), and (30), the equations of equilibrium can be written in the form:

$$I_m \ddot{\phi}_m - k\phi_e = T_m \quad (35)$$

$$\begin{aligned} I_t \ddot{\phi}_r + k\phi_e + kg\dot{\phi}_r/|\dot{\phi}_r| \\ = m_1 A_1 (-a_1 \sin \phi + a_2 \cos \phi) - I_t \ddot{\theta}_3 + T_r. \end{aligned} \quad (36)$$

Equation (21) can be used to write equations (35) and (36) in terms of two unknowns:

$$I_m \ddot{\phi}_m - k(\phi_r - \phi_m) = T_m \quad (37)$$

$$I_t \ddot{\phi}_r + k(\phi_r - \phi_m) + kg\dot{\phi}_r/|\dot{\phi}_r| = T_I + T_r \quad (38)$$

where, for convenience, an effective hull inertia torque is defined as follows:

$$T_I \triangleq m_1 A_1 (-a_1 \sin \phi + a_2 \cos \phi) - I_t \ddot{\theta}_3. \quad (39)$$

For the elevation vibration, the corresponding equations have the same form as equations (37) and (38) except that the variable ϕ is replaced by α . The inertial torque T_I for this case will have the form:

$$\begin{aligned} T_I \triangleq -m_2 [(A_2 + A_3 \cos \alpha) a_3 + (a_1 \cos \phi + a_2 \sin \phi) (-B_2 + A_3 \sin \alpha)] \\ - I_t (-\ddot{\theta}_1 \sin \phi + \ddot{\theta}_2 \cos \phi). \end{aligned} \quad (40)$$

Before the solution to equations (37) and (38) is determined, an appropriate expression for the motor torque T_m must be obtained. This expression will be developed next. Both the azimuth and the elevation motions are

governed by the same type of servosystem; the only differences are in the inertial and geometrical parameters, and in the gear ratio used in each of these motions. A simplified block diagram for the servocontrol system is shown in Figure 7.

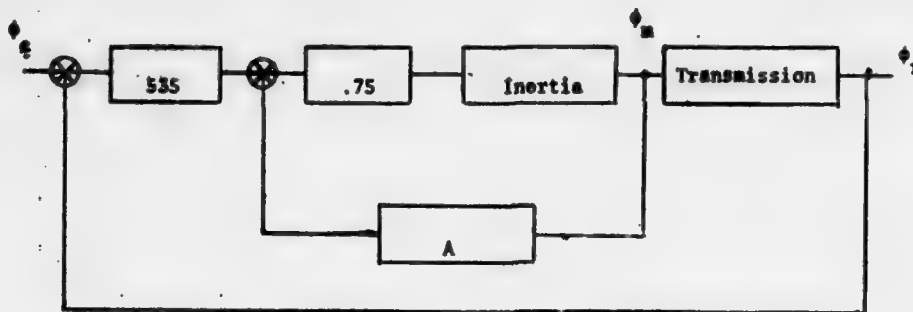


Figure 7. AH-1J Turret Servosystem Diagram

In the simplification of the actual servodiagram, certain very high-frequency effects were neglected. Basically, two feedback systems are present. The first feedback signal is the relative motion ϕ_r or α_r that is measured by use of a gear position resolver. This relative motion is then subtracted from the desired control signal ϕ_c or α_c . The second feedback is the speed of the motor that is measured by a tachometer and modified by a transfer function. The transfer function is defined in terms of the motor angular displacements ϕ_m or α_m , and the resulting signal is subtracted from the difference of the control and the resolver signals. Actually, before the subtraction takes place, the control signal is amplified by the factor 535, as is shown in Figure 7. The transfer function A, defined in terms of the transformed variable s, has the form:

$$A = \left(\frac{1}{1.3} \times \frac{0.1s}{1 + .1s} \times .067s + \frac{.0192s}{7.5} \right) n \quad (41)$$

where n is the gear ratio. For the azimuth motion, $n = 620$; for the elevation motion, $n = 810$. Consequently, in terms of the transformed variable, the motor torque for the azimuth motion is given by:

$$T_m = 535 \times 0.75n (\phi_c - \phi_r - \phi_s) \quad (42)$$

where ϕ_s is defined as

$$\phi_s \triangleq (A/535)\phi_m. \quad (43)$$

Writing the transfer function A over a common denominator and using $n = 620$ results in the following equation:

$$\phi_s = \frac{.0029667s + .0062692 s^2}{1 + 0.1s} \phi_m. \quad (44)$$

Equation (44) is given in terms of the transformed variable s ; but, for convenience, this equation will be expressed in differential form by the replacement of the parameter s with the time-differential operator:

$$\phi_s + .1 \frac{d\phi_s}{dt} = .0029667 \frac{d\phi_m}{dt} + .0062692 \frac{d^2\phi_m}{dt^2}. \quad (45)$$

For the case of the elevation motion, equation (45) is modified by the replacement of ϕ_s and ϕ_m with α_s and α_m , and by the multiplication of each term on the right side with the factor $810/620$. The motor torque at any given time is defined from equations (42) and (45), although it is expressed in the form of a differential equation.

The final form of the governing equations is given here in terms of the azimuth deflection variable ϕ , and similar types of equations are valid for the elevation parameter α . Consider the equation of motion (37) and substitute from equation (42) to get

$$I_m \ddot{\phi}_m - k(\phi_r - \phi_m) = 401.25n (\phi_c - \phi_r - \phi_s). \quad (46)$$

Equation (46), together with equations (38) and (45), represents a system of three governing equations in the variables ϕ_m , ϕ_r , and ϕ_s . For the case of the elevation motion, the variable ϕ is changed to α and the right side of equation (45) is altered by a multiplying constant, as indicated previously.

The solution to the three governing equations will be obtained numerically on a computer. To do this calls for the transformation of the three second-order equations to five first-order equations by the definition of the following five variables:

$$\phi_1 \triangleq \phi_r \quad (47a)$$

$$\phi_2 \triangleq \frac{d\phi_r}{dt} \quad (47b)$$

$$\phi_3 \triangleq \phi_m \quad (47c)$$

$$\phi_4 \triangleq \frac{d\phi_m}{dt} \quad (47d)$$

$$\phi_5 \triangleq \phi_s \quad (47e)$$

By the substitution of the above definitions in the governing equations (38), (45), and (46), the set of five first-order equations follows:

$$\frac{d\phi_1}{dt} = \phi_2 \quad (48a)$$

$$\frac{d\phi_2}{dt} = \frac{1}{I_t} [-k(\phi_1 - \phi_3) - k g \dot{\phi}_2 / |\dot{\phi}_2| + T_I + T_r] \quad (48b)$$

$$\frac{d\phi_3}{dt} = \phi_4 \quad (48c)$$

$$\frac{d\phi_4}{dt} = \frac{1}{I_m} [k(\phi_1 - \phi_3) + 401.24n (\phi_c - \phi_1 - \phi_5)] \quad (48d)$$

$$\begin{aligned} \frac{d\phi_5}{dt} = & -10\phi_5 + 0.029667 \phi_4 \\ & + 0.062692 \left[\frac{1}{I_m} k(\phi_1 - \phi_3) + 401.25n (\phi_c - \phi_1 - \phi_5) \right]. \end{aligned} \quad (48e)$$

Note that, in the last of equations (48), the second derivative of ϕ_m was replaced by the use of equation (46). Equations (48) are solved numerically, and the solution has been programmed on a digital computer.

The FORTRAN IV source program for the Gun-Turret Dynamic Model is listed in the Appendix 2. In this program, file 1 is the input file that contains the data passed from the Helicopter Vibration Model. A plot routine is provided, in the Gun-Turret Dynamic Model, to graph the dynamic responses in the azimuth and elevation directions on the CALCOMP Model 914 plotter.

E. Evaluation of the Gun Pointing Errors

The results of the Gun-Turret Dynamic Model, described in the previous section, are used to calculate the gun-pointing errors. These errors are calculated from the statistical properties of the angular dynamic responses of the weapon. The statistical properties include the mean and the standard deviation of the angular motions of the gun barrel about two mutually perpendicular axes. With the use of the initial gun barrel direction as the reference line, the gun-pointing errors can be defined by the deviation of the gun from this orientation. This deviation can be calculated by the rotation of the barrel about two mutually perpendicular axes, which, in this analysis, are chosen to be z_3 and z_2 . The choice of the z_3 axis is a natural one since it corresponds to the elevation motion previously defined by equation (20) and denoted by $\Delta \alpha$. This quantity contains two parts, the helicopter rotation α_0 and the relative rotation α_r . The helicopter vibration term α_0 can be obtained from the data generated by the Helicopter Vibration Model and it is related to the angular rotations of the helicopter at the attachment point of the turret. This relation can be obtained by the consideration of the coordinate transformation matrices for the three coordinate systems, shown in Figure 5. On the assumption that the coordinates x_1 and $-\xi_1$, x_2 and ξ_3 , and x_3 and ξ_2 differ by small angles and that the second-order terms in these angles are negligible, the coordinate transformations are then given by

$$\begin{pmatrix} x_1 \\ x_2 \\ x_3 \end{pmatrix} = \begin{bmatrix} -1 & 0 & 0 \\ 0 & 0 & 1 \\ 0 & 1 & 0 \end{bmatrix} \begin{pmatrix} \xi_1 \\ \xi_2 \\ \xi_3 \end{pmatrix}, \quad (49)$$

$$\begin{pmatrix} z_1 \\ z_2 \\ z_3 \end{pmatrix} = \begin{bmatrix} \cos \alpha \cos \phi & \sin \alpha & -\cos \alpha \sin \phi \\ -\sin \alpha \cos \phi & \cos \alpha & \sin \alpha \sin \phi \\ \sin \phi & 0 & \cos \phi \end{bmatrix} \begin{pmatrix} x_1 \\ x_2 \\ x_3 \end{pmatrix}, \quad (50)$$

and

$$\begin{bmatrix} z_1 \\ z_2 \\ z_3 \end{bmatrix} = \begin{bmatrix} -\cos\alpha \cos\phi, & -\cos\alpha \sin\phi, & \sin\alpha \\ \sin\alpha \cos\phi, & \sin\alpha \sin\phi, & \cos\alpha \\ -\sin\phi, & \cos\phi, & 0 \end{bmatrix} \begin{bmatrix} \xi_1 \\ \xi_2 \\ \xi_3 \end{bmatrix}. \quad (51)$$

Equations (49) to (51) represent coordinate transformations, but they are also valid for the transformation of small angular rotations about the various axes of the three coordinate systems.

Consider now the rotation about the z_3 axis that has been defined as the elevation motion and is given by equations (20) and (22). The contribution α_r is calculated directly by the Gun-Turret Dynamic Model, and the contribution α_o is related to the helicopter motion. Using the third of the transformation relations given in equation (51) and applying it to the small angular rotation vector $\{\theta\}$ yields the result

$$\alpha_o = -\theta_1 \sin\phi + \theta_2 \cos\phi, \quad (52)$$

since θ_1 , θ_2 , and θ_3 have been defined as the helicopter attachment point rotations about the ξ_1 axes. Therefore, the total angle used in the error analysis, in the elevation direction, is given by

$$\Delta\alpha = -\theta_1 \sin\phi + \theta_2 \cos\phi + \alpha_r. \quad (53)$$

Consider now the rotation about the z_2 axis, which is denoted by $\Delta\eta$ and is divided into two parts

$$\Delta\eta \triangleq \eta_o + \eta_r, \quad (54)$$

where η_o is the contribution from the helicopter structural vibration and η_r is the contribution from the turret motion. The term η_o is obtained by use of the second transformation in equation (51), and is given by

$$\eta_o = (\theta_1 \cos\phi + \theta_2 \sin\phi) \sin\alpha + \theta_3 \cos\alpha. \quad (55)$$

The second term η_r is related to the relative azimuth motion ϕ_r that is defined as the rotation about the x_2 or the ξ_3 axis. Therefore, the contribution of this rotation is again obtained by use of the second of the transformations in equation (51). Consequently, the total angle to be used in the calculation of the error analysis is given by

$$\Delta\eta = (\theta_1 \cos\phi + \theta_2 \sin\phi) \sin\alpha + (\theta_3 + \phi_r) \cos\alpha. \quad (56)$$

Equations (53) and (56) are used by the Gun-Turret Dynamic Model to compute the mean and the standard deviation of the gun barrel rotations about the two mutually perpendicular axes. Equation (53) represents the dynamic error in the elevation direction, and equation (56) represents the dynamic error about an axis orthogonal to both the elevation axis and the barrel axis. For convenience, the dynamic error $\Delta\alpha$ will be designated the turret elevation error, and the dynamic error $\Delta\eta$ will be designated the turret azimuth error.

F. Recoil Forces

During the present investigation, a number of different types of gun recoil forces were utilized. These forces correspond to different caliber weapons and have been generated by different methods including experimental and simulated approaches. The first set of data was measured experimentally (for the 20mm XM197 weapon) on the six-degree-of-freedom simulator, at the GEN Keith L. Ware Simulation Center. These data are summarized in Table 1; and the plots of three of these recoil forces, as a function of time, are given in Figures 8 to 10. The data presented in these figures are the total recoil force transmitted to the rigid turret structure for a twenty-round burst and correspond to different firing rates and to different turret positions. In each case the data points were recorded at one millisecond time intervals. The rates of fire were varied from 500 to 817 shots per minute.

TABLE 1
List of Experimentally Measured
Standard Recoil Data

<u>No.</u>	<u>Test No.</u>	<u>Date</u>	<u>Firing Rate</u> <u>spm</u>	<u>No. Shots</u>
1	2	3/26/74	670	20
2	3	3/26/74	500	20
3	1	3/28/74	669	20
4	2	3/28/74	817	20
5	3	3/28/74	500	20
6	4	3/28/74	660	5

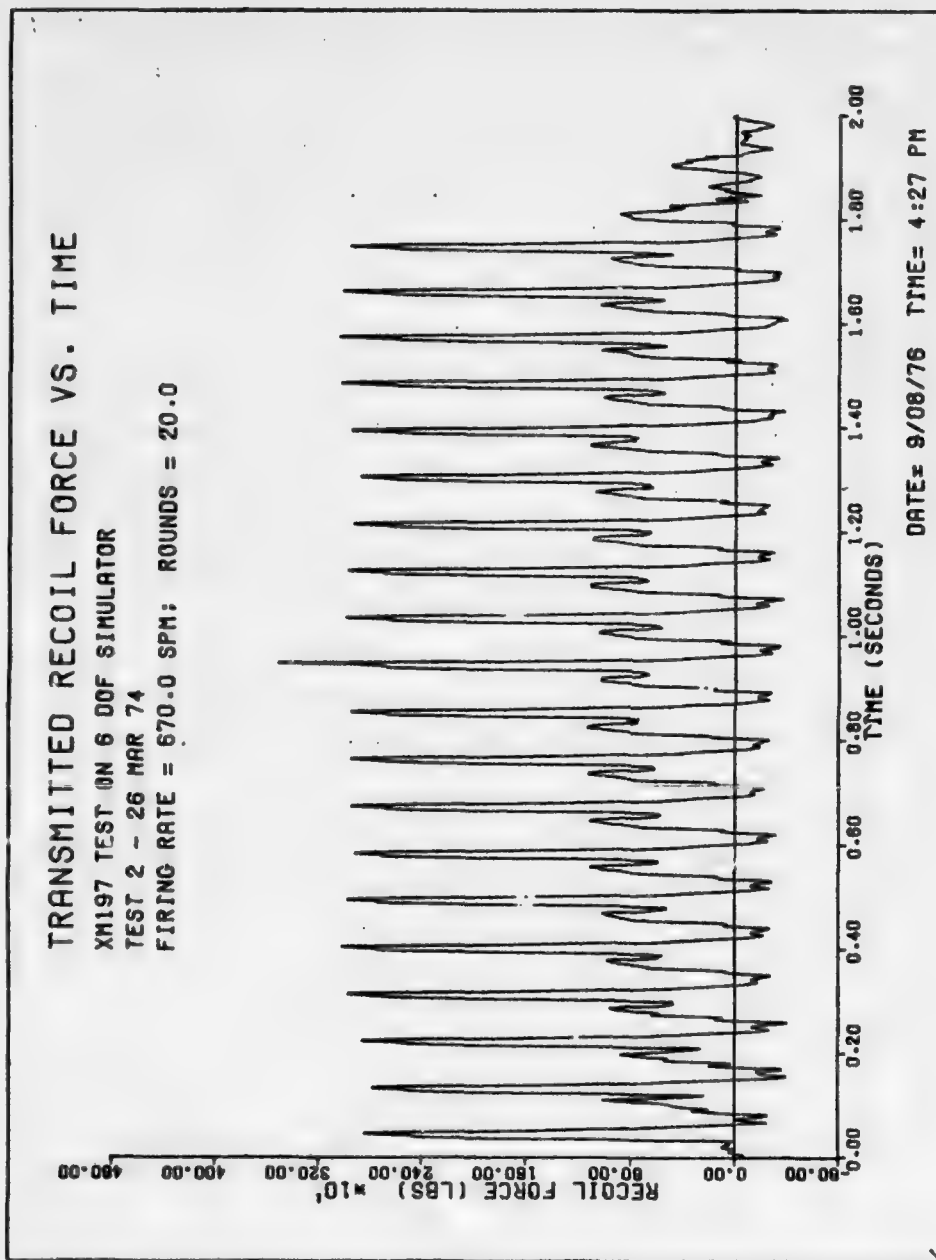


Figure 8. Recoil Force for the 20mm XM197 Gun; Test 2, 26 Mar 74; 20 Rounds; 670 spm

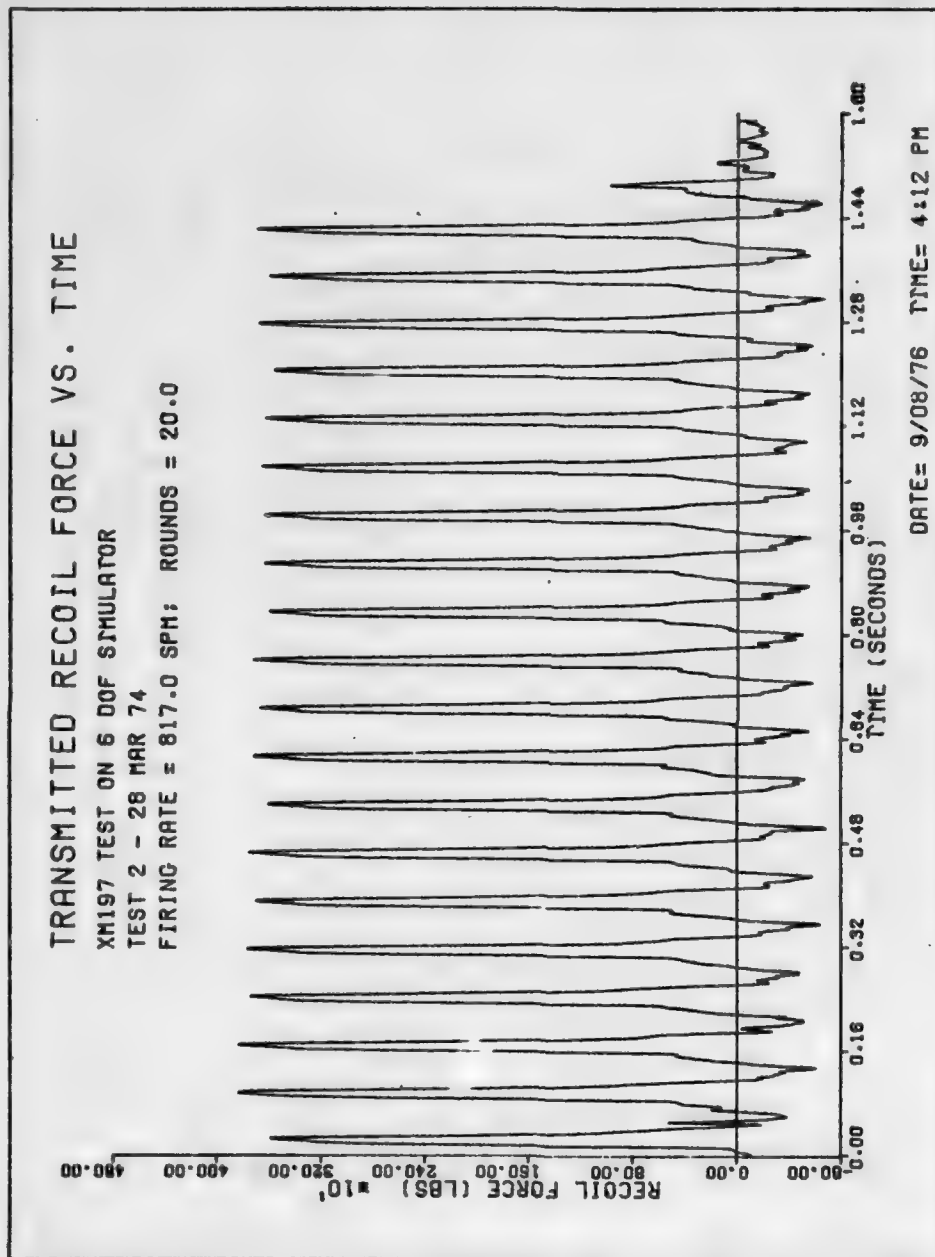


Figure 9. Recoil Force for the 20mm XM197 Gun; Test 2, 28 Mar 74; 20 Rounds; 817 spm

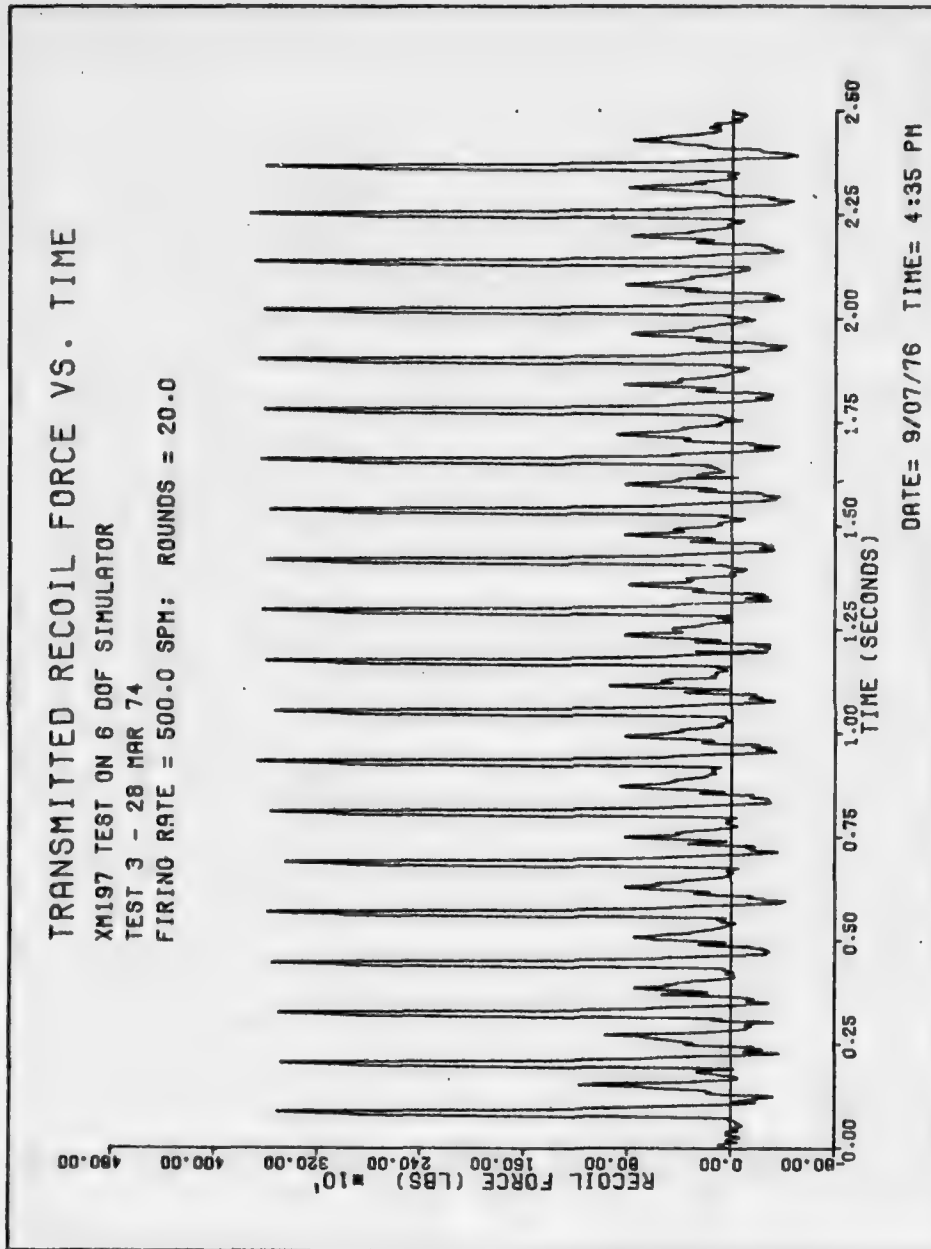


Figure 10. Recoil Force for the 20mm XM197 Gun; Test 3, 28 Mar 74; 20 Rounds, 500 spm

The second set of data used in the present study corresponds to constant recoil data that were provided by Honeywell Incorporated. These data contain eight different records and are summarized in Table 2. The data again represent the total recoil force transmitted to the turret for the 20mm gun mounted on a constant recoil mechanism. The plots of these data as a function of time are shown for three representative cases in Figures 11 to 13. The first six records of these data in Table 2 correspond to computer simulated results, and the last two of these simulated records contain misfires in the rounds 2 and 4 out of 25. The rates of fire for these six records were varied from 675 to 820 shots per minute. The data records 7 and 8 correspond to experimentally measured constant recoil forces at the rate of approximately 750 shots per minute; about 10 rounds were fired. The simulated and the measured constant recoil data are noticeably different; nevertheless, the peak-to-peak variation in the recorded constant recoil data is well below that of the test data recorded from standard spring adapter mounts.

TABLE 2
List of Honeywell XM197 20mm
Constant Recoil Data

<u>No.</u>	<u>Code Name</u>	<u>Round Impulse lb-sec</u>	<u>Firing Rate spm</u>	<u>No. Shots</u>	<u>Type of Data</u>
1	RAANM	34.56	750	25	Simulated
2	RALNM	34.56	675	25	Simulated
3	RLLNM	31.10	675	25	Simulated
4	RHHNM	38.02	820	25	Simulated
5	RAAM2	34.56	750	25	Simulated with misfire Rds. 2 and 4
6	RHHM2	38.02	820	25	Simulated with misfire Rds. 2 and 4
7	DDGGT	-	750	10	Experimental
8	DDFFTA	-	750	10	Experimental

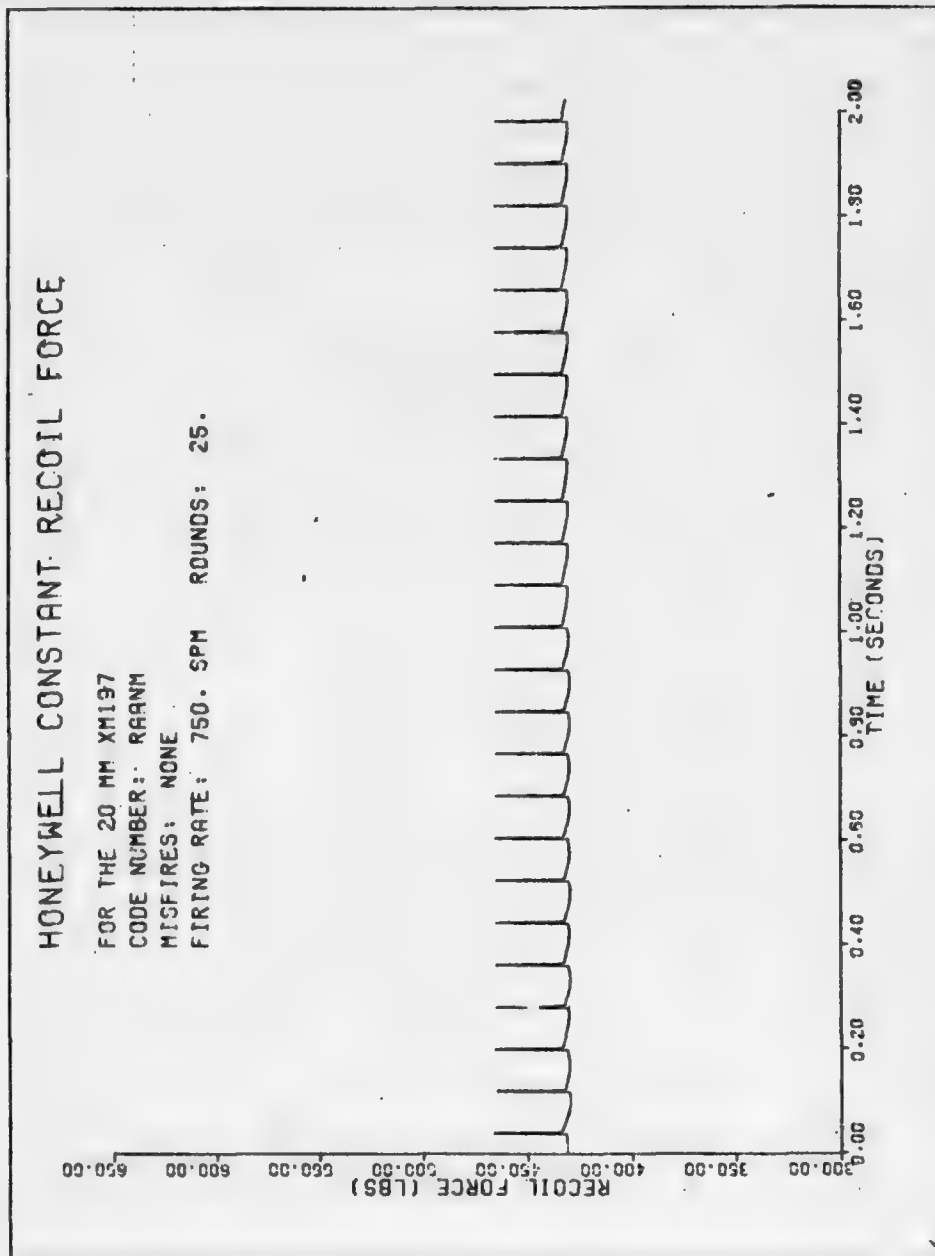


Figure 11. Honeywell Constant Recoil Force for the 20mm XM197 Gun; Code RAANM; 34.56 lb-sec Impulse; 25 Rounds; 750 spm; Mechanism Model Data

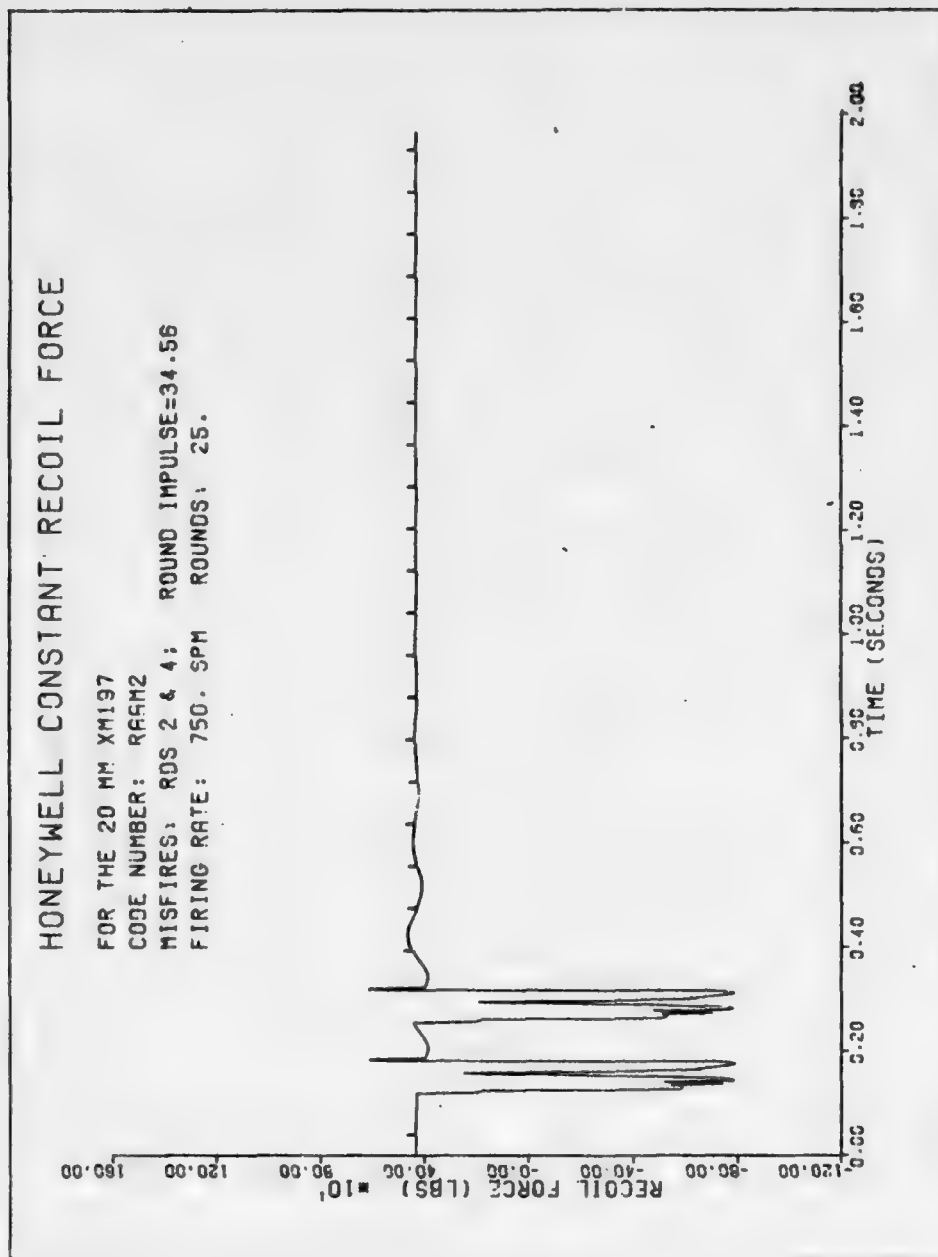


Figure 12. Honeywell Constant Recoil Force for the 20mm XM197 Gun; Code RAAMZ; 34.56 1b-sec Impulse; 25 Rounds; 750 spm; Misfires: RDS 2 and 4; Mechanism Model Data

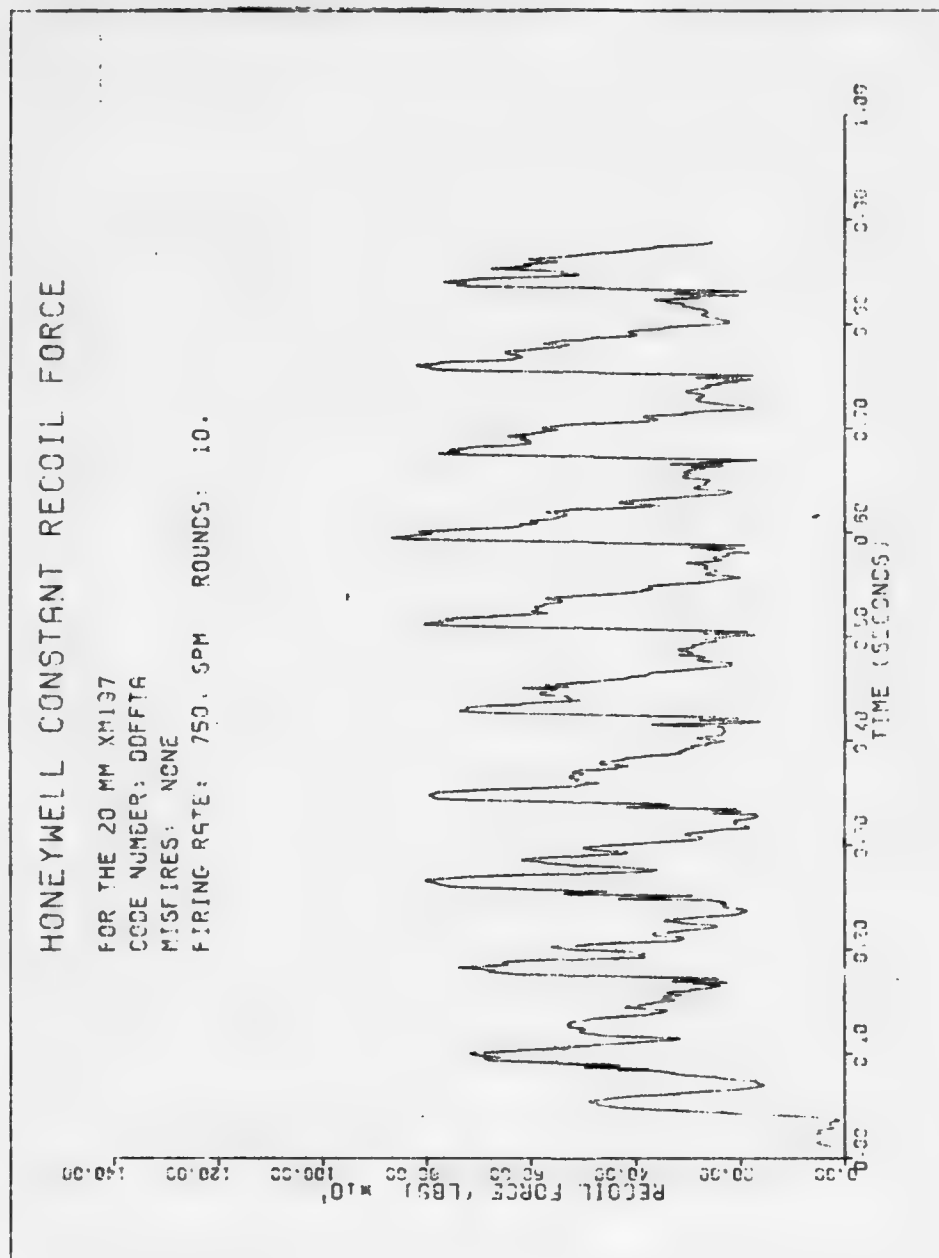


Figure 13. Honeywell Constant Recoil Force for the 20mm XM197 Gun; Code D0FFTA; 10 Rounds; 750 spm; Experimental Test Data

For the Bushmaster 25mm and the AMCAWS 30mm weapons, which were also examined, the detailed time records for the recoil forces were unavailable. The only available data for these weapons were limited to the peak recoil force, the total round impulse, and the rate of fire. With the use of this information, the recoil time records for the larger caliber weapons were generated by the modification of the 20mm recoil data. The modifications involved the adjustment of the rate of fire and the magnitude of the peak recoil forces. The rate of fire was adjusted by the changing of the time scale of the 20mm records, and the magnitude was altered by the multiplication of the force by a conversion factor. The actual numbers used for these changes will be given in the separate sections of this report that deal with the results for these particular weapons. In the case of the 25mm gun, both the regular and the constant recoil forces were used in the analysis. For the 30mm gun, only the constant recoil force was used in the analysis, because, without the use of a constant recoil device, the peak recoil force for this weapon would be too large for the practical operation on the AH-1G helicopter.

III. ANALYSIS OF THE 20mm XM197 WEAPON

A. Weapon Description

The XM197 weapon is a three-barrel 20mm automatic gun. The rate of fire of this weapon can be varied; however, for helicopter applications, the weapon firing rate is normally selected at about 750 shots per minute. The gun is supported by the XM97 turret, which controls the motion of the gun in the azimuth and in the elevation directions. The azimuth orientation can be varied from 0° (front of helicopter) to $\pm 110^\circ$. The elevation motion, measured positive up from the horizontal plane of the helicopter, can be varied between 5° and about -50° . The various servocontrol parameters have been defined in the Section II-D in which the Gun-Turret Dynamic Model is treated. Additional parameters, by which the physical properties of the weapon are defined, consist of the inertial parameters and the positions of the centers of mass of the moving parts of the turret and the gun. These positions are defined in Figure 4 by the parameters A_1 , A_2 , A_3 , B_1 , and B_2 . By an examination of the specifications of the gun and the turret, these parameters were chosen to have the following values:

$A_1 = 2.4"$, $A_2 = 2.4"$, $A_3 = 10"$, $B_1 = 6"$, and $B_2 = 6"$. The two masses that are considered in the analysis are the mass of the moving part of the turret and the mass of the gun. These masses were estimated as 130 and 170 pounds, respectively. The moments of inertia of the rotating components of the assembled gun and turret about the azimuth and the elevation pivots are 20.7 and 13.7 slug-ft², respectively. The axial moments of inertia for the two electric drive motors are identical and are 2.4×10^{-4} slug-ft². The gear ratios for the azimuth and the elevation motions are 620 and 810, respectively; the transmission stiffness in each drive was chosen as 5×10^5 lb-ft/rad. The structural damping factor of the drive system was taken as 0.0001.

The various weapon parameters defined in this section were used in the numerical analysis of the dynamic motion of the gun mounted on the AH-1J or on the AH-1G helicopter frame. The results of these calculations are discussed in the next two sections of this report.

B. Analysis of the AH-1J Helicopter

The first phase of investigation involved the analysis of the pointing

errors of the 20mm XM197 gun attached to the AH-1J helicopter frame. The analysis was performed for five different recoil force histories. Three of these histories correspond to experimentally measured forces and are listed as forces No. 3, 4, and 5 in Table 1. These forces were chosen to cover a broad range of firing rates; these rates correspond to 669, 817, and 500 spm. The remaining two forces are the Honeywell simulated constant recoil forces obtained by a mechanism model of that device. These forces are identified by the codes RAANM and RAAM2; the first code refers to the data with no misfires and the second refers to the data with two misfires. These are two of the forces described in Table 2 and plots of these two forces are provided in Figures 11 and 12. Both of these forces had a firing rate of 750 spm.

For each of the five forces, the dynamic helicopter and turret models were analyzed for 12 different angular orientations of the gun barrel. The orientations include combinations of the four different azimuth angles of 0, 22.5, 45, and 67.5 degrees, and the three different elevation angles of -5, -25, and -45 degrees. In each case, the results of the calculations are presented in terms of the mean and the standard deviation of the angular motion error in both the azimuth and the elevation directions. The results are presented in Tables 3 to 7, in which the values of the statistical error parameters are given in units of milliradians. The most important statistical parameter is the standard deviation because it represents the theoretical gun scatter. The maximum standard deviation error, from the recoil force excitation, occurs when the gun is fired from the side of the helicopter, that is, at the maximum azimuth angle. This result was expected since, for large azimuth orientations, the recoil torque imparts a predominant torsional mode of vibration in the helicopter frame. In the comparison of the responses of the standard recoil forces (Tables 3 to 5) with the corresponding responses of the constant recoil forces (Tables 6 and 7), the conclusion can be made that the constant recoil mechanism is effective in the reduction of the dynamic motion, even when misfires occur.

TABLE 3
AM-1J Analysis Results for Test 1
3/28/74 (669 spm) Standard Recoil

TURNET ORIENTATION		AZIMUTH ERROR (mrad)		ELEVATION ERROR (mrad)	
Elevation (deg)	Azimuth (deg)	Mean	Std. Dev.	Mean	Std. Dev.
-5°	0.0°	0.50	0.61	0.35	1.23
	22.5°	0.34	0.54	0.24	1.43
	45.0°	0.23	0.68	1.63	8.37
	67.5°	0.15	0.86	3.70	17.50
-25°	0.0°	0.47	0.55	0.57	1.17
	22.5°	0.31	0.50	0.48	1.20
	45.0°	0.20	0.60	1.27	6.27
	67.5°	0.14	0.75	3.00	13.68
-45°	0.0°	0.35	0.44	0.78	1.04
	22.5°	0.24	0.40	0.70	0.83
	45.0°	0.15	0.44	0.65	3.34
	67.5°	0.10	0.53	1.70	7.71

TABLE 4
AM-1J Analysis Results for Test 2
3/28/74 (817 spm) Standard Recoil

TURNET ORIENTATION		AZIMUTH ERROR (mrad)		ELEVATION ERROR (mrad)	
Elevation (deg)	Azimuth (deg)	Mean	Std. Dev.	Mean	Std. Dev.
-5°	0°	0.46	0.84	0.31	1.22
	22.5°	0.32	1.16	0.23	1.41
	45°	0.20	1.69	0.09	3.44
	67.5°	0.13	2.10	0.13	5.90
-25°	0°	0.42	0.76	0.52	1.28
	22.5°	0.29	1.01	0.45	1.39
	45°	0.19	1.48	0.27	2.87
	67.5°	0.02	1.84	0.23	4.79
-45°	0°	0.33	0.57	0.71	1.20
	22.5°	0.23	0.71	0.65	1.19
	45°	0.15	1.05	0.49	1.91
	67.5°	0.09	1.32	0.32	2.99

TABLE 5
AH-1J Analysis Results for Test 3
3/28/74 (500rpm) Standard Recoil

TURRET ORIENTATION		AZIMUTH ERROR (mrad)		ELEVATION ERROR (mrad)	
Elevation (deg)	Azimuth (deg)	Mean	Std. Dev.	Mean	Std. Dev.
-5°	0.0°	0.33	0.63	0.22	1.12
	22.5°	0.23	1.57	0.15	1.05
	45.0°	0.22	2.42	0.58	6.12
	67.5°	0.29	2.87	1.70	13.60
-25°	0.0°	0.31	0.56	0.38	1.04
	22.5°	0.21	1.32	0.31	0.93
	45.0°	0.15	2.11	0.44	4.51
	67.5°	0.17	2.55	1.35	10.46
-45°	0.0°	0.24	0.44	0.51	1.10
	22.5°	0.16	0.85	0.46	0.96
	45.0°	0.10	1.40	0.34	2.60
	67.5°	0.06	1.76	0.68	5.62

TABLE 6
AH-1J Analysis Results for Honeywell
Constant Recoil Force (Code RAANYM)

TURRET ORIENTATION		AZIMUTH ERROR (mrad)		ELEVATION ERROR (mrad)	
Elevation (deg)	Azimuth (deg)	Mean	Std. Dev.	Mean	Std. Dev.
-5°	0°	-0.27	0.20	-0.17	0.26
	22.5°	-0.19	0.20	-0.14	0.29
	45.0°	-0.12	0.20	0.0	0.34
	67.5°	-0.08	0.20	0.14	0.43
-25°	0°	-0.24	0.20	-0.30	0.26
	22.5°	-0.17	0.20	-0.27	0.29
	45.0°	-0.11	0.20	-0.13	0.33
	67.5°	-0.06	0.20	-0.01	0.39
-45°	0°	-0.19	0.2	-0.42	0.27
	22.5°	-0.13	0.20	-0.38	0.29
	45.0°	-0.08	0.20	-0.27	0.31
	67.5	-0.05	0.20	-0.14	0.32

TABLE 7
AH-1J Analysis Results for Honeywell
Constant Recoil Force (Code RAAM2)

TURRET ORIENTATION		AZIMUTH ERROR (mrad)		ELEVATION ERROR (mrad)	
Elevation (deg)	Azimuth (deg)	Mean	Std. Dev.	Mean	Std. Dev.
-5°	0°	-0.24	0.23	0.16	0.31
	22.5°	-0.17	0.26	-0.11	0.67
	45.0°	-0.11	0.35	0.0	1.42
	67.5°	-0.07	0.42	0.07	2.70
-25°	0°	-0.22	0.22	-0.26	0.57
	22.5°	-0.15	0.25	-0.22	0.66
	45.0°	-0.10	0.32	-0.11	1.17
	67.5°	-0.06	0.38	-0.02	2.22
-45°	0°	-0.17	0.22	-0.36	0.62
	22.5°	-0.12	0.23	-0.33	0.64
	45.0°	-0.07	0.27	-0.24	0.86
	67.5°	-0.05	0.30	-0.13	1.33

C. Analysis of the AH-1G Helicopter

The AH-1J helicopter model is sufficiently accurate to predict the dynamic response to weapon recoil forces. The model, however, contains some deficiencies that needed to be corrected to improve the accuracy of the results. In particular, the dynamic predictions of the AH-1J model are valid only for frequencies below 20 Hz; however, the weapon recoil force data usually include large amplitude Fourier series components that correspond to frequencies above 20 Hz. To improve the accuracy of the model, a more detailed representation of the AH-1 helicopter structure was therefore required, which would yield accurate solutions in the frequency range from zero to about 40 Hz. Another problem encountered with the AH-1J model is that the elastic axis model of the forward fuselage structure does not represent the torsional stiffness of the actual helicopter structure in sufficient detail. For these reasons, Bell Helicopter Company was contracted to provide a NASTRAN model of the AH-1G helicopter that includes a detailed representation of the fuselage structure. The resulting model contains

over 1700 independent degrees of freedom compared with about 300 for the AH-1J model. The free vibration solution for the AH-1G model is provided in Reference 2. This solution includes the generalized mass and stiffness matrices, the natural frequencies, and the matrix of mode shapes. Again, only the 30 lowest natural frequencies and the corresponding mode shapes were used in the forced-vibration analysis with the Helicopter Vibration Model.

In the subsequent analyses with the Helicopter Vibration Model, the data from the AH-1G NASTRAN model were used in place of the data from the AH-1J model. Before any new problems were solved, however, some comparisons of results obtained with the AH-1J and with the AH-1G models were made for the dynamic response of the 20mm XM197 gun. The calculations were performed for several of the 20mm recoil forces listed in Tables 1 and 2; and the results obtained from the AH-1G model version were compared with the corresponding results obtained previously from the AH-1J model version. The analysis was performed for each combination of the four initial azimuth angles (0° , 22.5° , 45° , and 67.5°) and for the three initial elevation angles (-5° , -25° , and -45°). Again, the dynamic responses of the gun barrel in the azimuth and elevation directions were determined during the burst interval; and, from these results, the statistical means and standard deviations were calculated.

An example of the dynamic response of the 20mm weapon mounted on the AH-1G airframe is provided in Figures 14 and 15 for one set of conditions. The case presented is that of the standard 20mm recoil force with a 670 spm firing rate and an initial gun position of 45° in azimuth and -5° in elevation. The recoil force excitation is plotted in Figure 8, and the azimuth and elevation vibration patterns are plotted in Figures 14 and 15, respectively. Also, the statistical mean and standard deviation parameters determined from the vibration patterns are given in Figures 14 and 15. Note that, in this particular case, the peak amplitudes of the elevation vibration are significantly larger than those of the azimuth vibration.

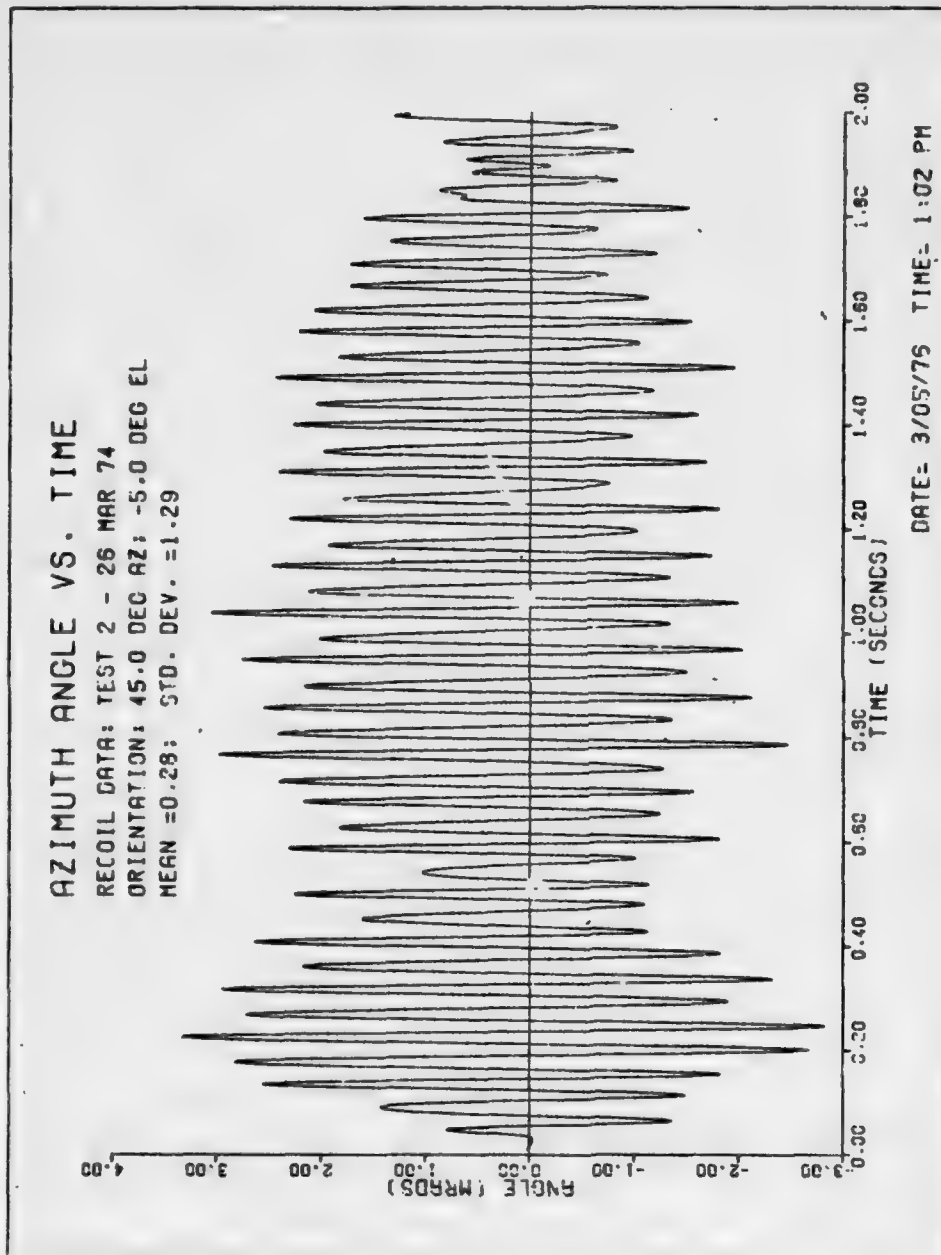


Figure 14. Dynamic Azimuth Response to the 670 spm Standard 20mm XM197 Recoil Force at the 45° Azimuth and -5° Elevation Position

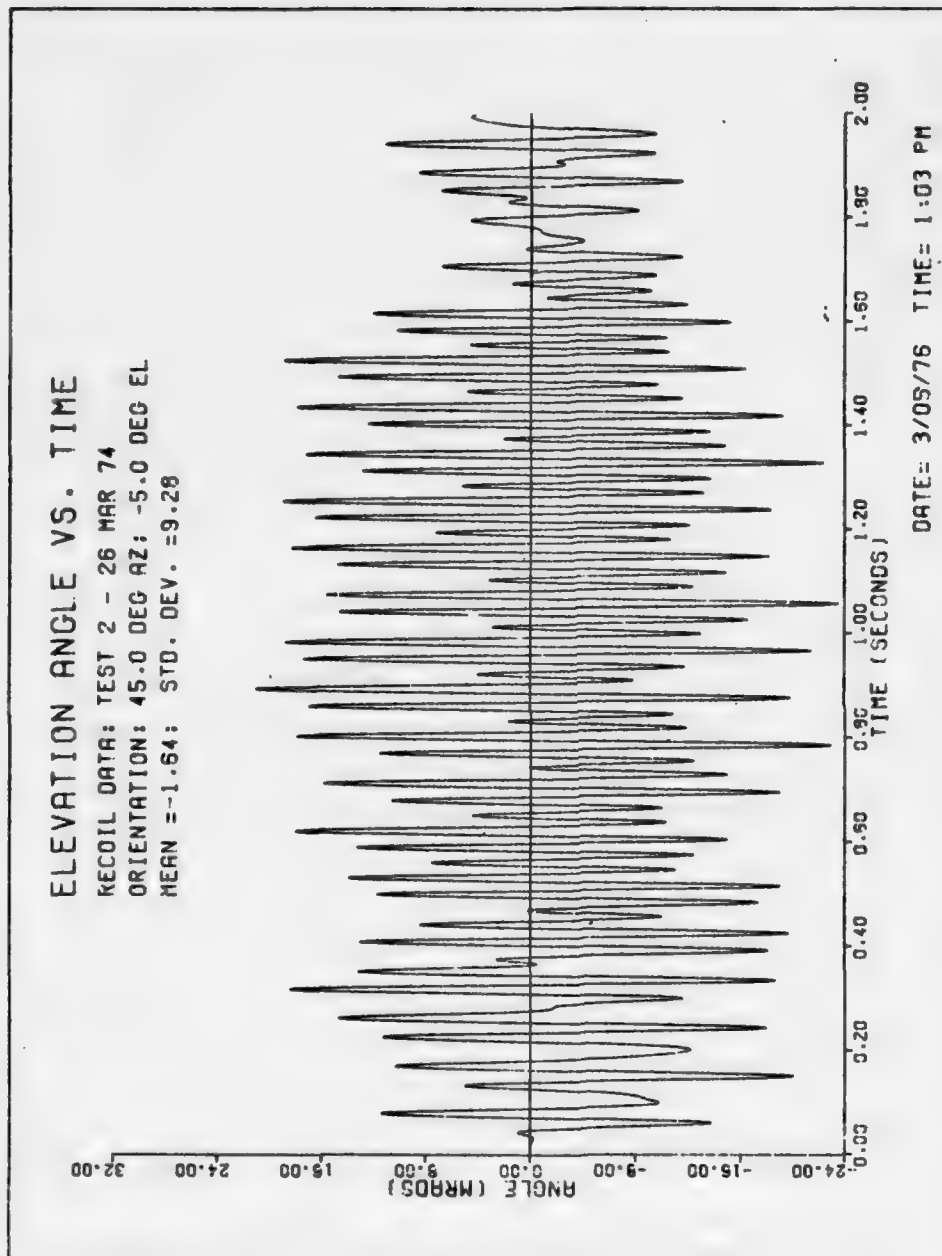


Figure 15. Dynamic Elevation Response to the 670 spm Standard 20mm XM197 Recoil Force at the 45° Azimuth and -5° Elevation Position

The dynamics of the elevation mechanism are affected to a large extent by both the azimuth orientation of the turret and the mass unbalance of the weapon, as defined by the parameter A_3 in Figure 4. At large azimuth orientations, the recoil force induces predominantly large torsional vibrations of the helicopter structure. The torsional vibrations of the turret platform directly affect the dynamic motions of the elevation mechanism; and, furthermore, the platform accelerations induce large inertial torques about the elevation trunnion. Ideally, the turret should be designed in such a manner that the center of mass of the weapon lies along the intersection of the azimuth axis and the elevation trunnion axis. For practical reasons, however, mass unbalances cannot always be eliminated.

A second example of the dynamic azimuth and elevation responses is provided in Figures 16 and 17, respectively. In this example, the applied excitation force is the Honeywell constant recoil force that is specified by the code DDFFTA and is shown in Figure 13. The initial turret orientation was the same as that of the previous example, namely, 45° in azimuth and -5° in elevation. Again, the predominant vibration pattern occurs in the elevation mechanism; however, the magnitudes of the statistical errors are much less than the corresponding results in the previous example. For instance, the standard deviation error in the elevation motion is reduced from a value of 9.28 to a value of 1.73, by the use of the constant recoil mount.

The sensitivity of the gun-pointing error to the initial turret azimuth orientation is illustrated by a set of results presented in Figures 18, 19, and 20 that correspond to three types of weapon recoil forces. In these figures, each of the four statistical errors is plotted versus the turret azimuth orientation and the initial turret elevation angle is set at -25° . The results for the 817 spm standard recoil force are shown in Figure 18; the results for the Honeywell constant recoil mechanism model data (code RAANM) are shown in Figure 19; and the results for the Honeywell constant recoil test data (code DDFFTA) are shown in Figure 20. In each case, the mean and standard deviation errors associated with the elevation vibration are the predominant errors, especially when the initial turret azimuth position is greater than about 30° . At the -25° elevation

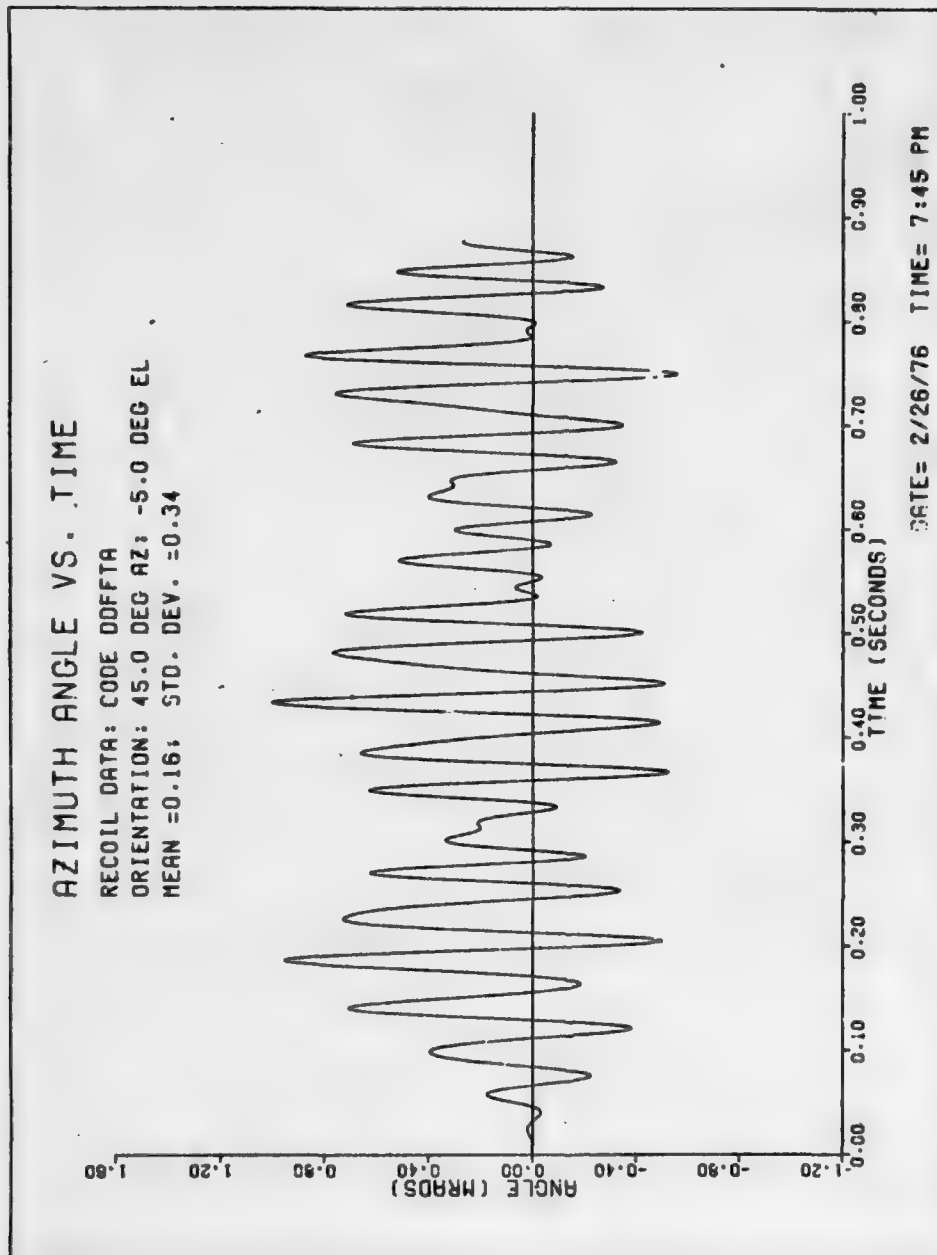


Figure 16. Dynamic Azimuth Response to the Honeywell Constant Recoil Force (Code DDFFTA) at the 45° Azimuth and -5° Elevation Position

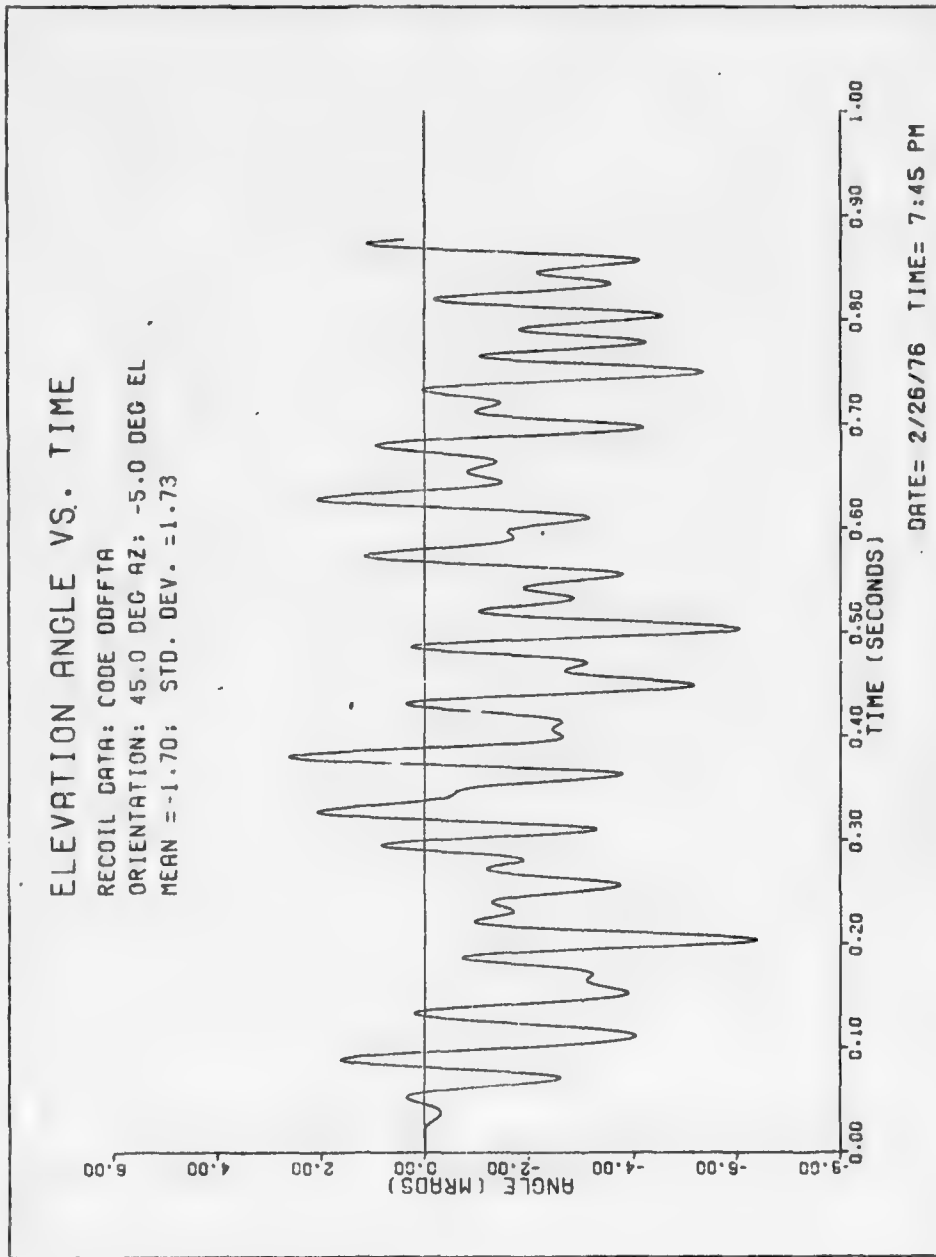


Figure 17. Dynamic Elevation Response to the Honeywell Constant Recoil Force (Code DDFFTA) at the 45° Azimuth and -5° Elevation Position

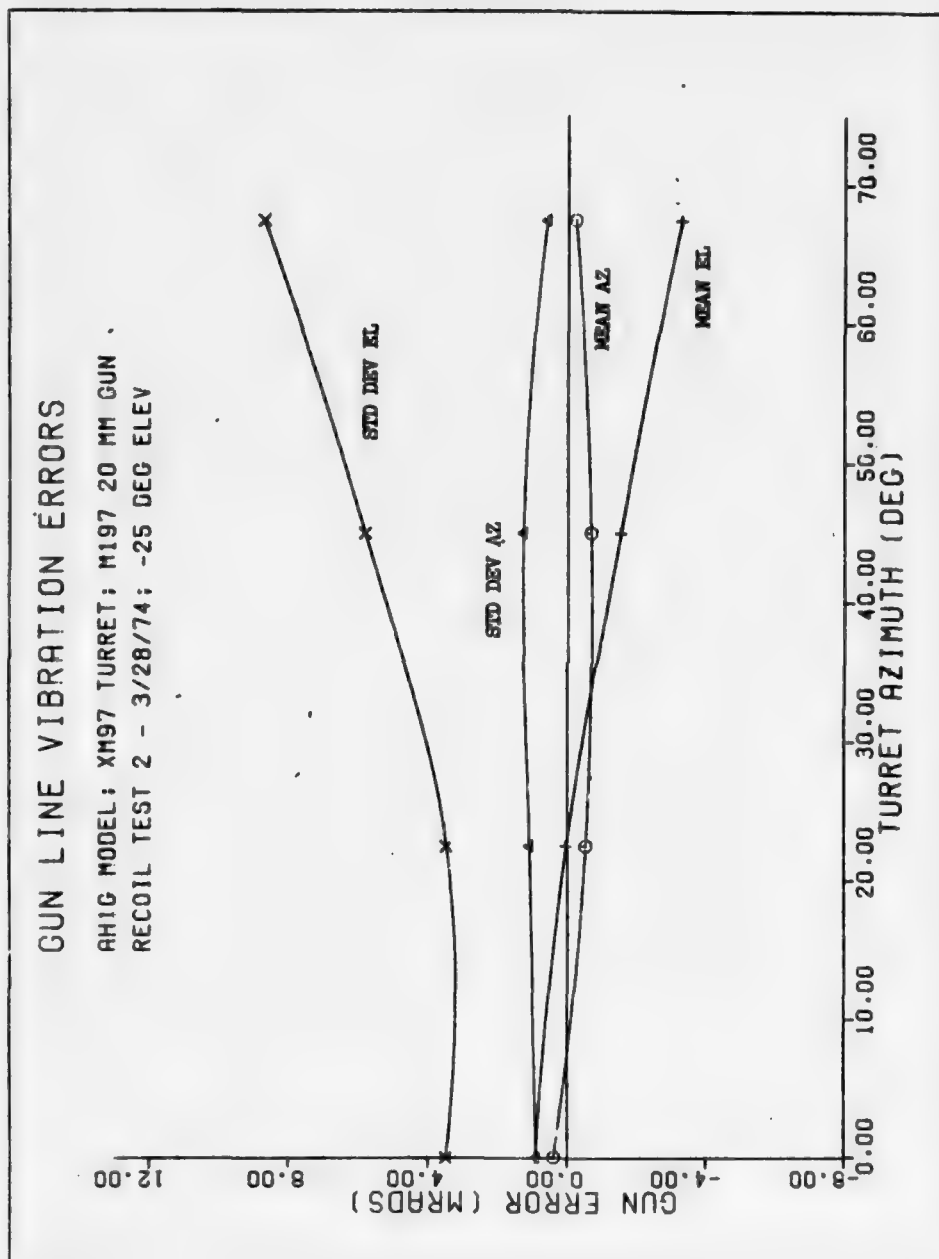


Figure 18. Statistical Gun Vibration Errors vs. Turret Azimuth Angle for the Test 2-3/28/74 Recoil Force, -25° Turret Elevation Angle

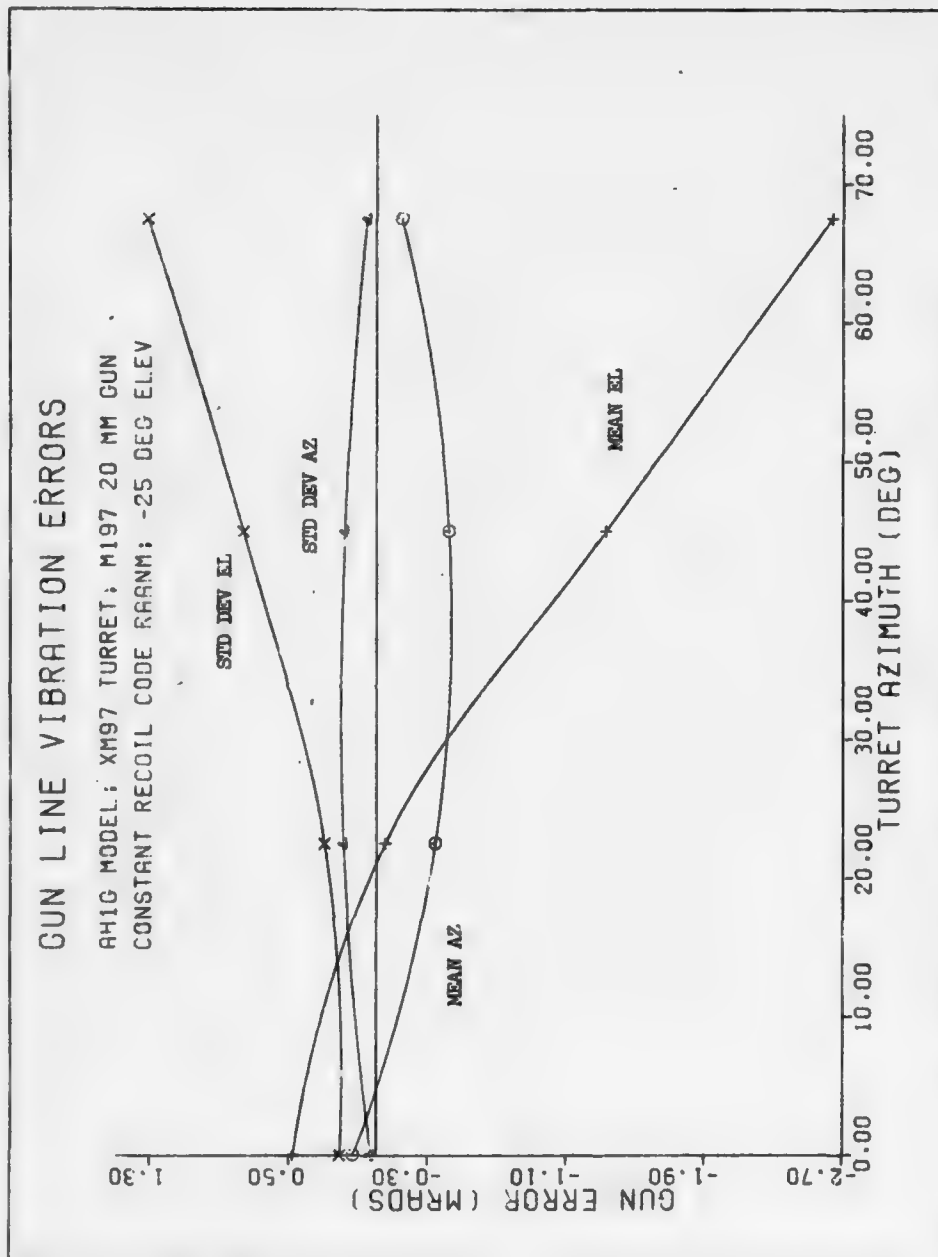


Figure 19. Statistical Gun Vibration Errors vs. Turret Azimuth Angle for the Honeywell Constant Recoil Mechanism Model Data (Code RAANM), -25° Turret Elevation Angle

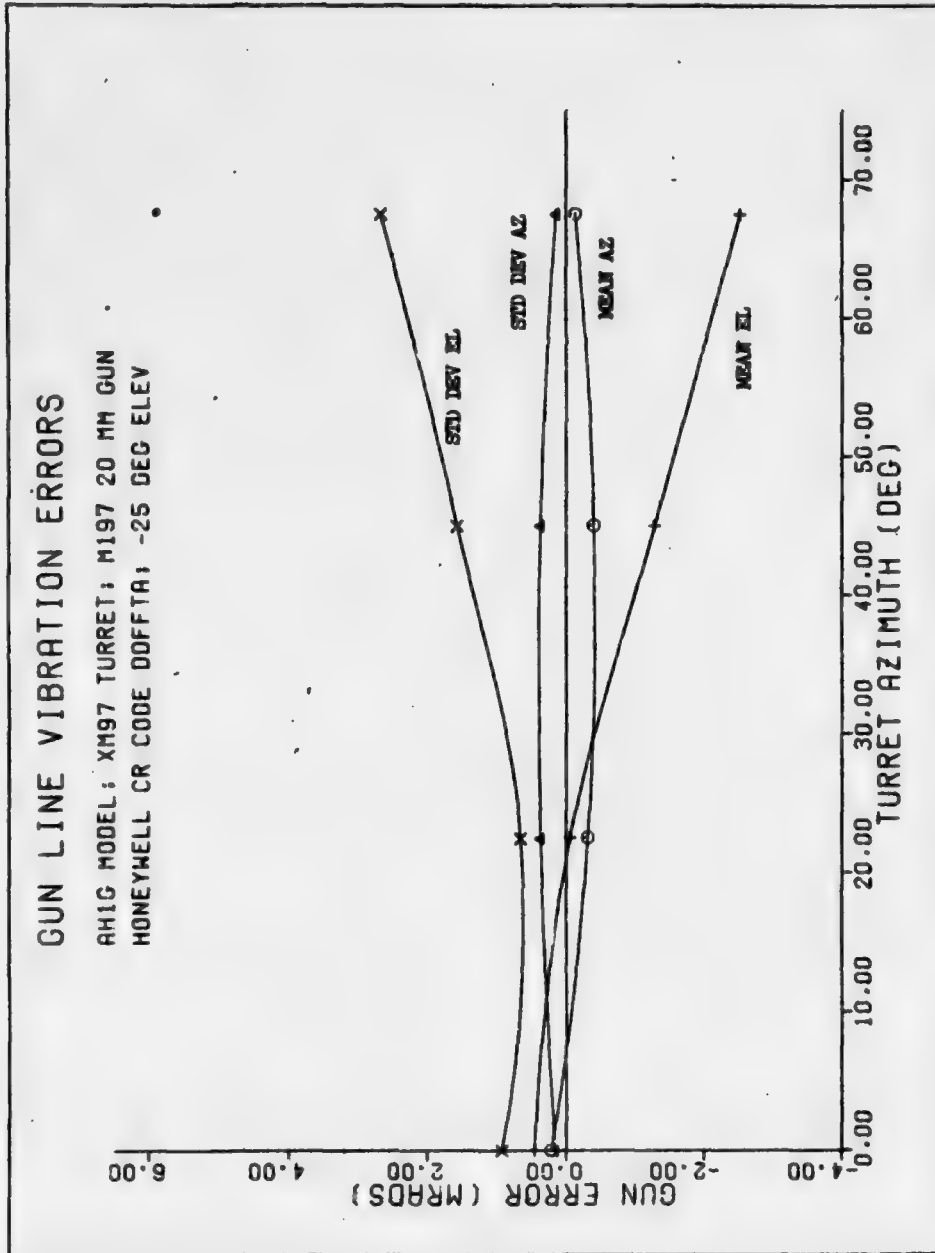


Figure 20. Statistical Gun Vibration Errors vs. Turret Azimuth Angle for the Honeywell Constant Recoil Test Data (Code D0FFTA), -25° Turret Elevation Angle

setting, the elevation error parameters generally become larger as the turret azimuth angle increases. The azimuth errors, however, are relatively insensitive to the turret azimuth position. As expected, the constant recoil device had a noticeable effect in the reduction of the magnitudes of the statistical errors.

The improvement in the gun-pointing accuracy as a result of the constant recoil device is further illustrated in Figure 21. In this figure, the standard deviation error in elevation is plotted versus the initial turret azimuth angle for the standard recoil force (Test 2-3/26/74), for the Honeywell constant recoil test data (code DDFFTA), and for the Honeywell constant recoil mechanism model data (code RAANM). The case represented again corresponds to an initial elevation angle of -25° . The standard deviation error function for the constant recoil test data (code DDFFTA) lies slightly above the error function for the idealized mechanism model data (code RAANM); nevertheless, both graphs for the constant recoil forces lie well below the graph for the standard recoil force. In this particular example, the firing rate for the standard recoil force was 670 shots per minute, and the firing rate for both sets of constant recoil data was 750 shots per minute.

The sensitivity of the gun-pointing error to the weapon firing rate was also investigated for the 20mm XM197 weapon. The weapon recoil data listed in Tables 1 and 2 were recorded at several different firing rates that ranged from about 500 spm to 820 spm. In addition, the constant recoil mechanism model data were recorded with slightly different round impulses. Each of these recoil forces was used in the sensitivity investigations. For each particular turret orientation, the statistical error predictions obtained for each of the different constant recoil forces did not vary appreciably, regardless of the firing rate or the round impulse. Only the occurrence of misfires in the constant recoil force data affected the results by a noticeable degree.

An examination of the results obtained for the standard recoil forces reveals, however, that the weapon firing rate significantly affects the vibration patterns. In Figure 22, the standard deviation error in elevation

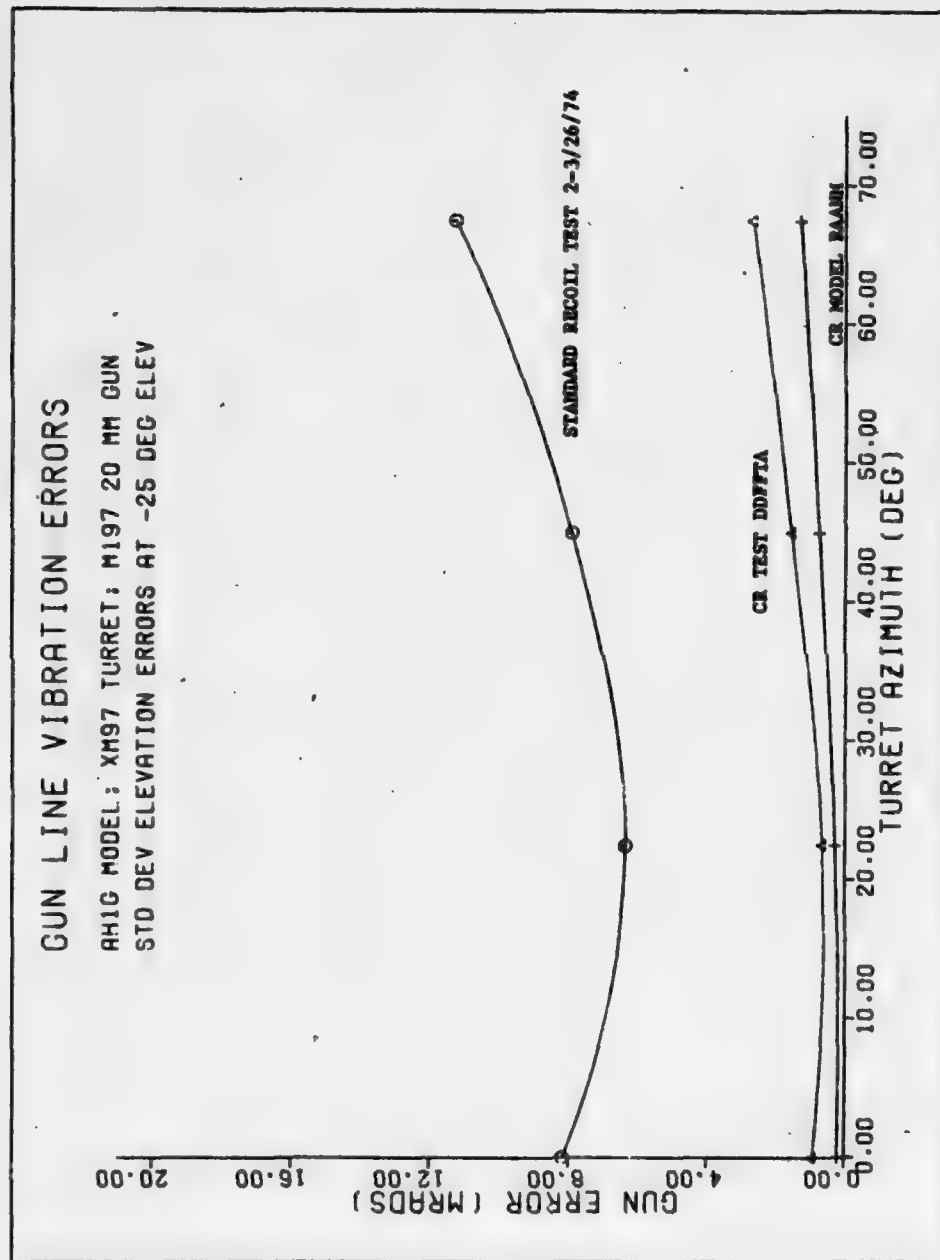


Figure 21. Comparison of the Standard Deviation Elevation Error at -25° Elevation Angle vs. Turret Azimuth Angle, Standard Recoil Test 2-3/26/74 and Constant Recoil Codes RAANM and DDFFTA

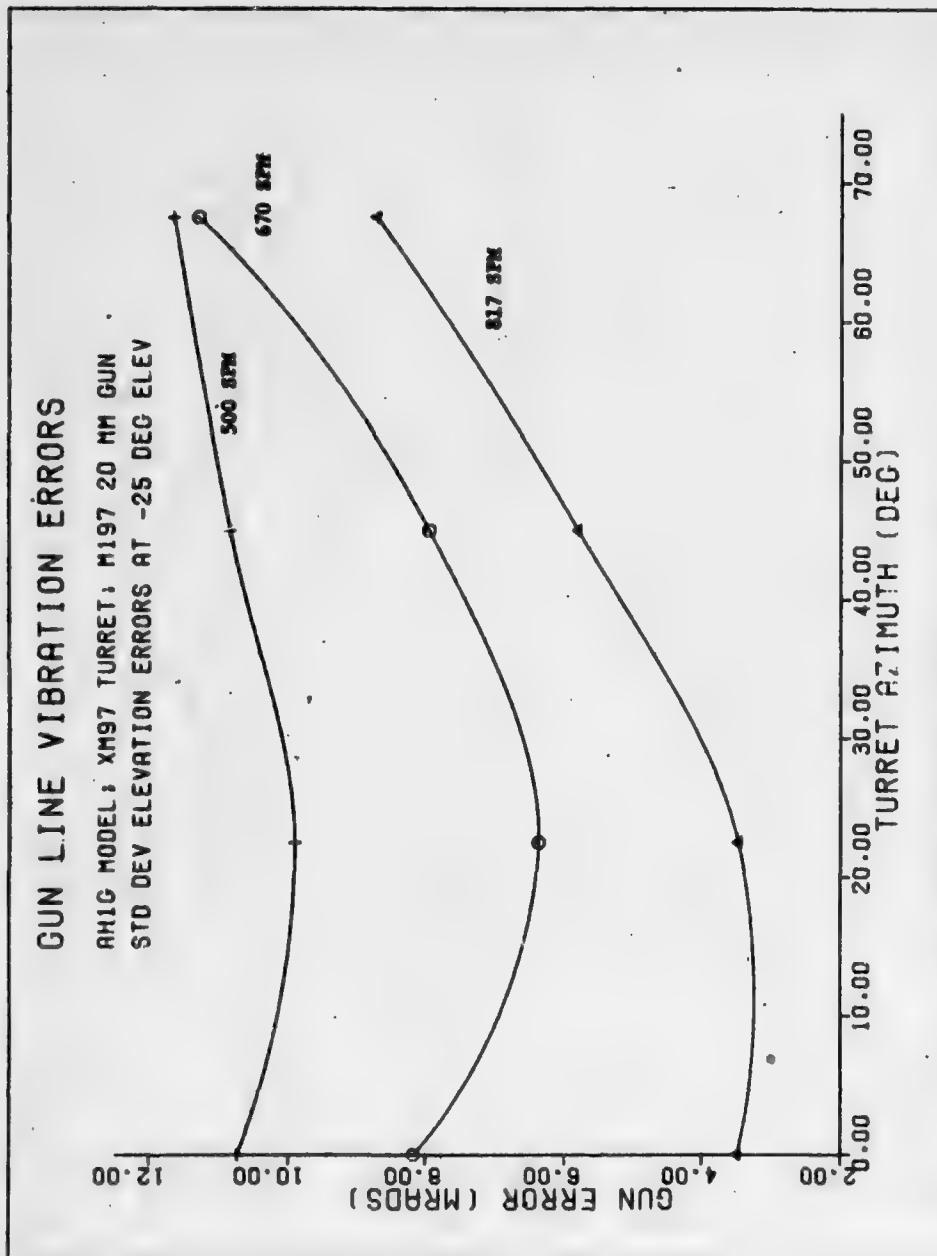


Figure 22. Comparison of the Standard Deviation Elevation Error at -25° Elevation Angle vs. Turret Azimuth Angle for Different Standard Recoil Firing Rates

is plotted versus the turret azimuth angle for three standard recoil force excitations. The weapon firing rates correspond to 500, 670, and 817 shots per minute. The weapon firing rate not only affects the magnitudes of the statistical errors at each particular turret orientation, but also affects the functional dependency of the statistical errors on the turret azimuth position angle. These observations were anticipated because the vibration amplitudes of each natural mode of the helicopter are dependent upon both the frequency spectrum and the direction of the applied force. Based on these results, the conclusion is made that the dynamic response of a given weapon system to the standard weapon recoil loads can be significantly improved by the adjustment of the firing rate. If, however, the weapon system includes a constant recoil mount, then the weapon firing rate will not appreciably affect the dynamic response.

The results of the AH-1G structural sensitivity analysis for the 20mm XM197 gun are summarized in Tables 8 to 12. Tables 8, 9, and 10 contain the statistical error predictions for three of the standard recoil forces that are listed in Table 1. Tables 11 and 12 contain the results for the Honeywell constant recoil forces that are designated by the codes RAA NM and DDFFTA. A comparison of the results summarized in these five tables reveals again that the Honeywell constant recoil mechanism is very effective in the reduction of the angular gun vibrations. The constant recoil mount is particularly effective in the reduction of the standard deviation error in the elevation mechanism. For example, the standard deviation error in elevation is greater than 13 milliradians, for the case in which the initial elevation angle is -5° and a standard recoil force is applied at a 500 spm firing rate. These results are shown in Table 10. The corresponding results for the Honeywell constant recoil force DDFFTA, which are shown in Table 12, range from 0.84 to 2.90 milliradians. In this case, the use of the constant recoil mount resulted in a significant improvement in the gun-pointing accuracy. Moreover, in all of the other cases analyzed, large improvements in the standard deviation errors resulted from the use of the constant recoil mount. The constant recoil mount, however, is not very effective in the reduction of the mean errors in gun pointing. The mean error appears to depend primarily on the mean

TABLE 8
AN-1G Analysis Results For
Test 2 - 3/26/74 (670 spm) Standard Recoil

Angle		Azimuth Statistical Error Parameters		Elevation Statistical Error Parameters	
Azimuth ϕ	Elevation α	Mean	Std. Dev.	Mean	Std. Dev.
-3°	0°	0.42	0.52	2.28	11.72
	22.5°	0.30	1.09	0.83	8.99
	45.0°	0.28	1.29	-1.64	9.28
	67.5°	0.38	0.88	-1.34	12.11
-23°	0°	0.35	0.42	1.89	8.17
	22.5°	-0.52	1.48	0.70	6.38
	45.0°	-0.89	1.97	-1.16	7.95
	67.5°	-0.56	1.34	-2.43	11.29
-43°	0°	0.16	0.30	1.12	3.01
	22.5°	-1.34	1.75	0.45	2.89
	45.0°	-2.05	2.48	-0.64	5.50
	67.5°	-1.63	1.76	-1.39	8.62

TABLE 9
AN-1G Analysis Results For
Test 2 - 3/28/74 (817 spm) Standard Recoil

Angle		Azimuth Statistical Error Parameters		Elevation Statistical Error Parameters	
Azimuth ϕ	Elevation α	Mean	Std. Dev.	Mean	Std. Dev.
-3°	0°	0.46	1.10	0.85	5.29
	22.5°	0.30	0.80	-0.11	5.13
	45.0°	0.29	0.89	-2.07	7.15
	67.5°	0.41	0.89	-4.20	9.95
-23°	0°	0.39	0.89	0.91	3.49
	22.5°	-0.57	1.18	0.04	3.48
	45.0°	-0.96	1.80	-1.52	5.81
	67.5°	-0.60	1.55	-3.28	8.70
-43°	0°	0.19	0.54	1.17	2.40
	22.5°	-1.46	2.91	0.50	2.23
	45.0°	-2.21	2.88	-1.05	3.66
	67.5°	-1.78	2.45	-2.24	6.32

TABLE 10
AR-16 Analysis Results For
Test 3 - 3/28/74 (500 rpm) Standard Recoil

Angle		Azimuth Statistical Error Parameters		Elevation Statistical Error Parameters	
Azimuth ϕ	Elevation α	Mean	Std. Dev.	Mean	Std. Dev.
-3°	0°	0.33	1.21	2.08	15.43
	22.5°	0.22	1.65	1.07	13.70
	45.0°	0.21	1.90	-0.81	13.43
	67.5°	0.32	1.86	-2.82	13.25
-23°	0°	0.21	0.72	1.79	10.75
	22.5°	-0.41	1.11	1.01	9.91
	45.0°	-0.70	1.39	-0.51	10.85
	67.5°	-0.45	1.41	-2.25	11.64
-45°	0°	0.12	0.60	1.08	4.04
	22.5°	-1.05	1.15	0.59	4.35
	45.0°	-1.64	1.89	-0.47	6.08
	67.5°	-1.32	2.02	-1.69	7.77

TABLE 11
AR-16 Analysis Results For
Honeywell Constant Recoil Force (Code RAAND)

Angle		Azimuth Statistical Error Parameters		Elevation Statistical Error Parameters	
Azimuth ϕ	Elevation α	Mean	Std. Dev.	Mean	Std. Dev.
-5°	0°	0.25	0.05	0.25	0.15
	22.5°	0.18	0.03	-0.35	0.29
	45.0°	0.17	0.05	-1.78	0.88
	67.5°	0.25	0.10	-3.23	1.52
-25°	0°	0.13	0.03	0.48	0.21
	22.5°	-0.37	0.21	-0.05	0.30
	45.0°	-0.60	0.26	-1.33	0.77
	67.5°	-0.38	0.14	-2.64	1.31
-45°	0°	-0.002	0.09	0.68	0.26
	22.5°	-0.91	0.39	0.27	0.30
	45.0°	-1.38	0.49	-0.70	0.57
	67.5°	-1.09	0.34	-1.70	0.93

TABLE 12
AH-1G Analysis Results For
Honeywell Constant Recoil Force (Code HDPFTA)

Angle		Azimuth Statistical Error Parameters		Elevation Statistical Error Parameters	
Azimuth °	Elevation °	Mean	Std. Dev.	Mean	Std. Dev.
-3°	0°	0.26	0.19	0.24	1.15
	22.5°	0.18	0.29	-0.33	0.84
	45.0°	0.16	0.23	-1.76	1.73
	67.5°	0.24	0.26	-3.09	2.90
-25°	0°	0.22	0.16	0.46	0.93
	22.5°	-0.34	0.40	-0.05	0.66
	45.0°	-0.57	0.53	-1.28	1.57
	67.5°	-0.35	0.36	-2.53	2.67
-45°	0°	0.09	0.13	0.65	0.57
	22.5°	-0.85	0.59	0.25	0.44
	45.0°	-1.30	0.82	-0.67	1.20
	67.5°	-1.03	0.61	-1.64	2.01

level of the weapon recoil force instead of the peak-to-peak variation in the force.

The results presented in Tables 8 to 12, which were obtained using the AH-1G model version, can be compared directly with the results shown in Tables 3 to 7, which were obtained using the AH-1J model version. In both the AH-1J and the AH-1G analyses, the applied excitation forces consisted of a selection of three standard recoil forces, with firing rates of approximately 500, 670, and 817 shots per minute, and two Honeywell constant recoil forces. An examination of the AH-1J and the AH-1G model results for the same type of recoil force shows that both models give results of the same order of magnitude. The differences in the predictions of the two models are most pronounced in the variations of the standard deviation errors with the turret azimuth position. With the AH-1G model, these errors are relatively large for all turret positions; whereas, with the AH-1J model, these errors generally increase in magnitude from a relatively small

azimuth position angle increases from 0° to 67.5° .

This discrepancy is a consequence of the much more accurate torsional stiffness representation in the AH-1G model. In this model, the torsional and the bending mode shapes for the forward fuselage structure are strongly coupled; however, in the AH-1J model, the bending and the torsional modes are primarily uncoupled. Hence, the AH-1J model exhibits a greater sensitivity to the turret azimuth position than the AH-1G model.

D. The XM97 Turret Servocontrol Modifications

The results presented in the two previous sections of this report showed that, under certain conditions, the dynamic motion of the gun would produce relatively large gun errors, especially the error in the standard deviation of the elevation motion. Closer examination of the computer results revealed that the dynamic motion was predominantly of one frequency, which is closely related to the natural frequency of the turret elevation mechanism. Consequently, any reduction of this motion would involve a reduction of the natural frequency response of the turret. One objective of the overall study was to determine whether such a reduction is possible by the modification of the existing XM97 servocontrols, with the addition of a rate gyro sensor attached at one of several possible locations in the system. Altogether, four different modifications of the controls have been tried; these are labeled as Methods 1 to 4.

Method 1

In Method 1, the rate gyro is placed on the gun and the signal from this gyro is fed back into the servoloop. The corresponding modification of the controlsystem is illustrated in Figure 23 and the unmodified system is shown in Figure 7. The rate gyro modification is represented by a loop containing the total angular displacement of the gun, or its time derivative. This displacement is denoted by $\phi_r + \phi_o$ for the azimuth motion. The expressions for the elevation motion are similar; therefore, the development of duplicate relations will not be necessary. The term ϕ_r is the feedback signal from the azimuth gear position resolver. This term represents the relative displacement between the turret attachment platform and the rotating azimuth mechanism. The term ϕ_o is the absolute displacement of the turret attachment platform, in the azimuth direction. Some additional

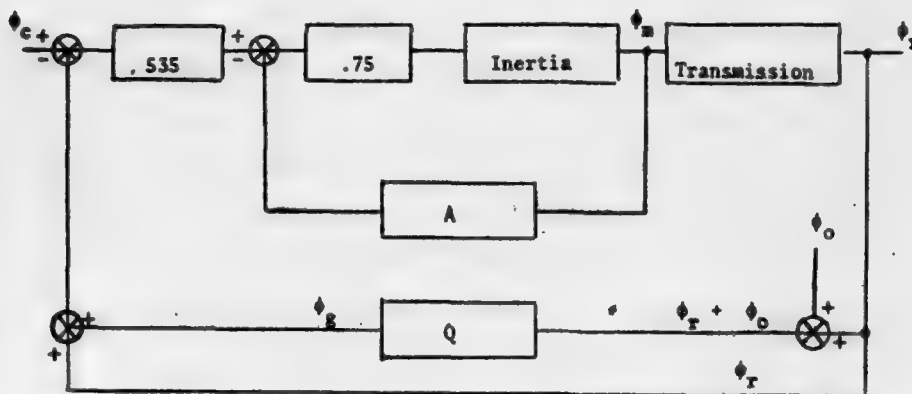


Figure 23. Modified AH-1J Turret Servosystem Diagram

aircraft instrumentation, such as a rate gyro or some other type of inertial sensor, would be required to measure the displacement ϕ_o .

In the feedback loop, the total angular displacement signal is processed through a transfer function, Q . To choose an expression for the transfer function, Q , requires a consideration of the basic purpose of this function. As mentioned in the beginning of this section, the main angular response of the gun and turret occurs at a predominant frequency related to the natural frequency of the elevation drive system. Consequently, in the modification of the control system, a transfer function is desirable that would have certain frequency characteristics. Specifically, the transfer function would amplify the signal in the control loop by the maximum amount, when the predominant frequency of this signal is at or near the natural frequency of the turret. Furthermore, the effect of the transfer function, Q , should decrease at frequencies that are above and below this natural frequency. The Laplace transformation of the expression for the feedback signal is given by

$$\phi_g(s) = Q(s) [\phi_r(s) + \phi_o(s)] \quad (57a)$$

and a transfer function $Q(s)$ that would have these desired characteristics might be represented by

$$Q(s) = \frac{G}{(1 + sT_1)^2} \quad (57b)$$

where s is the transform variable, G is an amplifying constant, and T_1 is a time parameter used to define the maximum amplification frequency. The parameter T_1 is chosen to be very close to the natural period of vibration of the turret drive system. An illustration of the transfer function, Q , is provided in Figure 24, in which the graph of $Q(s)$ is plotted on a semi-log scale for a particular choice of the parameters T_1 and G . The actual values that were chosen for the parameters T_1 and G , in the modified gun-turret analysis, are presented later in this section.

The additional feedback signal in the modified servocontrol loop, namely ϕ_g , is used to modify the drive motor torque. With reference to equation (42), the new expression for the motor torque T_m becomes:

$$T_m = 401.25n (\phi_c - \phi_r - \phi_s - \phi_g) \quad (58)$$

For the incorporation of this modification into the gun-turret, equation (57a) is first transformed in the time domain and the resulting differential equation is given by

$$T_1^2 \frac{d^2 \phi_g}{dt^2} + 2T_1 \frac{d\phi_g}{dt} + \phi_g = \frac{d\phi_o}{dt} + \frac{d\phi_r}{dt} \quad (59)$$

This equation is then written in terms of two first-order equations by the definition of two new variables ϕ_6 and ϕ_7 where

$$\phi_6 = \phi_g \quad (60)$$

and

$$\phi_7 = \frac{d\phi_6}{dt} \quad (61)$$

With the use of these definitions, equation (59) can be written:

$$\frac{d\phi_7}{dt} = \frac{1}{T_1} \left[\frac{d\phi_o}{dt} + \phi_2 - 2T_1 \phi_7 - \phi_6 \right] \quad (62)$$

The two first-order equations (61) and (62) are added to the set of equations (48) to modify the dynamic model. Accordingly, the Gun-Turret Model computer program was modified and then an analysis was performed to check

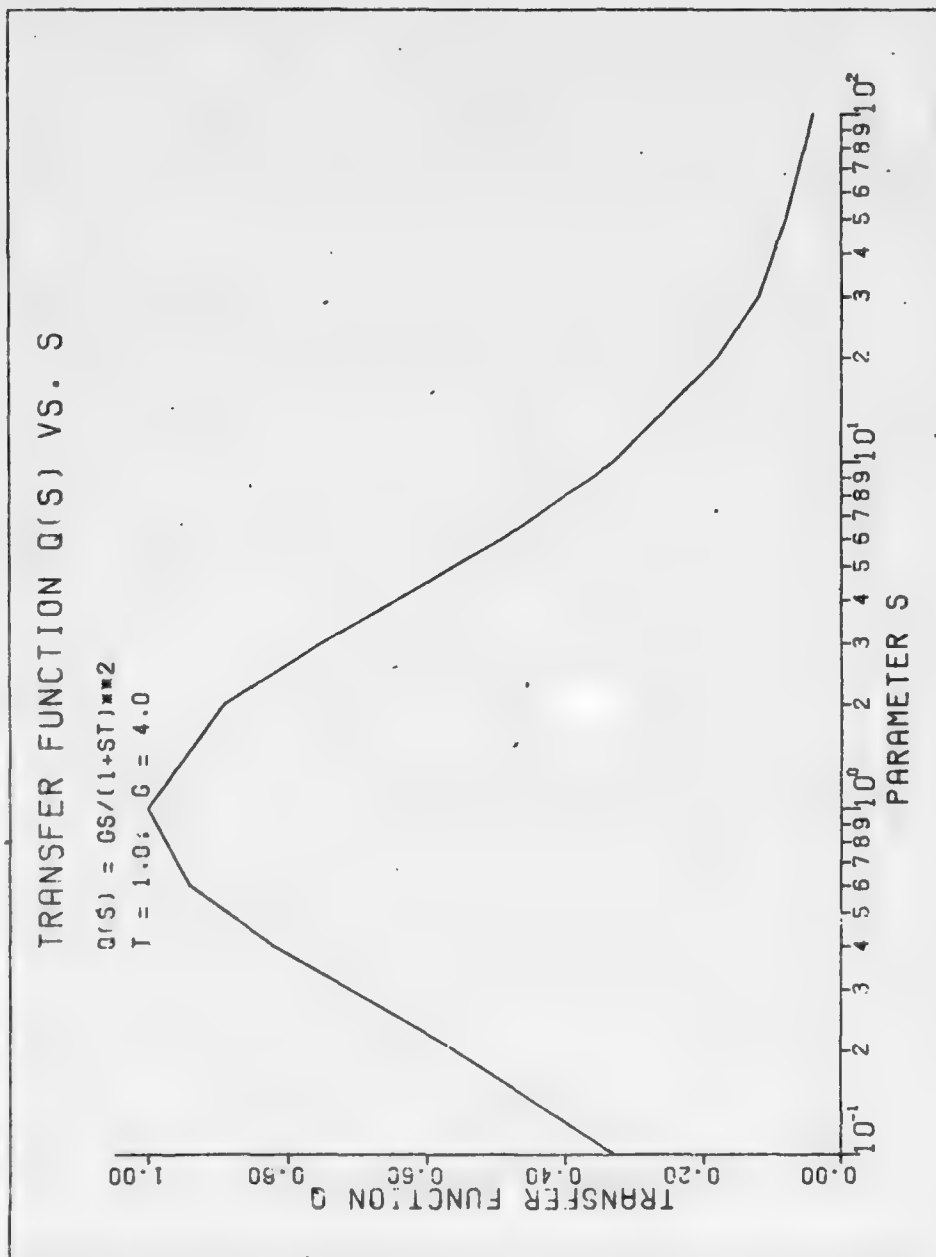


Figure 24. Transfer Function $Q(S)$ For The Modified Turret Servocontrol System

out the effect of this modification. An examination of the response of the modified system revealed that, for this study, the term $\frac{d\phi_o}{dt}$ is small compared with the term $\frac{d\phi_r}{dt}$ in equation (59), and therefore this term was neglected.

A specific angular orientation was chosen to check the servocontrol modification and this orientation corresponds to an azimuth angle of 67.5° and an elevation angle of -5° . Usually, the largest gun-pointing error was obtained at this particular turret orientation. In Section III-B the results of the analysis with the AH-1J Helicopter Vibration Model and the unmodified Turret Dynamic Model are presented. One specific set of results is presented in Table 3 for the standard 20mm recoil force with a firing rate of 669 shots per minute. The predominant turret vibration, in this analysis, is characterized by the standard deviation of the elevation motion, and the value obtained for this parameter at the chosen turret orientation is 17.5 milliradians. The amount of improvement obtained in this standard deviation is, therefore, one way to estimate the effectiveness of the present modification to the control system. Consequently, in this section, a ratio of the new value to the previous value of this standard deviation is presented as a measure of the effectiveness of the servocontrol modification. This ratio is denoted by the term "modified ratio".

In the present modification, the two additional servocontrol parameters that are defined in equation (57b) are G and T_1 . So that a reasonable value for T_1 could be obtained, the natural frequency of the drive system was examined in the azimuth and in the elevation modes. These frequencies were calculated from the servoparameters and have been found to be 1.91×10^2 and 1.55×10^2 radians per second for the elevation and for the azimuth motions, respectively. Consequently, the parameter T_1 for the elevation motion was chosen to be 5.6×10^{-3} , by the requirement that $\omega T_1 = 1$, in which ω is the natural frequency of the drive system. However, since this is only an approximate estimate, several different values of the parameter T_1 were examined. The numerical results are shown in Cases a. and b. of Table 13. The numerical results in Case a. show the modified ratio for $T_1 = 5.6 \times 10^{-3}$ and for different values of the parameter G defined in equation (57b). Note that, in Case a., G is varied over a range of 0.1 to

TABLE 13

Effect on Dynamic Response
Due to Servocontrol Modifications

Case a.		Case b.	
$T_1 = 5.6 \times 10^{-3}$ seconds		$G = .05$	
G	Modified Ratio	T_1	Modified Ratio
.1	1.21	1.0×10^{-3}	1.4
.05	1.18	5.6×10^{-3}	1.08
-.05	2.1	10×10^{-3}	1.01
-.1	6.4	20×10^{-3}	1.00
		50×10^{-3}	0.99

Case c.		Case d.	
$T_1 = 5.6 \times 10^{-3}$ seconds		G	Modified Ratio
G	Modified Ratio		
10.	1.18	4×10^{-2}	1.32
-10.	420.	1×10^{-2}	1.15
		-1×10^{-2}	1.10
		-4×10^{-2}	1.70

Case e.	
G	Modified Ratio
2×10^{-4}	1.25
0.5×10^{-4}	1.04
-0.5×10^{-4}	1.14
-2×10^{-4}	1.45

-0.1 and that a minimum value for the modified ratio of 1.18 is obtained for $G = 0.05$. Increasing or decreasing G from this value produced larger motions. Since none of the values of G produced a value below 1.0 for the modified ratio, the modified control system, therefore, did not improve the dynamic motion. The sensitivity of the modified ratio to the variable T_1 was then examined and the results of this investigation are presented in Case b. of Table 13 for $G = 0.05$ and for different values of T_1 . Note that in Case b. the modified ratio reaches approximately a constant value of one for large values of T_1 . Similar results were also obtained for $G = 0.1$. On the basis of these results, the conclusion is made that the present modification would not, in most instances, improve the dynamic response of the control system.

Method 2

The second type of modification of the control system, which was examined, consisted of a similar approach to Method 1, but with a slight difference in the transfer function Q . The new transfer function is given by

$$Q(s) = G/(1 + sT_1)^2. \quad (63)$$

Note that this function is similar to the one in equation (57b) except that the parameter s is omitted from the numerator. The effect of this change is to produce a response that, for sinusoidal inputs, will differ by a 90-degree phase angle from that of equation (57b).

With the use of equation (63) instead of equation (57b), the governing equation (62) is modified to read

$$\frac{d\phi_7}{dt} = \frac{1}{T_1} (\phi_0 + \phi_1 - 2T_1 \phi_7 - \phi_6). \quad (64)$$

Equations (61) and (64) are now the two additional first-order equations that are used to modify the existing Gun-Turret Model.

As in the case of Method 1, the new model was applied to the case in which the azimuth and the elevation angles are given by 67.5° and -5° , respectively. The modified ratio was determined for values of G equal to 10 and -10 and for the parameter T_1 equal to 5.6×10^{-3} seconds. The results of this investigation are shown in Case c. of Table 13. Note from these results that choosing either value for G increases the modified ratio. In fact, the large result that occurs for $G = -10$ indicates an unstable system. Other values of T_1 were also examined, but were found to give similar results; that is, no reduction in the dynamic motion was obtained. On the basis of these results, the conclusion is made that this modification does not improve the response of the control system.

Method 3

In this approach and in Method 4 to be described next, a slightly different technique was used to modify the control system. Specifically, the motor torque is modified by a function proportional to angular velocity of the gun. Consequently, equation (42) is modified to read:

$$T = 401.25 n(\phi_c - \phi_r - \phi_s - G \dot{\phi}_r) . \quad (65)$$

The gun-turret model was modified accordingly and the numerical results for the modified model are shown in Case d. of Table 13 for different values of the parameter G . These results show that a minimum value of the modified ratio is obtained if G is set equal to -1×10^{-2} and, on either side of this value, the modified ratio increases. Again, a modified ratio of less than one was not obtained; consequently this approach also does not bring about a reduction in the gun motion.

Method 4

In Method 4, the motor torque is modified by the gun-barrel acceleration feedback rather than by the velocity feedback. Using a rate gyro with this approach would require a differentiating circuit. With this approach, the motor torque is given by

$$T_m = 401.25n (\phi_c - \phi_r - \phi_s - G\ddot{\phi}_r) . \quad (66)$$

The results of this modification are summarized in Case e. of Table 13. A minimum value for the modified ratio was obtained for $G = 0.5 \times 10^{-4}$, but again none of the values of G were found to give a modified ratio of less than one.

On the basis of the results presented in this section, the conclusion is made that none of the simple modifications of the existing control system provide any effective reduction in the motion of the gun. What the numerical results do indicate is that a difficulty exists in the generating of enough motor torque to correct the elastic motion in the transmission. This difficulty may be caused by an upper bound on the motor torque due to amplifier saturation and, in all the modified model versions described here, this saturation effect was included. All the modifications described up to this point can be considered as external to the control system in the sense that the only change is an addition of an extra feedback signal to the control system. However, more fundamental changes could also be made to the controls and, therefore, the question arises about the effectiveness of such changes in reducing the dynamic motion. One method that has been suggested

to improve the response of the control system is the use of optimal control techniques in the design of the servocontrol system. Additional studies are therefore being planned to investigate the dynamic response of an optimally controlled turret.

IV. ANALYSIS OF THE 25mm WEAPON

A. Weapon Description

In the previous chapter, the analysis of gun pointing errors was presented for the 20mm XM197 weapon. As a continuation of this study, the helicopter model and the gun-turret model were used to evaluate the dynamic responses of the larger caliber weapons, including the 25mm and 30mm automatic cannons. This section of the report deals with the 25mm gun; the 30mm gun analysis is described in the following section.

The weapon used in this study is the 25mm Bushmaster cannon that is an automatic, single-barrel weapon with the rate of fire in the vicinity of 500 spm. This gun has a round impulse of about 57 lb-sec which can be compared with 33.15 lb-sec for the 20mm XM197 weapon.

B. Recoil Force

Two different recoil forces were used in this study. The first of these is a standard recoil force and the second is a constant recoil force. Since no experimentally measured recoil data were available for the 25mm gun, the necessary data were generated by use of the measured recoil force for the XM197 20mm weapon, which is described as recoil force No. 3 in Table 1. The original data were generated for a firing rate of 669 spm, but these data were converted to the 500 spm firing rate, which was assumed to be representative of the 25mm gun. This conversion was made by an increase in the time scale of the weapon recoil data by a factor of 669/500. In addition to the adjustment for the different firing rates, an adjustment was made on the amplitude of the recoil force. If the assumption is made that the recoil traces for the 20mm and 25mm weapons are similar except for the amplitude, then the maximum force of each weapon will be proportional to the impulse. On the basis of a round impulse of 33.15 lb-sec for the XM197 gun and 57 lb-sec for the Bushmaster 25mm gun, the correction for the maximum force was obtained by the application of the factor 57/33.15 to the recoil force. This constant was included in the computer program of the AH-1G Helicopter Vibration Model, as a multiplying factor to the vector B(1) in subroutine REDREC.

The 25mm constant recoil force data were generated from the Honeywell data with the code name DDFFTA, which was again originally obtained for the

20mm weapon. Since these data correspond to a 750 spm firing rate, the time scale was modified by a factor of 750/500. The modification of the peak force was the same as that used for the standard recoil force; that is, the force was increased by a factor of 57/33.15.

C. Turret Controls

Since the characteristics of the turret for the 25mm weapon are not as yet determined, the decision was made to use the XM97 turret with a few design modifications. These modifications were performed, in order to improve the dynamic response of the turret drive systems to the transmitted recoil force of the higher impulse weapon. They include the increasing of the motor torque response from 0.10 to 0.13 lb-ft per volt for both the azimuth and the elevation drives, the increasing of the motor saturation voltage from 26 to 35 volts, and the increasing of the transmission stiffness from 5×10^5 to 10×10^5 lb-ft/rad.

D. Mass and Inertia Properties

The mass of the modified XM97 turret was taken to be 220 pounds and that of the gun to be 250 pounds. The position of the center of gravity of the gun relative to the elevation trunnion axis plays an important role in the dynamic analysis because a large mass unbalance is produced by the location of the gun center of gravity at a large distance from the pivot. Since the final gun-mounting position, relative to trunnion location, is not firm at this stage, four different weapon-mounting positions were examined. These four positions are listed in Table 14, in which the parameters A_1 and A_3 are the distances that were defined previously in Figure 4. The trunnion elevation axis was assumed to intersect the turret azimuth axis and to be perpendicular to the azimuth axis. The center of gravity of the combined gun and turret, denoted by the parameter A_1 , will vary depending on the position of the gun from the elevation trunnion, represented by the parameter A_3 . Table 14 contains a listing of the parameters A_1 and A_3 for each of the selected gun positions. For the 25mm turret configuration, the distances A_2 , B_1 , and B_2 were assumed to be zero.

The maximum value of A_3 was chosen to be 2.67 feet (32 inches) and the minimum value was taken to be zero, in which case the gun center of gravity

TABLE 14
Position of Gun Center of Gravity
for the 25mm Analysis

Gun Center of Gravity Position	Distance A_1 (ft)	Distance A_3 (ft)	Azimuth Moment of Inertia (slug-ft ²)	Elevation Moment of Inertia (slug-ft ²)
1	1.2	2.67	65.0	63.0
2	0.89	2.0	41.0	39.0
3	0.59	1.33	23.7	21.7
4	0.0	0.0	10.0	8.0

would be directly on the turret elevation axis. The distance A_1 was chosen to be about 45 percent of A_3 . This choice is somewhat arbitrary, but should be quite close to the actual value. The largest effect of these distances is on the rotational moments of inertia. These rotational moments of inertia, both for the azimuth and for the elevation motions, are given in Table 14. Both of these inertias are expressed in relation to the turret and gun pivot points and were calculated on the assumption that the turret moment of inertia about its azimuth axis is 2.0 slug-ft² and that the gun-saddle moment of inertia about any axis normal to the barrel is approximately 8.0 slug-ft². Consequently, the total inertia for the azimuth motion was calculated from the relation

$$I_a = 2.0 + 8.0 + 250(A_3)^2/32.2$$

where the last term represents the gun-mass unbalance and is proportional to the square of the distance A_3 . The corresponding expression for the elevation motion was calculated from

$$I_e = 8.0 + 250(A_3)^2/32.2.$$

E. Results

The 25mm analysis was performed with the AH-1G version of the Helicopter Vibration Model and with the modified Gun Turret Model. Calculations were performed for the four different center of gravity positions given in Table 14, and for the two different recoil forces described previously.

The results of these calculations are the statistical means and the standard deviations of the dynamic errors in the azimuth and elevation gun-position angles. For each gun-center-of-gravity position in Table 14, calculations were performed for twelve different angular positions of the weapon. These positions involve three different elevation angles of -5° , -25° , and -45° ; and four azimuth angles of 0° , 22.5° , 45° , and 67.5° . The results of these calculations are given in Tables 15 to 22. Tables 15 to 18 contain the results for the standard recoil force, and Tables 19 to 22 contain the results for the constant recoil force. Each table corresponds to a different position of the gun center of gravity. The statistical errors are in units of milliradians. These results reveal that the maximum values of the standard deviation parameters were obtained for the gun-center-of-gravity position No. 1, which corresponds to the largest mass unbalance.

The maximum standard deviation occurs in the elevation motion and corresponds to the largest azimuth angle. In that respect, the helicopter response to the 25mm standard recoil force is similar to that of the 20mm weapon. Some quantitative comparisons of the results for the 20mm and the

TABLE 15
Statistical Error Parameters for the
Standard 25mm Force and Gun CG Position No. 1

Turret Orientation		Azimuth Error (mrad)		Elevation Error (mrad)	
Elevation Angle α	Azimuth Angle ϕ	Mean	Std. Dev.	Mean	Std. Dev.
-5°	0°	.45	.56	1.26	5.18
	22.5°	.28	1.08	0.25	4.98
	45.0°	.37	1.45	-2.90	7.74
	67.5°	.36	1.10	-4.90	11.29
-25°	0°	.29	.27	.81	1.84
	22.5°	-.65	.94	.04	2.91
	45.0°	-1.38	2.41	-1.76	11.09
	67.5°	-1.00	1.80	-3.62	19.34
-45°	0°	.13	.42	3.16	3.84
	22.5°	-1.99	1.64	2.03	4.11
	45.0°	-2.89	2.50	-.83	8.24
	67.5°	-2.29	2.30	-2.32	14.36

TABLE 16
Statistical Error Parameters for the
Standard 25mm Force and Gun CG Position No. 2

Turret Orientation		Azimuth Error (mrad)		Elevation Error (mrad)	
Elevation Angle α	Azimuth Angle θ	Mean	Std. Dev.	Mean	Std. Dev.
-5°	0°	.39	.58	1.43	6.63
	22.5°	.23	1.04	.43	7.05
	45.0°	.23	1.20	-2.12	8.38
	67.5°	.32	.87	-4.66	10.10
-25°	0°	.30	.31	1.25	3.72
	22.5°	-.66	1.08	.44	4.22
	45.0°	-1.56	2.58	-1.40	9.74
	67.5°	-1.09	2.04	-4.71	13.71
-45°	0°	-.14	.45	3.13	4.49
	22.5°	-2.00	2.00	1.26	3.79
	45.0°	-3.00	2.93	-1.81	5.63
	67.5°	-2.51	2.91	-2.76	9.18

TABLE 17
Statistical Error Parameters for the
Standard 25mm Force and Gun CG Position No. 3

Turret Orientation		Azimuth Error (mrad)		Elevation Error (mrad)	
Elevation Angle α	Azimuth Angle θ	Mean	Std. Dev.	Mean	Std. Dev.
-5°	0°	-.39	.99	1.17	5.50
	22.5°	.27	1.36	-.21	4.67
	45.0°	.24	1.39	-3.09	5.39
	67.5°	.35	1.33	-5.79	7.13
-25°	0°	.29	.45	1.26	4.34
	22.5°	-.65	1.01	.03	3.48
	45.0°	-1.32	2.91	-3.42	8.47
	67.5°	-.51	3.00	-7.33	12.53
-45°	0°	.15	.47	2.38	4.29
	22.5°	-2.02	1.73	.92	3.58
	45.0°	-2.85	2.91	-1.68	6.10
	67.5°	-1.95	3.20	-4.47	9.31

TABLE 18
Statistical Error Parameters for the
Standard Force and Gun CG Position No. 4

Turret Orientation		Azimuth Error (mrad)		Elevation Error (mrad)	
Elevation Angle α	Azimuth Angle ϕ	Mean	Std. Dev.	Mean	Std. Dev.
-5°	0°	.43	.27	.36	1.31
	22.5°	.24	.31	-.68	1.79
	45.0°	.18	.40	3.26	3.41
	67.5°	.32	.50	-5.80	5.17
-25°	0°	.34	.16	.79	.86
	22.5°	-.64	.55	-.14	1.18
	45.0°	-1.82	1.34	-4.23	4.57
	67.5°	-1.20	.98	-8.26	7.33
-45°	0°	.15	.44	1.99	2.03
	22.5°	-2.03	1.39	.69	2.07
	45.0°	-3.06	2.15	-2.26	3.20
	67.5°	-2.45	2.04	-5.38	5.00

TABLE 19
Statistical Error Parameters for the
25mm Constant Recoil Force and Gun CG Position No. 1

Turret Orientation		Azimuth Error (mrad)		Elevation Error (mrad)	
Elevation Angle α	Azimuth Angle ϕ	Mean	Std. Dev.	Mean	Std. Dev.
-5°	0°	.31	.23	.33	1.36
	22.5°	1.92	.88	-.54	1.94
	45.0°	.19	1.28	-2.35	4.39
	67.5°	.27	.90	-3.87	6.74
-25°	0°	.23	.14	.72	.95
	22.5°	-.58	.76	-.10	1.70
	45.0°	-.94	1.17	-1.53	4.28
	67.5°	-.62	.75	2.83	6.68
-45°	0°	.04	.13	1.04	.83
	22.5°	-1.05	.71	.38	1.37
	45.0°	-1.58	1.04	-.58	3.72
	67.5°	-1.27	.79	-1.72	5.67

TABLE 20
Statistical Error Parameters for the
25mm Constant Recoil Force and Gun CG Position No. 2

Turret Orientation		Azimuth Error (mrad)		Elevation Error (mrad)	
Elevation Angle α	Azimuth Angle ϕ	Mean	Std. Dev.	Mean	Std. Dev.
-3°	0°	.31	.40	.36	2.45
	22.5°	.20	.62	-.57	2.21
	45.0°	.15	.79	-2.83	2.94
	67.5°	.28	.62	4.99	4.71
-25°	0°	.23	.23	.72	1.59
	22.5°	-.58	.64	-.12	1.25
	45.0°	-.93	.91	-2.12	2.61
	67.5°	-.62	.66	-4.03	4.41
-45°	0°	.04	.13	1.04	.80
	22.5°	-1.04	.70	.39	.84
	45.0°	-1.57	1.01	-1.11	2.23
	67.5°	-1.27	.82	-2.61	3.57

TABLE 21
Statistical Error Parameters for the
25mm Constant Recoil Force and Gun CG Position No. 3

Turret Orientation		Azimuth Error (mrad)		Elevation Error (mrad)	
Elevation Angle α	Azimuth Angle ϕ	Mean	Std. Dev.	Mean	Std. Dev.
-3°	0°	.32	1.01	.32	2.08
	22.5°	.20	.66	-.60	1.37
	45.0°	.15	.45	-2.87	2.23
	67.5°	.26	.78	-5.10	3.71
-25°	0°	.23	.53	.70	1.64
	22.5°	-.58	.55	-.12	1.01
	45.0°	-.94	.76	-2.15	1.97
	67.5°	-.63	.98	-4.21	3.31
-45°	0°	.03	.12	1.04	.80
	22.5°	-1.06	.67	.39	.72
	45.0°	-1.58	.99	-1.13	1.49
	67.5°	-1.28	1.06	-2.73	2.45

TABLE 22
Statistical Error Parameters for the
25mm Constant Recoil Force and Gun CG Position No. 4

Turret Orientation		Azimuth Error (mrad)		Elevation Error (mrad)	
Elevation Angle α	Azimuth Angle δ	Mean	Std. Dev.	Mean	Std. Dev.
-5°	0°	.32	.13	.13	.52
	22.5°	.17	.12	-.59	.61
	45.0°	.14	.15	-2.86	1.92
	67.5°	.26	.23	5.15	3.36
-25°	0°	.24	.11	.72	.51
	22.5°	-.59	.45	-.12	.54
	45.0°	-.95	.60	-2.15	1.16
	67.5°	-.63	.39	-4.22	2.85
-45°	0°	.04	.12	1.05	.68
	22.5°	-1.05	.65	.40	.63
	45.0°	-1.59	.91	-1.13	1.16
	67.5°	-1.29	.72	-2.74	2.00

25mm weapon systems are now given. The results were obtained for the 20mm XM197 weapon mounted on the unmodified XM97 turret and for the 25mm Bushmaster weapon mounted on the modified XM97 turret. The firing rate was 500 spm for both weapons, but the two weapon systems used in the comparisons differed in several respects besides the weapon caliber. In both analyses, the AH-1G version of the helicopter dynamic model was used.

Consider first the azimuth and the elevation angles of 67.5° and -5°, respectively. For this orientation of the gun, the standard deviation of the elevation vibration was found, in Table 10 for the 20mm weapon, to be 13.25 milliradians and the corresponding value for the 25mm weapon, given in Table 15, is 11.29 milliradians. This value corresponds to the largest mass unbalance, whereas the corresponding value for the smallest unbalance, given in Table 18, is 5.17 milliradians. Consider now the gun orientation of 67.5° and -45°, for the azimuth and for the elevation, respectively. At that orientation, the 20mm analysis gave the result for the elevation standard deviation of 7.77 milliradians; the corresponding

values for the 25mm analysis vary from 14.36 to 5.00 milliradians. The largest standard deviation found in these studies is 19.3 milliradians in the elevation motion and it corresponds to an initial angular orientation of 67.5° in azimuth and -25° in elevation. This value was obtained for the largest mass unbalance from Table 15. From these results, the conclusion is made that, if the mass unbalance of the weapon is large, the 25mm weapon standard recoil force can lead to gun vibration errors of approximately twice those obtained for the 20mm weapon.

The significance of the gun-mass-unbalance parameter, A_3 , is illustrated in Figure 25. This figure contains plots of the standard deviation error for the elevation motion versus the turret azimuth orientation. The plots correspond to three separate values of the gun position parameter A_3 and the initial turret elevation orientation was -25° in each case. As expected, the smallest standard deviation error is generated when the parameter A_3 is zero. For larger values of the parameter A_3 , the standard deviation error in elevation usually increases, although this does not always happen. Usually, however, the dynamic response of the turret would be improved by the reduction of the distance A_3 to as small a value as is possible.

Consider now the comparison of the response to the standard recoil force with the response to the constant recoil force. The effect of the constant recoil mechanism can be seen by a comparison of the results in Tables 15 to 18 with the corresponding results in Tables 19 to 22. For each position of the gun center of gravity, the constant recoil force yields appreciable smaller values of the standard deviations. This is especially apparent for the standard deviation error in the elevation angle. The constant recoil force yields a reduction in this error that ranges from about 30 to 60 percent of the corresponding result for the standard recoil force. A constant recoil mechanism would, therefore, bring about a significant reduction in the dynamic gun-pointing error.

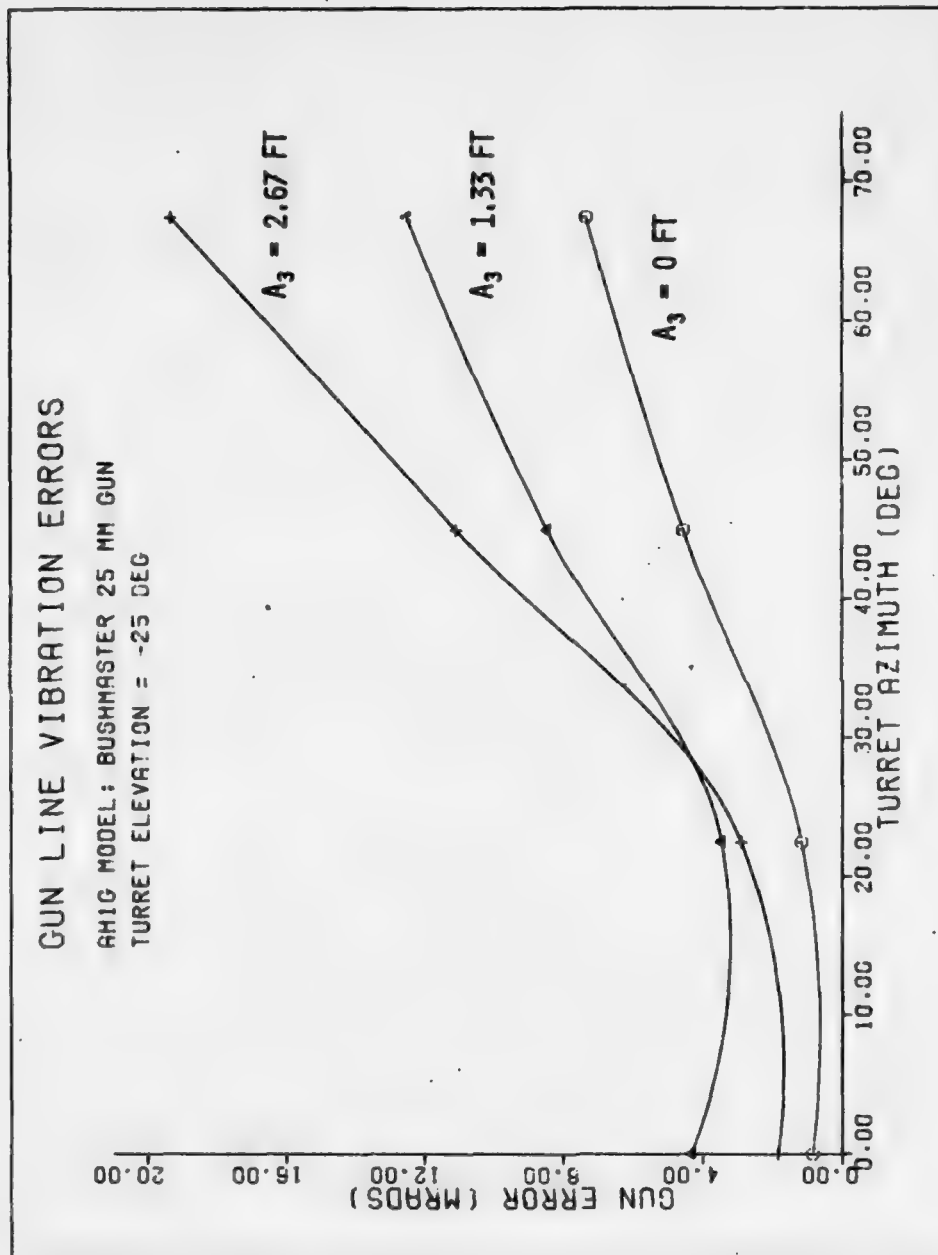


Figure 25. Standard Deviation Elevation Error at -25° Turret Elevation Angle vs. Turret Azimuth Angle for the Bushmaster 25mm Gun at Three Different Gun CG Positions.

V. ANALYSIS OF THE 30mm WEAPON

A. Weapon Description

The dynamic response of the AH-1G helicopter and the gun-turret system was next examined with the application of the weapon recoil forcing function for the AMCAWS 30mm weapon. This weapon is a single-barrel automatic cannon and has an approximate firing rate of 450 spm and a very large round impulse of approximately 150 lb-sec.

In the performance of this analysis, the decision was made to use only the constant recoil force because the magnitude of the peak recoil of this weapon is very large. A peak recoil force of about 15,000 pounds was measured for the AMCAWS 30mm weapon on a hard stand. Consequently, on the basis of the results for the 20mm gun, extremely large motions of the helicopter and the gun-turret configuration would probably result without the use of the constant recoil mechanism. In addition, the AH-1G helicopter is not designed to withstand peak recoil forces of this magnitude. Such large motions could not be tolerated by the system.

Since no turret has yet been designed to house the AMCAWS 30mm gun, the present analysis makes use of a modified XM97 turret. The computer program for the analysis of the original XM97 turret has been modified and used in the present investigation.

B. Recoil Force

Two different types of weapon recoil data were used to provide the dynamic excitation force. The first of these is a simulated constant recoil force with no misfires and the second is a simulated constant recoil force with two misfired rounds.

No experimental data are available at the present time for the recoil history of the AMCAWS 30mm weapon and, consequently, the appropriate data for this analysis were generated from existing constant recoil data supplied by the Honeywell, Inc., for the 20mm weapon. The two data sets that were used are identified by codes RAANM and RHMM2 and are described in Table 2. To use these data for the AMCAWS 30mm gun required the modification of both the round impulse and the firing rate. The projected firing rate of the AMCAWS 30mm gun is 450 shots per minute and, therefore,

the time scale of the RAANM data was increased by a factor of 750/450 and the time scale of the RHHM2 data was increased by 820/450. To account for the higher impulse of the AMCAWS 30mm weapon an increase was made to the constant recoil amplitude of the 20mm recoil force by a factor of 3.

C. Turret Controls

Some design modifications were performed on the XM97 turret servo-control system so that the turret would respond adequately to the higher impulse loading of the AMCAWS 30mm weapon. The first modification involved a change in the servocontrol drive motor torque response, which was increased from 0.1 ft-lb per volt to 0.13 ft-lb per volt. The second modification concerned the motor saturation voltage that was raised from 26 to 35 volts. The third change involved the motor inertia that was increased from 2.4×10^{-4} to 4.0×10^{-4} slug-ft². The final change was an increase in the stiffness of the gear transmission. The original stiffness was 5×10^5 lb-ft/rad and it was increased to 10×10^5 and 15×10^5 lb-ft/rad. Both of these larger values of the transmission stiffness were used in the analysis.

D. Mass and Inertia Properties

Before the dynamic analysis of the turret could be performed, some estimates had to be made as regards the mass and the moments of inertia of the AMCAWS 30mm gun and turret. The total mass of the gun and the turret was estimated at 400 pounds, and the moments of inertia about both the azimuth and the elevation axes were chosen as 50 slug-ft². Furthermore, the gun and the turret centers of gravity were assumed to coincide, and the position of the gun center of gravity was chosen to be at the gun elevation pivot point. The pivot was chosen to be on the turret azimuth axis and 29.5 inches below the turret attachment point.

These modifications to the turret geometric parameters were performed, in spite of practical considerations, to minimize the vibration amplitude of the turret drive mechanisms. Although, in this regard, the modified 30mm turret is an idealized design concept, the results of the AMCAWS 30mm gun-pointing error analysis should provide an indication of the practicality

of mounting a large impulse weapon on a helicopter.

E. Results

Two sets of numerical results were obtained corresponding to the two different values of the transmission stiffness, k . For each case, the results are given by the mean value and by the standard deviation of the dynamic motion in both the azimuth and the elevation directions. These results are obtained for different orientations of the gun. The orientations of the gun correspond to two elevation angles of -5° and -45° , and four azimuth angles of 0° , 22.5° , 45° , and 67.5° . These results are summarized in Tables 23 and 24. The results in Table 23 correspond to the transmission stiffness $k = 10 \times 10^5$ lb-ft/rad; the results in Table 24 are for $k = 15 \times 10^5$ lb-ft/rad. Each table contains results for the constant recoil forces RAANM and RHHM2. As expected, the recoil force with misfires produces the largest standard deviation, which occurs in the elevation mode for large azimuth angles. These results are similar to the results for the 20mm gun, but are larger in magnitude. A comparison of the results in Tables 23 and 24 shows that a large increase in the transmission stiffness appears to cause a slight decrease in the dynamic response. In most cases, the statistical errors for the idealized AMCAWS 30mm constant recoil force (code RAANM modified) are less than 2 milliradians. The corresponding results for the idealized constant recoil force with misfires (code RHHM2 modified) are much larger; however, the statistical errors did not exceed 10 milliradians, for any turret orientation. Before a complete assessment of the dynamic errors can be made for the AMCAWS 30mm weapon, this analysis should be repeated with experimental data measured from an actual constant recoil mechanism. To date, no constant recoil mount design has been developed for the AMCAWS 30mm weapon. Such a device might, however, be expected to yield results which are slightly larger than the results that are presented in this section for the idealized constant recoil force. Nevertheless, from the results of this analysis the feasibility of mounting the AMCAWS 30mm gun on an attack helicopter has been demonstrated.

TABLE 23

Dynamic Response of AH-1G Model
to 30mm Constant Recoil Force
Transmission Stiffness $k = 10 \times 10^5$ lb-ft/rad

Recoil Force: RAANH Modified

Azimuth Angle	Elevation Angle = -5°				Elevation Angle = -45°			
	Azimuth Motion		Elevation Motion		Azimuth Motion		Elevation Motion	
	M	SD	M	SD	M	SD	M	SD
0°	-.18	.05	-.18	.139	-.0187	.008	-.63	.228
22.5°	-.23	.07	.38	.282	-.163	.0509	-.263	.26
45.0°	-.27	.106	1.8	1.07	-.173	.0718	.732	.65
67.5°	-.305	.135	3.2	1.86	-.177	.086	1.72	1.16

Recoil Force: RHHM2 Modified

Azimuth Angle	Elevation Angle = -5°				Elevation Angle = -45°			
	Azimuth Motion		Elevation Motion		Azimuth Motion		Elevation Motion	
	M	SD	M	SD	M	SD	M	SD
0°	-.15	.090	-.168	.891	-.124	.0819	-.559	1.07
22.5°	-.218	.362	.332	1.93	-.139	.242	-.191	1.58
45.0°	-.247	.638	1.49	5.88	-.154	.397	.594	3.86
67.5°	-.273	.822	2.75	9.59	-.167	.501	1.41	6.11

TABLE 24

Dynamic Response of AH-1G Model
to 30mm Constant Recoil Force
Transmission Stiffness $k = 15 \times 10^5$ lb-ft/rad

Recoil Force: RAANH Modified

Azimuth Angle	Elevation Angle = -5°				Elevation Angle = -45°			
	Azimuth Motion		Elevation Motion		Azimuth Motion		Elevation Motion	
	M	SD	M	SD	M	SD	M	SD
0°	-.185	.06	-.196	.133	-.159	.025	-.627	.227
22.5°	-.234	.0779	.396	.255	-.165	.048	-.228	.258
45.0°	-.265	.111	1.80	.809	-.175	.0733	.736	.507
67.5°	-.288	.136	3.23	1.41	-.18	.0859	1.72	.844

Recoil Force: RHHM2 Modified

Azimuth Angle	Elevation Angle = -5°				Elevation Angle = -45°			
	Azimuth Motion		Elevation Motion		Azimuth Motion		Elevation Motion	
	M	SD	M	SD	M	SD	M	SD
0°	-.148	.090	-.155	.704	-.148	.061	-.543	1.07
22.5°	-.201	.358	.346	1.60	-.141	.241	-.184	1.43
45.0°	-.246	.635	1.59	5.04	-.142	.396	.653	3.24
67.5°	-.27	.819	2.73	8.44	-.151	.499	1.51	5.24

VI. EXTRAPOLATION MODEL

During the present investigation, large amounts of data were obtained for the statistical gun-pointing errors from various helicopter, gun, and turret configurations. For each type of helicopter model, recoil force, and weapon configuration, the statistical errors were evaluated for specific azimuth and elevation angles of the gun. However, in an analysis with the complete Helicopter Weapon System Model, shown schematically in Figure 3, gun orientations different from those that have been examined may frequently arise. In this situation, the helicopter vibration analysis and the turret dynamic analysis could be repeated for the desired orientation. However, this approach is not practical since these two models are relatively complex and require an appreciable amount of computer storage and execution time. To remedy this difficulty, an extrapolation model was developed.

With this approach, the statistical mean and standard deviation quantities for any desired angular gun orientation are extrapolated from a table of results, obtained for a specific set of initial turret orientations. The model incorporates a linear extrapolation procedure to calculate the desired statistical quantities. One requirement of this approach is that the desired orientation of the gun should be within, or close to, the range of the angular orientations that have previously been analyzed. The computer program is relatively simple and requires little storage or execution time. The input for the extrapolation model computer program consists of matrices containing the statistical results for a particular type of recoil force. Each element of this matrix corresponds to one combination of the azimuth and elevation angles. The computer program allows for the storage of more than one set of data, and each set of data corresponds to a particular recoil force.

VII. SUMMARY AND CONCLUSIONS

The gun-pointing errors induced by weapon recoil forces, in a helicopter weapon system, were analyzed for several weapons of different caliber. In these investigations, the weapons were mounted on a biaxial turret and the gun-pointing accuracies were determined for various turret configurations. Three distinct models were used to carry out the analysis. The first model - a NASTRAN finite-element model of the helicopter structural airframe - was used to solve the free-vibration problem, and the primary outputs of this model are the natural frequencies and mode shapes of the helicopter airframe. These data are required by the Helicopter Vibration Model to solve the forced-vibration problem for weapons recoil force excitations. In particular, the Helicopter Vibration Model is used to predict the displacement, velocity, and acceleration components of the turret attachment platform. These data are then fed into the Gun-Turret Dynamic model, and this model is used to determine the dynamics of the turret drive systems in the azimuth and in the elevation directions. As a final step in the analysis, the statistical mean and the standard deviation parameters are estimated from the vibrations of the azimuth and the elevation drive mechanisms. These statistical parameters provide a convenient measure of the angular errors in gun-pointing.

A structural sensitivity analysis is carried out, with the use of these models, by the evaluation of the statistical gun-pointing error components for several discrete initial orientations of the turret. Normally the analysis is carried out for a selection of twelve discrete turret orientations, which correspond to a wide range of azimuth and elevation angles. The results of this analysis reveal the sensitivity of each gun-pointing error component to the initial turret orientation. This procedure has been applied to the investigation of the 20mm XM197, the 25mm Bushmaster, and the 30mm AMCAWS weapon systems. In each investigation, the effects of different turret and mount configurations on the gun-pointing error components were determined.

For the 20mm XM197 weapon, the weapon recoil data were obtained from

both experimental tests and computer simulations. These data consisted of standard recoil data, measured from recoil adapter mounts, and constant recoil data, obtained from a Honeywell constant recoil mount mechanism. Data were recorded on each type of mount for several weapon firing rates.

The basic weapon system configuration, which was used for the analysis of the 20mm automatic cannon, consisted of the XM197 gun, the XM97 turret, and the Bell AH-1 helicopter airframe. Two different NASTRAN models were used to represent the free-vibration characteristics of the model AH-1J and the model AH-1G airframes. The models differed primarily in the detail of the structural representation. For example, the AH-1G model was refined and contained about 1800 independent degrees of freedom, whereas the AH-1J model was much simpler and contained only about 300 degrees of freedom.

The results of the structural sensitivity analysis of the 20mm XM197 weapon are presented in Chapter III. Analytical predictions of the gun-pointing error components were obtained for both the AH-1J and the AH-1G versions of the structural model. In general, the error predictions for the two models were of the same order of magnitude. However, the results of the AH-1J model revealed a greater sensitivity to the turret azimuth angle than the corresponding results of the AH-1G model. The discrepancies in the model predictions are caused by the differences in the AH-1J and the AH-1G model representations. Since the AH-1G model contains a more refined representation of the helicopter structure, the analytical results for the AH-1G model are probably more accurate than the corresponding results of the AH-1J model.

In almost all cases analyzed, the largest statistical error component was the standard deviation of the elevation motion. In general, the value obtained for this error was dependent upon the type of weapon mount, the weapon firing rate, and the turret orientation. For the analysis of the AH-1G helicopter weapon system with an applied 20mm standard recoil force, this error varied between about 1.2 milliradians and 15.5 milliradians. In this analysis, the results showed that the gun-pointing error is very sensitive to the weapon firing rate and to the turret orientation. The largest errors usually occurred at the largest azimuth orientation of the turret. At this orientation, large torques are applied to the helicopter

structure, about the longitudinal axis.

The magnitudes of the error components obtained for the 20mm constant recoil forces were significantly lower than the magnitudes obtained for the corresponding analysis of the standard recoil forces. In particular, the statistical error components were almost always less than 3 milliradians; and, in almost all instances, the errors were less than 2 milliradians. These results, therefore, show that the constant recoil mount is very effective in the reduction of the gun-pointing errors. The amount of improvement obtained from the constant recoil mechanisms was dependent on the initial turret orientation and on the weapon firing rate. However, the constant recoil device usually resulted in the reduction of the gun-pointing errors by a factor of 3 or more. In addition, the gun-pointing errors for the 20mm constant recoil force excitations were somewhat insensitive to the firing rate, whereas the results for the standard recoil force excitation showed a much greater sensitivity to the firing rate.

Other studies were conducted for the 20mm XM197 weapon system to determine whether the XM197 turret servocontrol response could be improved by the incorporation of an additional feedback in the servocontrol loop. This additional feedback was expressed in the form of an angular rate signal or an acceleration signal. This type of feedback could be measured by a rate gyro or an accelerometer mounted on the gun or turret. None of the proposed turret servocontrol modifications affected a noticeable improvement in the dynamic response of the gun. Possibly, a better method for improving the turret servocontrol system would be to redesign the system on the basis of optimal control techniques rather than to add a feedback to the classical control system. Plans are, therefore, being made for an investigation of the dynamic response of an optimally controlled turret.

After the completion of the 20mm weapon system analysis, an investigation was carried out for the larger caliber Bushmaster 25mm and the AMCAWS 30mm weapons and the results of the investigation are presented in Chapters IV. and V. The analysis of the 25mm gun was conducted for both the standard recoil adapter mount and the constant recoil mount. However, the analysis of the 30mm weapon was limited to the constant recoil

mount only. Since no experimental recoil data were available for either of these weapons, the recoil traces for the 25mm and for the 30mm guns were estimated from the weapon design specifications and from the assumption that the 25mm and 30mm recoil traces are similar to the recoil traces for the 20mm weapon. Because the larger caliber weapons are more massive and larger in size than the 20mm XM197 gun, certain improvements had to be made to the physical design characteristics of the XM97 turret. Some of these improvements involved the relocation of the turret trunnion axis and the relocation of the center of gravity positions of the gun and the major turret components. As a result of these improvements, the mass unbalances in the turret were reduced considerably and, hence, the vibrations of the turret azimuth and elevation drive systems were also reduced.

After these changes had been made to the turret design, the structural sensitivity analysis was carried out for the Bushmaster 25mm weapon and for the AMCAWS 30mm weapon. In the analysis of the 25mm weapon, different values were selected for the parameter A_3 by which the mass unbalance of the gun is defined. As expected, the gun-pointing errors were generally larger for large mass unbalances than for small mass unbalances. The largest mass unbalance corresponded to a turret mounting configuration which was similar to that used for the 20mm XM197 weapon. In this case, the results for the 25mm analysis were about twice as large as the corresponding results for the 20mm standard recoil analysis. For the case in which the mass unbalance parameter was equal to zero, the results for the 25mm standard recoil analysis were not excessively large. The magnitudes of the statistical gun-pointing errors did not exceed 8.26 milliradians and, in most cases, these errors were much smaller. An even greater improvement in the gun-pointing errors occurred when the gun was mounted on a constant recoil mechanism. In this case, the errors were reduced by a factor of 2 or more.

In the analysis of the AMCAWS 30mm weapon, the gun mass unbalance parameter was set equal to zero, and different values were selected for the transmission stiffness. The choice of the transmission stiffness, however, had little effect on the numerical results. Almost all predicted

gun-pointing errors were small for the case in which an idealized constant recoil force was applied to the modified turret. In fact, the maximum errors occurred for the 67.5° azimuth angle position and these errors did not exceed 3.2 milliradians. The idealized 30mm constant recoil force that contained misfires, however, caused larger errors to occur in the elevation mechanism, especially at large azimuth angle positions.

From the AMCAWS 30mm gun-pointing error analysis, the feasibility of the use of a high-performance weapon in aircraft applications has been demonstrated, with the provision that the gun is to be attached to a constant recoil mount. These results, however, are somewhat tentative in that no actual weapon recoil test data were available to perform the analysis. A continuation of the structural sensitivity analysis is recommended for the Bushmaster 25mm weapon and for the AMCAWS 30mm weapon, in which actual experimental recoil force data are used in place of the computer simulated data. Before this analysis can be undertaken, a prototype design of a constant recoil mount for these weapons would have to be built and tested. Recently, a theoretical study has been initiated on the concept development of a constant recoil mount for the AMCAWS 30mm gun; however, no hardware development program has been initiated yet.

Other types of mount designs have been developed for various aircraft weapons that may also improve the dynamic responses of the turret drive systems. For example, General Electric Company has developed a new spring mount for the 30mm XM188 weapon that transmits smaller peak recoil forces than the standard spring adapter mount. The force transmitted by the improved spring mount may not be as smooth as the force transmitted by a constant recoil mount; nevertheless, the improved spring mount is more compact and less expensive than the constant recoil mount. An analysis is, therefore, recommended to quantify the amount of improvement in gun-pointing accuracy that could be achieved by the replacement of the standard spring adapter mount with the improved mount.

Besides the lack of suitable recoil data, a problem that arose in the analysis of the 25mm and 30mm weapons was the lack of a suitable turret for mounting these weapons. A modified version of the XM97 turret was, therefore, used in the 25mm and 30mm investigations, and, in most instances,

the resulting gun-pointing error predictions for the modified turret design were not excessively large. A much greater improvement in the dynamic response of a large caliber turret would probably be achieved by a complete design optimization of the turret. An extension of the 25mm and 30mm recoil sensitivity investigations is, therefore, recommended that would include the optimization of both the physical design characteristics and the servocontrol characteristics of the turret for precise dynamic gun pointing. In this investigation, the weights, center of gravity locations, trunnion locations, and other important design parameters of the turret will be chosen to minimize the dynamic effects of weapon recoil forces. Furthermore, the classical servocontrol system will be replaced by a control system design developed on the basis of an optimal control technique. Some additional turret instrumentation such as rate gyros or accelerometers may be incorporated in the optimal control system design concept.

In all probability, the design of a high-performance 25mm or 30mm weapon system would be intended for use on a next-generation helicopter such as the Advanced Attack Helicopter (AAH). After the Army has made a selection between the Bell and the Hughes versions of the AAH, the structural sensitivity analysis should be repeated for the selected AAH. The results of the structural sensitivity investigations for the AH-1G helicopter airframe revealed that the gun-pointing error is very sensitive to the natural frequencies of vibration and to the mode shapes of the helicopter structure. Since the free-vibration characteristics of the AAH helicopter might be quite different from that of the AH-1G helicopter, the results of a gun-pointing error analysis for the AAH helicopter weapon system may differ appreciably from the AH-1G results. An investigation of the gun-pointing errors is, therefore, recommended for the AAH weapon system.

In all completed analyses of the various factors that contribute to the total dynamic gun-pointing error, the dynamic gun barrel whip had not been considered. Often the flexural vibration amplitudes of the gun barrel are less than one milliradian and, therefore, these vibrations can be neglected in comparison with the turret and helicopter vibrations. For the larger impulse weapons such as the Bushmaster 25mm and the AMCAWS 30mm

AD-A035 138

ROCK ISLAND ARSENAL ILL GENERAL THOMAS J RODMAN LAB
THE INVESTIGATION OF DYNAMIC GUN POINTING ERRORS FOR HELICOPTER--ETC(U)
NOV 76 T D HUTCHINGS, A R ZAK

F/G 1/3

UNCLASSIFIED

RIA-R-TR-76-042

NL

2 OF 2
AD-A
035 138



END
DATE
FILMED
3 / 77
NTIS

weapons, the gun barrels are rather long (85 inches for the AMCAWS 30mm gun); consequently, the flexural vibrations of the gun barrels of these larger caliber weapons may be a significant source of gun-pointing error. An analysis should, therefore, be carried out for these weapons, to quantify the magnitudes of the dynamic oscillations of the gun barrel during a firing event. The analytical modeling techniques that are needed to perform the barrel vibration calculations have already been developed, and these techniques can readily be applied to the investigations of the Bushmaster 25mm and the AMCAWS 30mm weapons.

In conclusion, the structural sensitivity analysis has proven to be a valuable tool for the evaluation and quantification of the dynamic performance of existing or conceptual helicopter weapon systems. Furthermore, the dynamic error prediction techniques have been useful for the identification of potential problem areas, such as the excitation of vibration resonance at certain weapon firing rates, and these techniques have also been beneficial for the evaluation of certain concept improvements, such as the constant recoil mount.

APPENDIX

A. FORTRAN IV Source Listing of the Helicopter Vibration Model

```

C
C *****
C HELICOPTER VIBRATION MODEL: MAIN PROGRAM
C *****
C PURPOSE:
C DETERMINES THE SOLUTION TO THE FORCED VIBRATION PROBLEM FOR THE
C HELICOPTER STRUCTURAL AIRFRAME. THE MODEL GENERATES THE DISPLACEMENTS,
C VELOCITIES, AND ACCELERATIONS AT THE TURRET ATTACHMENT POINT.
C
C COMMON BLOCKS AND THE PROGRAMS THAT REQUIRE THEM:
C /ANGLE/ LOAD.MAIN
C /DIST/ LOAD.MAIN
C /MODE/ MAIN,OUPT,QMODE,QUAD
C /RED/ MAIN,OUTP,REDREC
C /WHY/ MAIN, QMODE, QUAD
C
C SUBROUTINES CALLED:
C DIME
C MODSEN
C NOW
C OUTP
C QUAD
C REDREC
C RLOT
C
C COMMON /ANGLE/ ALPHA,PHI,SA,CA,SP,CP
C COMMON /DIST/ B1,B2,D1,D2
C COMMON/MODE/A(180,30),GM(30),GF(30),NG(6),NMOD,NDF,MITER,WORK(900)
C *,NIN,NOUT
C COMMON /RED/ XO,H,C(4003)
C COMMON /WHY/ Y(90),IMODE(30)
C DIMENSION IDISP(30),IVEL(30),IACC(30)
C DIMENSION YOUT(251),TIME(251)
C DIMENSION PRMT(5)
C DIMENSION RPLT(5),CONFID(3)
C
C --- INITIALIZE TIMER
C --- TIMER RESOLUTION = 16440 MICROSECONDS
C
C ITIME=0
C CALL NOW(ITIME)
C
C READ DISTANCES B1 B2 B3 AND D1 D2 D3
C

```

```

      READ (5.1000) B1,B2,D1,D2
      WRITE (6.2002) B1,B2,D1,D2
C
C      READ CONSTANT ALPHA AND PHI
C
      READ(5.1000)DALPHA,DPHI
      PI=3.1415927
      CPI=PI/180.
      ALPHA=CPI*DALPHA
      PHI=CPI*DPHI
      SA=SIN(ALPHA)
      CA=COS(ALPHA)
      SP=SIN(PHI)
      CP=COS(PHI)
C
C      READ NUMBER OF MODES AND DEGREES OF FREEDOM
C
      READ(5.1001) NMOD,NDF
      IF(NMOD.GT.30) NMOD=30
      IF(NDF.GT.180) NDF=180
      DO 40 I=1,NDF
      DO 40 J=1,NMOD
40  A(I,J)=0.0
C
C      --- READ THE NUMBER OF MODAL EQUATIONS TO BE INTEGRATED
C
      READ (5.1001) NMODE
      READ (5.1001) (IMODE(I),I=1,NMODE)
C
C      READ GLOBAL POSITION OF TURRET DISPLACEMENTS
C
      READ(5.1001) (NQ(I),I=1,6)
C
C      --- READ EIGENVALUES, GENERALIZED MASSES
C
      READ (5.1008) ((OF(I),GM(I)),I=1,NMOD)
      ND2=2*NMODE
C
C      READ INITIAL DISPLACEMENTS AND VELOCITIES
C
      DO 60 I=1,ND2
60  Y(I)=0.0
C
C      READ LOWER AND UPPER BOUNDS,INITIAL INCREMENT,HMIN,HMAX
C

```

```

      READ (5.1005) PRMT
      WRITE(6.2003)
      DO 62 I=1,NMODE
62  YOUT(I) = SQRT(GF(IMODE(I)))/(2.*PI)
      WRITE(6.2004) ((IMODE(I),YOUT(I)) ,I=1,NMODE)
C
C --- DETERMINE STEP SIZE FOR INTEGRATION
C
      H=PRMT(3)
      IF(IMODE(NMODE).LE.6) GO TO 63
      TAUMIN=2.0*3.1415927/SQRT(GF(IMODE(NMODE)))
      H=0.05*TAUMIN
63  SD=0.02
      DELTA=PRMT(2)-PRMT(1)
      HMIN = PRMT(4)
      HMAX = PRMT(5)
      IF(H.LT.HMIN) H=HMIN
      IF(H.GT.HMAX) H=HMAX
      L=H/HMIN
      HX=H/HMIN
      NH=(HX+L+1.5)/2
      H=NH*HMIN
      PRMT(3)=H
      NITER=1+DELTA/H
      IF(NITER.LE.4001) GO TO 65
      PRMT(2)=4000.*H+PRMT(1)
      NITER=4001
65  WRITE (6.2005) (PRMT(I),I=1,3)
      XO=PRMT(1)
      WRITE(6.2006)DALPHA,DPHI
C
C *** READ TEST NUMBER AND DATE
C
      READ(11.2222)RPLT
      WRITE(6.2223)RPLT
C
C *** READ HELICOPTER CONFIGURATION
C
      READ(5.1111)CONFIG
      WRITE(6.1112)CONFIG
C
C *** READ RECOIL FORCE DATA FROM UNIT 11
C
      CALL REDREC(NH,NITER)
C

```

```

C --- PLOT RECOIL FORCE
C
    HDIV=DELTA/250.
    DO 68 J=1,251
    X=XO+(J-1)*HDIV
    CALL RECOIL(X,RF)
    YOUT(J)=RF
68  TIME(J)=X
    WRITE(6,2007)
    CALL PLOT(251,TIME,YOUT)
    CALL DIME(RR,SS,TT)
    WRITE (6,4000) SS

C
C  READ MATRIX OF MODESHAPES
C
    NS=NG(1)
    NE=NG(6)
    READ(5,1005) ((A(I,J),I=NS,NE),J=7,NMOD)
    CALL DIME(RR,SS,TT)
    WRITE (6,4001) SS

C
C --- COMPRESS MODESHAPE MATRIX
C
    NMOD=NMODE
    DO 160 I=1,NMOD
    DO 160 J=1,NDF
160  A(J,I)=A(J,IMODE(I))

C
C --- ZERO THE TEMPORARY I/O FILE 14
C
    NIN = 13
    NOUT = 14
    MITER = NITER/100
    IF(NITER.NE.100*MITER) MITER = MITER + 1
    DO 170 I=1,900
170  WORK(I) = 0.
    DO 180 I=1,MITER
    WRITE(14) WORK
180  CONTINUE

C
C --- SOLVE MODAL EQUATIONS
C
200  DO 210 I=1,NMODE
    KMA=IMODE(I)
    OMEGA=SQRT(OF(IMODE(I)))

```



```

ALP=-0.5*SD*OMEGA
BETA=0.5*OMEGA*SQR(4.-SD**2)
CALL QUAD(NITER,ALP,BETA,XO,H,I,KMA)
CALL DIME(RR,SS,TT)
WRITE(6,4006) KMA,SS
210 CONTINUE
CALL OUTP(RPLT,CONFID,DALPHA,OPHI,NITER)
CALL DIME(RR,SS,TT)
999 WRITE(6,4005) TT
1000 FORMAT(6F10.5)
1001 FORMAT(6I10)
1005 FORMAT(6E12.5)
1006 FORMAT (E12.6,5X,E12.6)
1008 FORMAT (E12.6,E12.6)
1111 FORMAT(3A4)
1700 FORMAT (E15.8)
2002 FORMAT (3X,'B1,B2,D1,D2'/3X,4F12.6)
2003 FORMAT('0',5X,'MODE',5X,'EIGENVALUE')
2004 FORMAT(5X,I3,6X,E12.6)
1112 FORMAT(1X,'CONFIGURATION=',3A4)
2005 FORMAT('0','RKOS PARAMETERS:'/5X,'START TIME =',F8.3/
* 5X,'STOP TIME =',F8.3/5X,'INCREMENT =',F6.4)
2006 FORMAT('0','ALPHA=',F5.1,1X,'DEGREES',15X,'PHI=',F5.1,1X,
$ 'DEGREES')
2007 FORMAT(' ','RECOIL FORCE')
2222 FORMAT(5A4)
2223 FORMAT('1',5A4)
4000 FORMAT ('1','PREPROCESSOR CPU TIME =',F8.3,' SECONDS')
4001 FORMAT('0','MODESHAPE READ/WRITE CPU TIME =',F8.3,' SECONDS')
4003 FORMAT('0','PLOTTER CPU TIME =',F8.3,' SECONDS')
4004 FORMAT('0','PRINTER CPU TIME =',F8.3,' SECONDS')
4005 FORMAT('0','TOTAL CPU TIME =',F8.3,' SECONDS')
4006 FORMAT('0','CPU TIME FOR INTEGRATION OF MODAL EQUATION',I3,
* ' =',F8.3,' SECONDS')
4007 FORMAT('0','STAT CPU TIME =',F8.3,' SECONDS')
STOP
END

```


C		DQSF	10
C	DQSF	20
C		DQSF	30
C	SUBROUTINE DQSF	DQSF	40
C		DQSF	50
C	PURPOSE	DQSF	60
C	TO COMPUTE THE VECTOR OF INTEGRAL VALUES FOR A GIVEN	DQSF	70
C	EQUIDISTANT TABLE OF FUNCTION VALUES.	DQSF	80
C		DQSF	90
C	USAGE	DQSF	100
C	CALL DQSF (H,Y,Z,NDIM)	DQSF	110
C		DQSF	120
C	DESCRIPTION OF PARAMETERS	DQSF	130
C	H - DOUBLE PRECISION INCREMENT OF ARGUMENT VALUES.	DQSF	140
C	Y - DOUBLE PRECISION INPUT VECTOR OF FUNCTION VALUES.	DQSF	150
C	Z - RESULTING DOUBLE PRECISION VECTOR OF INTEGRAL	DQSF	160
C	VALUES. Z MAY BE IDENTICAL WITH Y.	DQSF	170
C	NDIM - THE DIMENSION OF VECTORS Y AND Z.	DQSF	180
C		DQSF	190
C	REMARKS	DQSF	200
C	NO ACTION IN CASE NDIM LESS THAN 3.	DQSF	210
C		DQSF	220
C	SUBROUTINES AND FUNCTION SUBPROGRAMS REQUIRED	DQSF	230
C	NONE	DQSF	240
C		DQSF	250
C	METHOD	DQSF	260
C	BEGINNING WITH Z(1)=0. EVALUATION OF VECTOR Z IS DONE BY	DQSF	270
C	MEANS OF SIMPSONS RULE TOGETHER WITH NEWTONS 3/8 RULE OR A	DQSF	280
C	COMBINATION OF THESE TWO RULES. TRUNCATION ERROR IS OF	DQSF	290
C	ORDER H**5 (I.E. FOURTH ORDER METHOD). ONLY IN CASE NDIM=3	DQSF	300
C	TRUNCATION ERROR OF Z(2) IS OF ORDER H**4.	DQSF	310
C	FOR REFERENCE, SEE	DQSF	320
C	(1) F.B.HILDEBRAND, INTRODUCTION TO NUMERICAL ANALYSIS,	DQSF	330
C	MCORAW-HILL, NEW YORK/TORONTO/LONDON, 1956, PP.71-76.	DQSF	340
C	(2) R.ZURMUEHL, PRAKTISCHE MATHEMATIK FUEER INGENIEURE UND	DQSF	350
C	PHYSIKER, SPRINGER, BERLIN/GOETTINGEN/HEIDELBERG, 1963,	DQSF	360
C	PP.214-221.	DQSF	370
C		DQSF	380
C	DQSF	390
C		DQSF	400
C	SUBROUTINE DQSF(H,Y,Z,NDIM)	DQSF	410
C		DQSF	420
C		DQSF	430
C	DIMENSION Y(1),Z(1)	DQSF	440
C	DOUBLE PRECISION Y,Z,H,HT,SUM1,SUM2,AUX,AUX1,AUX2	DQSF	450

C	HT=.333333333333333300=H	DQSF 460
	IF(NDIM-5)7.8.1	DQSF 470
C		DQSF 480
C	NDIM IS GREATER THAN 5. PREPARATIONS OF INTEGRATION LOOP	DQSF 490
1	SUM1=Y(2)+Y(2)	DQSF 500
	SUM1=SUM1+SUM1	DQSF 510
	SUM1=HT*(Y(1)+SUM1+Y(3))	DQSF 520
	AUX1=Y(4)+Y(4)	DQSF 530
	AUX1=AUX1+AUX1	DQSF 540
	AUX1=SUM1+HT*(Y(3)+AUX1+Y(5))	DQSF 550
	AUX2=HT*(Y(1)+3.87500*(Y(2)+Y(5))+2.62500*(Y(3)+Y(4))+Y(6))	DQSF 560
	SUM2=Y(5)+Y(5)	DQSF 570
	SUM2=SUM2+SUM2	DQSF 580
	SUM2=AUX2-HT*(Y(4)+SUM2+Y(6))	DQSF 590
	Z(1)=0.00	DQSF 600
	AUX=Y(3)+Y(3)	DQSF 610
	AUX=AUX+AUX	DQSF 620
	Z(2)=SUM2-HT*(Y(2)+AUX+Y(4))	DQSF 630
	Z(3)=SUM1	DQSF 640
	Z(4)=SUM2	DQSF 650
	IF(NDIM-6)5.5.2	DQSF 660
C		DQSF 670
C	INTEGRATION LOOP	DQSF 680
2	DO 4 I=7,NDIM.2	DQSF 690
	SUM1=AUX1	DQSF 700
	SUM2=AUX2	DQSF 710
	AUX1=Y(I-1)+Y(I-1)	DQSF 720
	AUX1=AUX1+AUX1	DQSF 730
	AUX1=SUM1+HT*(Y(I-2)+AUX1+Y(I))	DQSF 740
	Z(I-2)=SUM1	DQSF 750
	IF(I-NDIM)3.6.6	DQSF 760
3	AUX2=Y(I)+Y(I)	DQSF 770
	AUX2=AUX2+AUX2	DQSF 780
	AUX2=SUM2+HT*(Y(I-1)+AUX2+Y(I+1))	DQSF 790
4	Z(I-1)=SUM2	DQSF 800
5	Z(NDIM-1)=AUX1	DQSF 810
	Z(NDIM)=AUX2	DQSF 820
	RETURN	DQSF 830
6	Z(NDIM-1)=SUM2	DQSF 840
	Z(NDIM)=AUX1	DQSF 850
	RETURN	DQSF 860
C		DQSF 870
C	END OF INTEGRATION LOOP	DQSF 880
C		DQSF 890

7	IF(NOIM-3)12.11.8	DQSF 900
C	NOIM IS EQUAL TO 4 OR 5	DQSF 920
8	SUM2=1.12500*HT*(Y(1)+Y(2)+Y(2)+Y(2)+Y(3)+Y(3)+Y(3)+Y(4))	DQSF 930
	SUM1=Y(2)+Y(2)	DQSF 940
	SUM1=SUM1+SUM1	DQSF 950
	SUM1=HT*(Y(1)+SUM1+Y(3))	DQSF 960
	Z(1)=0.00	DQSF 970
	AUX1=Y(3)+Y(3)	DQSF 980
	AUX1=AUX1+AUX1	DQSF 990
	Z(2)=SUM2-HT*(Y(2)+AUX1+Y(4))	DQSF1000
	IF(NOIM-5)10.9.9	DQSF1010
9	AUX1=Y(4)+Y(4)	DQSF1020
	AUX1=AUX1+AUX1	DQSF1030
	Z(5)=SUM1+HT*(Y(3)+AUX1+Y(5))	DQSF1040
10	Z(3)=SUM1	DQSF1050
	Z(4)=SUM2	DQSF1060
	RETURN	DQSF1070
C		DQSF1080
C	NOIM IS EQUAL TO 3	DQSF1090
11	SUM1=HT*(1.2500*Y(1)+Y(2)+Y(2)-.2500*Y(3))	DQSF1100
	SUM2=Y(2)+Y(2)	DQSF1110
	SUM2=SUM2+SUM2	DQSF1120
	Z(3)=HT*(Y(1)+SUM2+Y(3))	DQSF1130
	Z(1)=0.00	DQSF1140
	Z(2)=SUM1	DQSF1150
12	RETURN	DQSF1160
	END	DQSF1170

SUBROUTINE LOAD

PURPOSE:

CALCULATES THE THREE FORCE COMPONENTS AND THE THREE
MOMENT COMPONENTS OF THE RECOIL FORCE VECTOR THAT IS
APPLIED TO THE HELICOPTER-TURRET ATTACH POINT. RESULTS
ARE STORED IN THE VECTOR FOR.

LISTING OF PARAMETERS:

X INPUT PARAMETER - TIME IN SECONDS

COMMON BLOCKS AND THE PROGRAMS THAT REQUIRE THEM:

```

/ANGLE/  LOAD.MAIN
/DIST/   LOAD.MAIN
/FORCE/  LOAD.QMODE

```

SUBROUTINES CALLED:

RECOIL

```

SUBROUTINE LOAD(X)
COMMON /ANGLE/ ALPHA,PHI,SA,CA,SP,CP
COMMON /DIST/ B1,B2,D1,D2
COMMON /FORCE/ FOR(6)
CALL RECOIL(X,RF)
FOR(1)=+RF*CA*CP
FOR(2)= RF*CA*SP
FOR(3)=-RF*SA
FX = RF*(-B1*SA+B2*CA+D2)
FOR(4) = -FX*SP
FOR(5) = FX*CP
FOR(6) = 0.0
999 CONTINUE
RETURN
END

```

```

C
C      SUBROUTINE OUTP
C
C      PURPOSE:
C      --- WRITES RECOIL FORCE DATA AND HELICOPTER ACCELERATION DATA ON
C      --- UNIT 12
C
C      LISTING OF PARAMETERS:
C          RPLT   ARRAY CONTAINING TITLE OF RECOIL FORCE
C          CONFIG ARRAY CONTAINING TITLE OF HELICOPTER
C                CONFIGURATION
C          DALPHA ELEVATION ANGLE IN DEGREES
C          DPHT   AZIMUTH ANGLE IN DEGREES
C          NITER  SIZE OF ARRAYS
C
C      COMMON BLOCKS AND THE PROGRAMS THAT REQUIRE THEM:
C          /MODE/   MAIN,OUTP,QMODE,QUAD
C          /RED/    MAIN,OUTP,REDREC
C
C      SUBROUTINES CALLED:
C          NONE
C
C      SUBROUTINE OUTP (RPLT,CONFIG,DALPHA,DPHT,NITER)
C      COMMON/MODE/8(180,30),GM(30),GF(30),NQ(6),NM00,N0F,NITER,WORK(900)
C      *,NIN,NOUT
C      COMMON /RED/ XO,H,A(4003)
C      DIMENSION RPLT(5),CONFIG(3),THETA(3),SE(3),AO(3)
C      WRITE (12) RPLT
C      WRITE (12) CONFIG
C      WRITE (12) DALPHA,DPHT,NITER,H,XO
C      WRITE (6,100) RPLT,CONFIG
C      WRITE (6,200) DALPHA,DPHT,NITER,H,XO
C      WRITE (6,400)
C
C      TRANSFER DATA FROM THE TEMPORARY FILE NOUT TO THE PERMANENT FILE 12
C
C      REWIND NOUT
C      IPRT = 0
C      DO 20 J=1,NITER
C      READ(NOUT) WORK
C      IJMIN = MIN0(100,NITER-(J-1)*100)
C      DO 20 J=1,IJMIN
C      INDX = J + (J-1)*100
C      DO 10 K=1,3
C      SE(K) = WORK(K+9*(J-1))

```



```

10 THETA(K) = WORK(K+3+9*(J-1))
   IPRT = IPRT + 1
   IF(IPRT.EQ.11) IPRT=1
   IF(INOX.EQ.NITER) IPRT=1
   IF(IPRT.EQ.1) WRITE(6,300) INOX,A(INOX),THETA,SE
20 CONTINUE
   WRITE(6,401)
   REWIND NOUT
   IPRT=0
   DO 30 I=1,NITER
   READ(NOUT) WORK
   IJMIN = MIN0(100,NITER-(I-1)*100)
   DO 30 J=1,IJMIN
   INOX = J + (I-1)*100
   DO 25 K=1,3
   SE(K) = WORK(K+9*(I-1))
   THETA(K) = WORK(K+3+9*(J-1))
25 AO(K) = WORK(K+6+9*(J-1))
   WRITE(12) A(INOX),SE,THETA,AO
   IPRT=IPRT+1
   IF(IPRT.EQ.11) IPRT=1
   IF(INOX.EQ.NITER) IPRT=1
   IF(IPRT.EQ.1) WRITE(6,300) INOX,A(INOX),AO
30 CONTINUE
100 FORMAT ('1',5A4/1X,3A4)
200 FORMAT (' ', 'ALPHA =',F5.1,10X,'DPHI =',F5.1,10X,'NITER =',
  * I4,10X,'H =',F8.5,10X,'X0 =',F8.5)
300 FORMAT (1X,I4,3X,F9.2,6(3X,E15.3))
400 FORMAT('0',T5,'I',T12,'RECOIL',T26,'T001',T44,'T002',T62,'T003',
  * T/9,'X1001',T97,'X1002',T115,'X1003')
401 FORMAT('0',T5,'I',T12,'RECOIL',T25,'THETA1',T43,'THETA2',T61,
  * 'THETA3')
   RETURN
   END

```



```

C
C      SUBROUTINE QUAD
C
C      PURPOSE:
C      --- INTEGRATES UNCOUPLED MODAL EQUATIONS AND DETERMINES TURRET
C      --- ANGULAR DISPLACEMENTS
C
C      FILES 13 AND 14 ARE USED TO TEMPORARILY STORE DATA BEFORE
C      IT IS WRITTEN ON OUTPUT FILE 12
C
C      LISTING OF PARAMETERS:
C      INPUT:
C          NITER  NUMBER OF DATA POINTS ON THE TIME INTERVAL
C          ALP    EXPONENTIAL DECAY FACTOR
C          BETA   DAMPED MODAL FREQUENCY
C          XO     STARTING TIME
C          H      TIME INCREMENT
C          N      COLUMN INDEX OF MATRIX A CONTAINING THE
C                MODESHAPE WITH INDEX IMX
C          IMX    MODAL COORDINATE INDEX
C
C      COMMON BLOCKS AND THE PROGRAMS THAT REQUIRE THEM:
C          /MODE/  MAIN,QUPT,QMODE,QUAD
C          /QR/    QMODE,QUAD
C          /WHY/   MAIN, QMODE, QUAD
C
C      SUBROUTINES CALLED:
C          QMODE
C          DQSF
C
C      SUBROUTINE QUAD(NITER,ALP,BETA,XO,H,N,IMX)
C      COMMON/MODE/A(180,30),QM(30),GF(30),NG(6),NMOD,NDF,NITER,WORK(900)
C      *,NIN,NOU
C      COMMON /QR/ QRHS(4001)
C      COMMON /WHY/ Y(90),IMODE(30)
C      DOUBLE PRECISION DH,DX,CB1,CB1,SB1,SB1,ETJ,QM1,QM01,QMOD1
C      DOUBLE PRECISION DQ(4001),QUAD1(4001)
C
C      GENERATE THE EXCITATION FORCE VECTOR
C
C      CALL QMODE(NITER,H,N,XO)
C
C      --- CHECK IF MODAL EQUATION REPRESENTS A RIGID BODY MOTION

```

```

C
C      IF(IMX.LE.6) GO TO 40
C
C --- FLEXURAL MODAL EQUATION
C
C      FORM THE SOLUTION INTEGRALS
C
C      E1=EXP(-ALP*X0)
C      DH=M
C      DO 10 I=1,NITER
C      DX=X0+(I-1)*DH
C      DEX=DEXP(-ALP*DX)
C      QUAD1(I)=QRHS(I)*DCOS(BETA*DX)*DEX
10  DQ(I)=QRHS(I)*DSIN(BETA*DX)*DEX
C      CALL DQSF(DH,QUAD1,QUAD1,NITER)
C      CALL DQSF(DH,DQ,DQ,NITER)
C      CB1=BETA*X0
C      SB1=DSIN(CB1)
C      CB1=DCOS(CB1)
C
C      READY THE INPUT AND OUTPUT FILES AND READ THE PARTIAL SOLUTION
C      FROM THE INPUT FILE
C
C      NIN = NOUT
C      NOUT = 13
C      IF(NOUT.EQ.NIN) NOUT = 14
C      REWIND 13
C      REWIND 14
C      DO 30 J=1,MITER
C      READ(NIN) WORK
C      IJMIN = MINO(100,NITER-(J-1)*100)
C
C      FORM THE SOLUTION TO THE N TH MODAL EQUATION
C
C      DO 20 IJ=1,IJMIN
C      I = (J-1)*100 + IJ
C      DX=X0+(I-1)*DH
C      SB1=DSIN(BETA*DX)
C      CB1=DCOS(BETA*DX)
C      ET1=DEXP(ALP*DX)
C      QMI = (SB1 *QUAD1(I)-CB1*DQ(I)+E1*((Y(NMOD+N)-ALP*Y(N))*(SB1*CB1-
C      *SB1*CB1)+Y(N)*BETA*(CB1*CB1+SB1*SB1)))*ET1/BETA
C      QMDI =ET1*((ALP*SB1+BETA*CB1)*QUAD1(I)-(ALP*CB1-BETA*SB1)*DQ(I)
C      *E1*(Y(NMOD+N)*BETA*(CB1*CB1+SB1*SB1)+(ALP*Y(NMOD+N)-(ALP**2+BETA

```

```

      2)*Y(N))*((SB1-CB1-SB1-CB1)))/BETA
      QMOD1 =QRHS(1)-2.*ALP*QMOD1 -(ALP**2+BETA**2)*QMI
C
C      ADD THE SOLUTION TO THE N TH MODAL EQUATION TO THE PARTIAL SUM
C      AND STORE THE RESULTS ON THE OUTPUT FILE
C
      DO 20 K=1,3
      K3 = K+3
      KJ = K+9*(IJ-1)
      KJ3 = KJ+3
      KJ6 = KJ+6
      WORK(KJ) = WORK(KJ) + A(NO(K),N)*QMOD1
      WORK(KJ3) = WORK(KJ3) + A(NO(K3),N)*QMOD1
20  WORK(KJ6) = WORK(KJ6) + A(NO(K3),N)*QMI
      WRITE(NOUT) WORK
30  CONTINUE
      RETURN
C
C ---- RIGID BODY MODAL EQUATION
C
      40 RETURN
      END

```

[illegible]

00000000000000000000000000000000

00000000000000000000000000000000

00000000000000000000000000000000

CCCCCCCCCCCCCCCC

[illegible]

0000000000000000

CCCCCCCCCCCCCCCC

ה

CCCCCCCC

CCCCCCCC

CCCCC

C
C
CC
C

CCC

C
C
C

CCC

C

```
20 DO 50 N=1,NITER
100 FORMAT(8F9.2)
DO 50 N=1,NITER
  L=(N-1)*NH/2
  XL=(N-1)*NH/2.
  IF(L.EQ.XL) GO TO 45
  L1=((N-1)*NH+1)/2
  L2=((N-1)*NH+3)/2
  A(N)=- (B(L1)+B(L2))/2.
  GO TO 50
45 A(N)=-B(L+1)
50 CONTINUE
  RETURN
```

C

C

C

C

THE ENTRY RECOIL ROUTINE DETERMINES THE RECOIL FORCE F AT AN ARBITRARY
POINT X BY LINEAR INTERPOLATION

```
ENTRY RECOIL(X,F)
Y=(X-X0)/H
L=Y
N=(L + Y + 1.6)/2 + 1
F=A(N)
RETURN
END
```

```

C
C   SUBROUTINE RLOT
C
C   PURPOSE:
C   --- A GENERAL PLOT ROUTINE, WHICH PLOTS A FUNCTION  $Y = Y(X)$  AT N DATA
C   --- POINTS  $(X(N), Y(N))$ 
C
C   LISTING OF PARAMETERS:
C       N = NUMBER OF DATA POINTS
C       X = VECTOR OF ABSCISSA DATA POINTS
C       Y = VECTOR OF ORDINATE DATA POINTS
C
C   SUBROUTINES CALLED:
C       NONE
C
C   SUBROUTINE RLOT (N,X,Y)
C   DIMENSION X(N), Y(N), AMARK(9)
C   INTEGER ORAPH(101)
C   DATA IBLANK/' ', IPLUS/'+' , IDASH/'-' , IDOT/'.' , ISTAR/'*' /
C
C   --- FIND THE MAXIMUM AMAX AND THE MINIMUM AMIN OF THE SET OF VALUES
C   --- TO BE PLOTTED
C
C       AMAX=Y(1)
C       AMIN=Y(1)
C       DO 20 J=1,N
C         IF(Y(J).LE.AMAX) GO TO 10
C         AMAX=Y(J)
C 10      IF(Y(J).GE.AMIN) GO TO 20
C         AMIN=Y(J)
C 20      CONTINUE
C         IF(AMAX.NE.AMIN) GO TO 25
C         WRITE (6,400) AMAX
C         RETURN
C 25      CONTINUE
C         WRITE(6,100) AMIN,AMAX
C
C   --- LABEL INCREMENTS ON THE Y-AXIS
C
C       RANGE=AMAX-AMIN
C       STEP=(AMAX-AMIN)/10.
C       RO=((0.0-AMIN)/RANGE)*100.
C       IO=RO
C       IO=((IO+RO+1.5)/2.

```



```

      IOZ=IO+2
      DO 30 J=1.9
30  AMARK(J)=AMIN+J*STEP
      WRITE(6,200) (AMARK(J),J=1.9)
C
C --- SCALE AND PLOT THE POINTS
C
      DO 70 J=1.N
      YY=Y(J)
      RY=((YY-AMIN)/RANGE)*100.
      IY=RY
      IY=(IY+RY+1.5)/2.
      IZ=IY+2
      DO 40 I=1.101
40  GRAPH(I)=IBLANK
      IF(IO.GE.0) GO TO 48
      IF(IY.EQ.1.OR.IY.EQ.0) GO TO 44
      DO 42 I=1.IY
42  GRAPH(I)=IDASH
44  DO 46 I=1.101.10
46  GRAPH(I)=IDOT
      GRAPH(IY+1)=IPLUS
      GO TO 66
48  IF(IO.LE.100) GO TO 66
      IF(IY.GT.98) GO TO 52
      DO 50 I=IZ.101
50  GRAPH(I)=IDASH
52  DO 54 I=1.101.10
54  GRAPH(I)=IDOT
      GRAPH(IY+1)=IPLUS
      GO TO 66
56  IF(IY.GT.IO-1) GO TO 69
      DO 58 I=IZ.IO
58  GRAPH(I)=IDASH
      GO TO 62
59  IF(IY.LE.IO+1) GO TO 62
      DO 60 I=IOZ.IY
60  GRAPH(I)=IDASH
62  DO 64 I=1.101.10
64  GRAPH(I)=IDOT
      GRAPH(IO+1)=ISTAR
      GRAPH(IY+1)=IPLUS
66  WRITE(6,300) X(J),Y(J),GRAPH
70  CONTINUE
100 FORMAT ('0',T21,'MINIMUM = ',E15.8,T97,'MAXIMUM = ',E15.8)

```

```
200 FORMAT ('O',4X,'X',9X,'Y',8X,9(1X,1PE9.2))
300 FORMAT(' ',F8.3,1X,1PE9.2,1X,10I1)
400 FORMAT ('C', 'CONSTANT VALUED FUNCTION =',E16.8)
      RETURN
      END
```

APPENDIX

B. FORTRAN IV Source Listing of the Gun-Turret Dynamic Model

```

C
C   TURRET DYNAMIC MODEL:  MAIN PROGRAM
C
C
C   PURPOSE:
C   DETERMINES THE DYNAMIC MOTIONS OF THE MAJOR COMPONENTS OF THE
C   TURRET AND CALCULATES THE ERROR IN THE GUN POSITION DURING THE
C   WEAPON FIRING INTERVAL.
C
C   COMMON BLOCKS AND THE PROGRAMS THAT REQUIRE THEM:
C   /ACCEL/ MAIN, IFORCE
C   /ANGLE/ MAIN, IFORCE, OUTP, RFORCE
C   /ANGROT/ MAIN, OUTP
C   /DIST/ MAIN, IFORCE
C   /MASS/ MAIN, FCT, IFORCE
C   /MOTION/ MAIN, CALCOM, IFORCE, OUTP, RFORCE
C   /NPLOT/ MAIN, CALCOM, OUTP
C   /NUMB/ MAIN, CALCOM, IFORCE, OUTP, POINT, RFORCE
C   /RED/ MAIN, CALCOM, RFORCE
C   /STIFF/ MAIN, FCT
C
C   SUBROUTINES CALLED:
C   CALCOM
C   PLOTS
C   RKQS
C   STATIS
C
C   COMMON /ACCEL/ T1(2600),T2(2600),T3(2600),UDD(2600),
C   * VDD(2600),WDD(2600)
C   COMMON /ANGLE/ PHI,ALPHA,SA,CA,SP,CP
C   COMMON /ANGROT/ AQ1(2600),AQ2(2600),AQ3(2600)
C   COMMON/DIST/A1,A2,A3,B1,B2
C   COMMON/MASS/AM,AI1,AI2,GR
C   COMMON/MOTION/IM,N
C   COMMON /NPLOT/ NP,TIME(2600),ANG(2600),WEAPON(8),DPHI,DALPHA,
C   * RATE,ROUNDS
C   COMMON /NUMB/ NITER,HDAT,XO,RPLT(5),CONFIG(3)
C   COMMON /RED/ FREC(2600)
C   COMMON/STIFF/TK,TQ
C   DIMENSION PRMT(5),DERY(5),AUX(8,5),Y(5)
C   EXTERNAL FCT,OUTP
C   CALL PLOTS (IBUF,IDUM,14)
C

```

```

C      READ PLOT TITLE PARAMETERS
C
C      READ(5,1007) WEAPON
C      READ(5,1005) RATE,ROUNDS
C
C      SET MOTION TO BE FIRST,IM=1 AZIMUTH,IM=2 ELEVATION
C
C      READ(5,1002) IM
C
C      SET NUMBER OF MOTIONS TO BE ANALYZED,1 OR 2
C
C      READ(5,1002) NM
C
C      READ CENTER OF GRAVITY OFFSET FEET
C
C      READ(5,1005) A1,A2,A3,B1,B2
C
C      READ DATA FROM UNIT 1
C
C      READ (1) RPLT
C      READ (1) CONFIG
C      READ (1) DALPHA,DPHI,NITER,HDAT,XO
C
C      TURRET INTERFACE GRID POINT PARAMETERS:
C
C      UDD = -XDD      LINEAR ACCELERATIONS
C      VDD = ZDD      LINEAR ACCELERATIONS
C      WDD = YDD      LINEAR ACCELERATIONS
C
C      T1 = -TDDX     ANGULAR ACCELERATIONS
C      T2 = TDDZ     ANGULAR ACCELERATIONS
C      T3 = TDDY     ANGULAR ACCELERATIONS
C
C      A01 = -TX      ANGULAR POSITIONS
C      A02 = TZ      ANGULAR POSITIONS
C      A03 = TY      ANGULAR POSITIONS
C
C      DO 4 I=1,NITER
C      READ(1) FREC(I),UDD(I),VDD(I),WDD(I),T1(I),T2(I),T3(I),
C      * A01(I),A02(I),A03(I)
C      4 CONTINUE
C
C      PRINT INPUT DATA
C
C      WRITE(6,100) WEAPON,RPLT,RATE,ROUNDS,CONFIG

```

```

WRITE(6.200) DALPHA,DPHI,NITER,HOAT,XO
WRITE(6.400)
IPRT = 0
DO 1 I=1,NITER
  IPRT = IPRT + 1
  IF(IPRT.EQ.11) IPRT = 1
  IF(I.EQ.NITER) IPRT = 1
  IF(IPRT.EQ.1) WRITE(6.300) I,FREC(I),T1(I),T2(I),T3(I),
    * UDD(I),VDD(I),WDD(I)
1 CONTINUE
  IPRT = 0
  WRITE(6.401)
  DO 2 I=1,NITER
    IPRT = IPRT + 1
    IF(IPRT.EQ.11) IPRT = 1
    IF(I.EQ.NITER) IPRT = 1
    IF(IPRT.EQ.1) WRITE(6.300) I,FREC(I),A01(I),A02(I),A03(I)
2 CONTINUE
C
C   INITIALIZE PARAMETERS
C
  PI=3.1415926/180.
  PHI=DPHI*PI
  ALPHA=DALPHA*PI
  SA=SIN(ALPHA)
  CA=COS(ALPHA)
  SP=SIN(PHI)
  CP=COS(PHI)
  PHI=PHI*PI
  ALPHA=ALPHA*PI
C
C   CONVERT LINEAR ACCELERATIONS TO FT/SEC**2 UNITS
C
  DO 5 I=1,NITER
    UDD(I)=UDD(I)/12.
    VDD(I)=VDD(I)/12.
5   WDD(I)=WDD(I)/12.
    DO 99 N=1,NM
      NP=0
      IF(IM.EQ.N) GO TO 12
      WRITE(6.1600)
      GO TO 13
12   WRITE(6.1600)
13   CONTINUE
C

```

```

C   READ MASS IN LBS AND MOMENTS OF INERTIA OF LOAD AND MOTOR
C   MOMENTS OF INERTIA IN SLUGS-FT**2
C
C   READ(5,1000)AM,AI1,AI2
C   AM=AM/32.2
C
C   READ GEAR BOX RATIO
C
C   READ(5,1000)OR
C
C   READ TRANSMISSION STIFFNESS,FT-LBS, AND DAMPING COEFFICIENT
C
C   READ(5,1003)TK,TQ
C   WRITE(6,2000) AM,AI1,AI2
C   WRITE(6,2001) A1,A2,A3,B1,B2
C   WRITE(6,2002) TK,TQ
C   WRITE(6,2003) OR
C
C   CONVERT MOTOR MOMENT OF INERTIA TO TURRET COORDINATES
C
C   AI2=AI2*(OR)**2
C
C   SET INITIAL DISPLACEMENTS
C
C   DO 10 I=1,5
10  Y(I)=0.0
C
C   SET ERROR WEIGHTS
C
C   DO 11 I=1,5
11  DERY(I)=.2
C
C   READ THE UPPER ERROR BOUND
C
C   READ(5,1001) PRMT(4)
C   PRMT(1)=X0
C   PRMT(2)=X0+(NITER-1)*H0AT
C   PRMT(3)=H0AT
C   WRITE(6,2005)
C
C   CALL THE RUNGE-KUTTA EQUATION SOLVER RKOS,
C   CALL THE STATISTICAL ERROR PARAMETER SUBROUTINE STATIS,
C   CALL THE CALCOMP PLOT SUBROUTINE CALCOM
C
20  CALL RKOS(PRMT,Y,DERY,S,IHLF,FCT,OUTP,AUX)

```

```

CALL STATIS(NITER,ANO,ANOAV,ANOSD)
CALL CALCOM(NM,ANOAV,ANOSD,PRMT)
IF(IM.EQ.N) GO TO 31
WRITE(6,2008)
WRITE(6,2007)
GO TO 32
31 CONTINUE
WRITE(6,2006)
WRITE(6,2007)
32 CONTINUE
WRITE(6,1006) ANOAV,ANOSD
99 CONTINUE
100 FORMAT('1',8A4/1X,5A4/
  * ' FIRING RATE =',F4.0,' SPM; ROUNDS =',F4.0/1X,3A4)
200 FORMAT(' ',DALPHA =',F5.1,10X,'DPHI =',F5.1,10X,'NITER =',
  * I4,10X,'H =',F8.5,10X,'XO =',F8.5)
300 FORMAT(1X,I4,3X,F9.2,8(3X,E15.8))
400 FORMAT('0',T5,'I',T12,'RECOIL',T26,'TDD1',T44,'TDD2',T62,'TDD3',
  * T79,'XDD1',T97,'XDD2',T115,'XDD3')
401 FORMAT('0',T5,'I',T12,'RECOIL',T25,'THETA1',T43,'THETA2',T61,
  * 'THETA3')
1000 FORMAT(F10.5,2E15.6)
1001 FORMAT(2F10.3)
1002 FORMAT(I10)
1003 FORMAT(E10.3,F10.5)
1005 FORMAT(5F10.3)
1006 FORMAT(5X,E15.6,10X,E15.6)
1007 FORMAT(20A4)
1500 FORMAT('1',50X,'AZIMUTH VIBRATION')
1600 FORMAT('1',50X,'ELEVATION VIBRATION')
2000 FORMAT(7X,'MASS TURRET INERTIA MOTOR INERTIA'/4X,3E18.6)
2001 FORMAT(7X,'CENTER OF GRAVITY AND PIVOT POSITIONS'/4X,5F18.6)
2002 FORMAT(7X,'GEAR STIFFNESS DAMPING COEFFICIENT'/4X,2E18.6)
2003 FORMAT(4X,' GEAR RATIO '/4X,F10.0)
2005 FORMAT(9X,'TIME , ANGULAR DISPLACEMENT IN RADIAN')
2006 FORMAT(5X,'AZIMUTH MOTION')
2007 FORMAT(5X,'MEAN VALUE STANDARD DEVIATION')
2008 FORMAT(5X,'ELEVATION MOTION')
STOP
END

```



```

C
C      INITIALIZE THE NEXT PLOT
C
CALL PLOT(0.,-15.,-3)
CALL PLOT(0.,14.,2)
CALL PLOT(1.,3.375,-3)
CALL FACTOR(0.75)
CALL RECT(0.,0., 9.,12.,0.,2)
CALL PLOT(1.,1.,-3)

C
C      SCALE AND DRAW THE AXES
C
N1=NP+1
N2=NP+2
CALL SCALE(ANG,7.,NP,1)
TIME(N1) = PRMT(1)
TIME(N2) = (PRMT(2) - PRMT(1))/10.
CALL AXIS(0.,0., 'TIME (SECONDS)',-14,10.,0.,TIME(N1),TIME(N2))
CALL GDATE(DAT)
CALL SYMBOL(6.,-0.8,0.14,DAT,0.,28)
CALL AXIS(0.,0., 'ANGLE (MRADS)', 13,7.,90.,ANG(N1),ANG(N2))

C
C      DRAW THE ZERO AXIS
C
ZEROP=ABS(ANG(N1)/ANG(N2))
CALL PLOT(0.,ZEROP,3)
CALL PLOT(10.,ZEROP,2)

C
C      WRITE THE HEADING FOR THE AZIMUTH OR ELEVATION ANGLE PLOT
C
IF(IM.EQ.N) GO TO 20
CALL SYMBOL(2.5,7.38,0.21, 'ELEVATION ',0.,10)
GO TO 30
20 CALL SYMBOL(2.5,7.38,0.21, 'AZIMUTH ',0.,8)
30 CALL SYMBOL(999.,999.,.21, 'ANGLE VS. TIME',0.,14)
CALL SYMBOL(2.5,7.,0.14, 'RECOIL DATA: ',0.,13)
CALL SYMBOL(999.,999.,0.14,RPLT,0.,20)
CALL SYMBOL(2.5,6.7,0.14, 'ORIENTATION: ',0.,13)
CALL NUMBER(999.,999.,0.14,DPhi,0.,1)
CALL SYMBOL(999.,999.,0.14, ' DEG AZ: ',0.,9)
CALL NUMBER(999.,999.,0.14,DALPHA,0.,1)
CALL SYMBOL(999.,999.,0.14, ' DEG EL',0.,7)
CALL SYMBOL(2.5,6.4,0.14, 'MEAN =',0.,6)
CALL NUMBER(999.,999.,0.14,ANGAV,0.,2)
CALL SYMBOL(999.,999.,0.14, ' STD. DEV. =',0.,14)

```

```

CALL NUMBER(999..999..0.14,ANOSD,0..2)

C
C
C
PLOT THE AZIMUTH OR ELEVATION ANGLE VS. TIME

CALL NEWPEN(2)
CALL LINE(TIME,ANG,NP,1,0,1)
CALL NEWPEN(1)
CALL FACTOR(1.0)
CALL PLOT(9.25,-15.,-3)
IF(N.NE.NM) RETURN

C
C
C
PLOT RECOIL FORCE

CALL PLOT(0..14..2)
CALL PLOT(1..3.375,-3)
CALL FACTOR(0.75)
CALL RECT(0..0.. 9..12..0..2)
CALL PLOT(1..1.,-3)
CALL SCALE(FREC,7..NP,1)
CALL AXIS(0..0.. 'TIME (SECONDS)',-14,10..0..TIME(N1),TIME(N2))
CALL SYMBOL(6..-0.8,0.14,DAT,0..28)
CALL AXIS(0..0.. 'RECOIL FORCE (LBS)',18,7..90..
* FREC(N1),FREC(N2))
ZEROP = ABS(FREC(N1)/FREC(N2))
CALL PLOT(0..ZEROP,3)
CALL PLOT(10..ZEROP,2)
CALL SYMBOL(2.0,7.38,0.21,
* 'TRANSMITTED RECOIL FORCE VS. TIME',0..33)
CALL SYMBOL(2.0,7.0,0.14,WEAPON,0..32)
CALL SYMBOL(2.0,6.7,0.14,RPLT,0..20)
CALL SYMBOL(2.0,6.4,0.14,'FIRING RATE = ',0..14)
CALL NUMBER(999..999..0.14,RATE,0..1)
CALL SYMBOL(999..999..0.14,' SPM: ROUNDS = ',0..16)
CALL NUMBER(999..999..0.14,ROUNDS,0..1)
CALL NEWPEN(2)
CALL LINE(TIME,FREC,NP,1,0,1)
CALL NEWPEN(1)
CALL FACTOR(1.0)
CALL PLOT(9.25,-15.,-3)
CALL PLOT(0..12..2)
CALL PLOT(4..0..999)
RETURN
END

```

[illegible]

CCC

CCC

1999

```

DERY(2)=-TK/AI1*(Y(1)-Y(3)+Y(2)/AF*TO)+(TR+TH)/AI1
DERY(3)=Y(4)
DERY(4)=TK/AI2*(Y(1)-Y(3))          +C/AI2
DERY(5)=(4.785047E-5*Y(4)+1.011186E-4*DERY(4))*OR-10.*Y(5)
RETURN
END

```

```
C
C
C
C
SUBROUTINE IFORCE
C
C
C
PURPOSE:
CALCULATES THE INERTIAL TORQUES CAUSED BY THE ACCELERATIONS OF THE
TURRET ATTACHMENT PLATFORM
C
C
LISTING OF PARAMETERS:
X = TIME INPUT
TH = INERTIAL TORQUE ABOUT THE ORIGIN OF THE TURRET
COORDINATE SYSTEM
C
C
COMMON BLOCKS AND THE PROGRAMS THAT REQUIRE THEM:
/ACCEL/ MAIN, IFORCE
/ANGLE/ MAIN, IFORCE, OUTP, RFORCE
/DIST/ MAIN, IFORCE
/MASS/ MAIN, FCT, IFORCE
/MOTION/ MAIN, CALCOM, IFORCE, OUTP, RFORCE
/NUMB/ MAIN, CALCOM, IFORCE, OUTP, POINT, RFORCE
/TORQUE/ IFORCE, OUTP, RFORCE
C
C
SUBROUTINES CALLED:
POINT
C
C
SUBROUTINE IFORCE(X,TH)
COMMON /ACCEL/ T1(2600),T2(2600),T3(2600),UDD(2600),
$ VDD(2600),WDD(2600)
COMMON /ANGLE/ PHI,ALPHA,SA,CA,SP,CP
COMMON/DIST/A1,A2,A3,B1,B2
COMMON/MASS/AM,AI1,AI2,GR
COMMON/MOTION/IM,N
COMMON /NUMB/ NITER,HDAT,XO,RPLT(5),CONFIG(3)
COMMON/TORQUE/TR,THDUM
C
C
CALCULATE THE ANGULAR AND LINEAR ACCELERATIONS OF THE TURRET
ATTACHMENT AT TIME X
C
CALL POINT(X,NUM,XN)
THX=-T1(NUM)+(T1(NUM)-T1(NUM+1))*((X-XN)/HDAT
THY=T3(NUM)+(T3(NUM+1)-T3(NUM))*((X-XN)/HDAT
```

```

      THZ=T2(NUM)+(T2(NUM+1)-T2(NUM))*(X-XN)/HOAT
      AX=-UDD(NUM)+(UDD(NUM)-UDD(NUM+1))*(X-XN)/HOAT
      AY=WDD(NUM)+(WDD(NUM+1)-WDD(NUM))*(X-XN)/HOAT
      AZ=VDD(NUM)+(VDD(NUM+1)-VDD(NUM))*(X-XN)/HOAT
      IF(IM.EQ.N) GO TO 9
C
C   FORCE FOR ELEVATION DIRECTION
C
      TH=-AM*((A2+A3*CA)* AY-(AX*CP-AZ*SP)*(-B2+A3*SA))-A11*
      * (THX*SP+THZ*CP)
      GO TO 10
9    CONTINUE
C
C   FORCE FOR AZIMUTH DIRECTION
C
      TH=AM*A1*(AX*SP+AZ*CP)-A11*THY
10   CONTINUE
      THOUM=TH
      RETURN
      END

```



```

C
C      CALCULATE THE ANGULAR POSITIONS AT THE TURRET ATTACHMENT POINT
C      AT THE TIME X
C
      CALL POINT(X,NUM,XN)
      Q1 = AQ1(NUM) + (AQ1(NUM+1) - AQ1(NUM)) * (X-XN)/HOUT
      Q2 = AQ2(NUM) + (AQ2(NUM+1) - AQ2(NUM)) * (X-XN)/HOUT
      Q3 = AQ3(NUM) + (AQ3(NUM+1) - AQ3(NUM)) * (X-XN)/HOUT
      IF(IM.EQ.N) GO TO 8
C
C      ELEVATION ANGLE
C
      ANG(NP) = (Y(1) - Q1*SP + Q2*CP)*1000.
      GO TO 9
8      CONTINUE
C
C      AZIMUTH ANGLE
C
      ANG(NP) = ((Y(1) + Q3)*CA + (Q1*CP + Q2*SP)*SA)*1000.
9      CONTINUE
      IF (NP.EQ.1) GO TO 10
      IF((NP/10)*10.NE.NP) RETURN
10     CONTINUE
      WRITE(6,1000) X,Y(1),ANG(NP)
1000  FORMAT(3X,6E15.6)
      RETURN
      END

```


C

10

TR=F*0.16*CA
CONTINUE
TRDUM=TR
RETURN
END

C		RKOS	10
C	RKOS	20
C		RKOS	30
C	SUBROUTINE RKOS	RKOS	40
C		RKOS	50
C	PURPOSE	RKOS	60
C	TO SOLVE A SYSTEM OF FIRST ORDER ORDINARY DIFFERENTIAL	RKOS	70
C	EQUATIONS WITH GIVEN INITIAL VALUES.	RKOS	80
C		RKOS	90
C	USAGE	RKOS	100
C	CALL RKOS (PRMT,Y,DERY,NDIM,IHLF,FCT,OUTP,AUX)	RKOS	110
C	PARAMETERS FCT AND OUTP REQUIRE AN EXTERNAL STATEMENT.	RKOS	120
C		RKOS	130
C	DESCRIPTION OF PARAMETERS	RKOS	140
C	PRMT - AN INPUT AND OUTPUT VECTOR WITH DIMENSION GREATER	RKOS	150
C	OR EQUAL TO 5, WHICH SPECIFIES THE PARAMETERS OF	RKOS	160
C	THE INTERVAL AND OF ACCURACY AND WHICH SERVES FOR	RKOS	170
C	COMMUNICATION BETWEEN OUTPUT SUBROUTINE (FURNISHED	RKOS	180
C	BY THE USER) AND SUBROUTINE RKOS. EXCEPT PRMT(5)	RKOS	190
C	THE COMPONENTS ARE NOT DESTROYED BY SUBROUTINE	RKOS	200
C	RKOS AND THEY ARE	RKOS	210
C	PRMT(1)- LOWER BOUND OF THE INTERVAL (INPUT).	RKOS	220
C	PRMT(2)- UPPER BOUND OF THE INTERVAL (INPUT).	RKOS	230
C	PRMT(3)- INITIAL INCREMENT OF THE INDEPENDENT VARIABLE	RKOS	240
C	(INPUT).	RKOS	250
C	PRMT(4)- UPPER ERROR BOUND (INPUT). IF ABSOLUTE ERROR IS	RKOS	260
C	GREATER THAN PRMT(4), INCREMENT GETS HALVED.	RKOS	270
C	IF INCREMENT IS LESS THAN PRMT(3) AND ABSOLUTE	RKOS	280
C	ERROR LESS THAN PRMT(4)/50, INCREMENT GETS DOUBLED.	RKOS	290
C	THE USER MAY CHANGE PRMT(4) BY MEANS OF HIS	RKOS	300
C	OUTPUT SUBROUTINE.	RKOS	310
C	PRMT(5)- NO INPUT PARAMETER. SUBROUTINE RKOS INITIALIZES	RKOS	320
C	PRMT(5)=0. IF THE USER WANTS TO TERMINATE	RKOS	330
C	SUBROUTINE RKOS AT ANY OUTPUT POINT, HE HAS TO	RKOS	340
C	CHANGE PRMT(5) TO NON-ZERO BY MEANS OF SUBROUTINE	RKOS	350
C	OUTP. FURTHER COMPONENTS OF VECTOR PRMT ARE	RKOS	360
C	FEASIBLE IF ITS DIMENSION IS DEFINED GREATER	RKOS	370
C	THAN 5. HOWEVER SUBROUTINE RKOS DOES NOT REQUIRE	RKOS	380
C	AND CHANGE THEM. NEVERTHELESS THEY MAY BE USEFUL	RKOS	390
C	FOR HANDING RESULT VALUES TO THE MAIN PROGRAM	RKOS	400
C	(CALLING RKOS) WHICH ARE OBTAINED BY SPECIAL	RKOS	410
C	MANIPULATIONS WITH OUTPUT DATA IN SUBROUTINE OUTP.	RKOS	420
C	Y - INPUT VECTOR OF INITIAL VALUES. (DESTROYED)	RKOS	430
C	LATERON Y IS THE RESULTING VECTOR OF DEPENDENT	RKOS	440
C	VARIABLES COMPUTED AT INTERMEDIATE POINTS X.	RKOS	450

C	DERY	- INPUT VECTOR OF ERROR WEIGHTS. (DESTROYED)	RKOS 460
C		THE SUM OF ITS COMPONENTS MUST BE EQUAL TO 1.	RKOS 470
C		LATERON DERY IS THE VECTOR OF DERIVATIVES, WHICH	RKOS 480
C		BELONG TO FUNCTION VALUES Y AT A POINT X.	RKOS 480
C	NDIM	- AN INPUT VALUE, WHICH SPECIFIES THE NUMBER OF	RKOS 500
C		EQUATIONS IN THE SYSTEM.	RKOS 510
C	IHLF	- AN OUTPUT VALUE, WHICH SPECIFIES THE NUMBER OF	RKOS 520
C		BISECTIONS OF THE INITIAL INCREMENT. IF IHLF OETS	RKOS 530
C		GREATER THAN 10. SUBROUTINE RKOS RETURNS WITH	RKOS 540
C		ERROR MESSAGE IHLF=11 INTO MAIN PROGRAM. ERROR	RKOS 550
C		MESSAGE IHLF=12 OR IHLF=13 APPEARS IN CASE	RKOS 560
C		PRMT(3)=0 OR IN CASE SIGN(PRMT(3)).NE.SIGN(PRMT(2)-	RKOS 570
C		PRMT(1)) RESPECTIVELY.	RKOS 580
C	FCT	- THE NAME OF AN EXTERNAL SUBROUTINE USED. THIS	RKOS 590
C		SUBROUTINE COMPUTES THE RIGHT HAND SIDES DERY OF	RKOS 600
C		THE SYSTEM TO GIVEN VALUES X AND Y. ITS PARAMETER	RKOS 610
C		LIST MUST BE X,Y,DERY. SUBROUTINE FCT SHOULD	RKOS 620
C		NOT DESTROY X AND Y.	RKOS 630
C	OUTP	- THE NAME OF AN EXTERNAL OUTPUT SUBROUTINE USED.	RKOS 640
C		ITS PARAMETER LIST MUST BE X,Y,DERY,IHLF,NDIM,PRMT.	RKOS 650
C		NONE OF THESE PARAMETERS (EXCEPT, IF NECESSARY,	RKOS 660
C		PRMT(4),PRMT(5),...) SHOULD BE CHANGED BY	RKOS 670
C		SUBROUTINE OUTP. IF PRMT(5) IS CHANGED TO NON-ZERO,	RKOS 680
C		SUBROUTINE RKOS IS TERMINATED.	RKOS 690
C	AUX	- AN AUXILIARY STORAGE ARRAY WITH 8 ROWS AND NDIM	RKOS 700
C		COLUMNS.	RKOS 710
C			RKOS 720
C	REMARKS		RKOS 730
C		THE PROCEDURE TERMINATES AND RETURNS TO CALLING PROGRAM. IF	RKOS 740
C	(1)	MORE THAN 10 BISECTIONS OF THE INITIAL INCREMENT ARE	RKOS 750
C		NECESSARY TO GET SATISFACTORY ACCURACY (ERROR MESSAGE	RKOS 760
C		IHLF=11).	RKOS 770
C	(2)	INITIAL INCREMENT IS EQUAL TO 0 OR HAS WRONG SIGN	RKOS 780
C		(ERROR MESSAGES IHLF=12 OR IHLF=13).	RKOS 790
C	(3)	THE WHOLE INTEORATION INTERVAL IS WORKED THROUGH.	RKOS 800
C	(4)	SUBROUTINE OUTP HAS CHANGED PRMT(5) TO NON-ZERO.	RKOS 810
C			RKOS 820
C	SUBROUTINES AND FUNCTION SUBPROGRAMS REQUIRED		RKOS 830
C		THE EXTERNAL SUBROUTINES FCT(X,Y,DERY) AND	RKOS 840
C		OUTP(X,Y,DERY,IHLF,NDIM,PRMT) MUST BE FURNISHED BY THE USER.	RKOS 850
C			RKOS 860
C	METHOD		RKOS 870
C		EVALUATION S DONE BY MEANS OF FOURTH ORDER RUNGE-KUTTA	RKOS 880
C		FORMULAE IN THE MODIFICATION DUE TO OILL. ACCURACY IS	RKOS 890
C		TESTED COMPARING THE RESULTS OF THE PROCEDURE WITH SINGLE	RKOS 900

C	AND DOUBLE INCREMENT.	RK0S 910
C	SUBROUTINE RK0S AUTOMATICALLY ADJUSTS THE INCREMENT DURING	RK0S 920
C	THE WHOLE COMPUTATION BY HALVING OR DOUBLING. IF MORE THAN	RK0S 930
C	10 BISECTIONS OF THE INCREMENT ARE NECESSARY TO GET	RK0S 940
C	SATISFACTORY ACCURACY, THE SUBROUTINE RETURNS WITH	RK0S 950
C	ERROR MESSAGE IHLF=11 INTO MAIN PROGRAM.	RK0S 960
C	TO GET FULL FLEXIBILITY IN OUTPUT, AN OUTPUT SUBROUTINE	RK0S 970
C	MUST BE FURNISHED BY THE USER.	RK0S 980
C	FOR REFERENCE. SEE	RK0S 990
C	RALSTON/WILF. MATHEMATICAL METHODS FOR DIGITAL COMPUTERS,	RK0S1000
C	WILEY, NEW YORK/LONDON, 1960. PP.110-120.	RK0S1010
C		RK0S1020
CRK0S1030	
C		RK0S1040
C	SUBROUTINE RK0S(PRMT,Y,DERY,NDIM,IHLF,FCT,OUTP,AUX)	RK0S1050
C		RK0S1060
C		RK0S1070
	DIMENSION Y(5),DERY(5),AUX(6,5),A(4),B(4),C(4),PRMT(6)	
	DO 1 I=1,NDIM	RK0S1090
1	AUX(6,I)=.06666667*DERY(I)	RK0S1100
	X=PRMT(1)	RK0S1110
	XEND=PRMT(2)	RK0S1120
	H=PRMT(3)	RK0S1130
	PRMT(5)=0.	RK0S1140
	CALL FCT(X,Y,DERY)	RK0S1150
C		RK0S1160
C	ERROR TEST	RK0S1170
	IF(H*(XEND-X))39,37,2	RK0S1180
C		RK0S1190
C	PREPARATIONS FOR RUNGE-KUTTA METHOD	RK0S1200
2	A(1)=.5	RK0S1210
	A(2)=.2928932	RK0S1220
	A(3)=1.707107	RK0S1230
	A(4)=.1666667	RK0S1240
	B(1)=2.	RK0S1250
	B(2)=1.	RK0S1260
	B(3)=1.	RK0S1270
	B(4)=2.	RK0S1280
	C(1)=.5	RK0S1290
	C(2)=.2928932	RK0S1300
	C(3)=1.707107	RK0S1310
	C(4)=.5	RK0S1320
C		RK0S1330
C	PREPARATIONS OF FIRST RUNGE-KUTTA STEP	RK0S1340
	DO 3 I=1,NDIM	RK0S1350

AUX(1,I)=Y(I)	RKQS1360
AUX(2,I)=DERY(I)	RKQS1370
AUX(3,I)=0.	RKQS1380
3 AUX(6,I)=0.	RKQS1390
IREC=0	RKQS1400
H=H+H	RKQS1410
INLF=-1	RKQS1420
ISTEP=0	RKQS1430
IEND=0	RKQS1440
C	RKQS1450
C	RKQS1460
C START OF A RUNGE-KUTTA STEP	RKQS1470
4 IF((X+H-XEND)≠H)7.6.5	RKQS1480
5 H=XEND-X	RKQS1490
6 IEND=1	RKQS1500
C	RKQS1510
C RECORDING OF INITIAL VALUES OF THIS STEP	RKQS1520
7 CALL OUTP(X,Y,DERY,IREC,NDIM,PRMT)	RKQS1530
IF(PRMT(5))40.8.40	RKQS1540
8 ITEST=0	RKQS1550
9 ISTEP=ISTEP+1	RKQS1560
C	RKQS1570
C	RKQS1580
C START OF INNERMOST RUNGE-KUTTA LOOP	RKQS1590
J=1	RKQS1600
10 AJ=A(J)	RKQS1610
BJ=B(J)	RKQS1620
CJ=C(J)	RKQS1630
DO 11 I=1,NDIM	RKQS1640
R1=H*DERY(I)	RKQS1650
R2=AJ*(R1-BJ*AUX(6,I))	RKQS1660
Y(I)=Y(I)+R2	RKQS1670
R2=R2+R2+R2	RKQS1680
11 AUX(6,I)=AUX(6,I)+R2-CJ*R1	RKQS1690
IF(J-4)12.15.15	RKQS1700
12 J=J+1	RKQS1710
IF(J-3)13.14.13	RKQS1720
13 X=X+.5*H	RKQS1730
14 CALL FCT(X,Y,DERY)	RKQS1740
GOTO 10	RKQS1750
C	RKQS1760
C	RKQS1770
C	RKQS1780
C TEST OF ACCURACY	RKQS1790
15 IF(ITEST)16.16.20	RKQS1800

C		RKGS1810
C	IN CASE ITEST=0 THERE IS NO POSSIBILITY FOR TESTING OF ACCURACY	RKGS1820
16	DO 17 I=1,NDIM	RKGS1830
17	AUX(4,I)=Y(I)	RKGS1840
	ITEST=1	RKGS1850
	ISTEP=ISTEP+ISTEP-2	RKGS1860
18	IHLF=IHLF+1	RKGS1870
	X=X-H	RKGS1880
	H=.5*H	RKGS1890
	DO 19 I=1,NDIM	RKGS1900
	Y(I)=AUX(1,I)	RKGS1910
	DERY(I)=AUX(2,I)	RKGS1920
19	AUX(6,I)=AUX(3,I)	RKGS1930
	GOTO 9	RKGS1940
C		RKGS1950
C	IN CASE ITEST=1 TESTING OF ACCURACY IS POSSIBLE	RKGS1960
20	IMOD=ISTEP/2	RKGS1970
	IF(ISTEP-IMOD-IMOD)21,23,21	RKGS1980
21	CALL FCT(X,Y,DERY)	RKGS1990
	DO 22 I=1,NDIM	RKGS2000
	AUX(5,I)=Y(I)	RKGS2010
22	AUX(7,I)=DERY(I)	RKGS2020
	GOTO 9	RKGS2030
C		RKGS2040
C	COMPUTATION OF TEST VALUE DELT	RKGS2050
23	DELT=0.	RKGS2060
	DO 24 I=1,NDIM	RKGS2070
24	DELT=DELT+AUX(8,I)*ABS(AUX(4,I)-Y(I))	RKGS2080
	IF(DELT-PRMT(4))28,28,25	RKGS2090
C		RKGS2100
C	ERROR IS TOO GREAT	RKGS2110
25	IF(IHLF-10)26,36,36	RKGS2120
26	DO 27 I=1,NDIM	RKGS2130
27	AUX(4,I)=AUX(5,I)	RKGS2140
	ISTEP=ISTEP+ISTEP-4	RKGS2150
	X=X-H	RKGS2160
	IEND=0	RKGS2170
	GOTO 18	RKGS2180
C		RKGS2190
C	RESULT VALUES ARE GOOD	RKGS2200
28	CALL FCT(X,Y,DERY)	RKGS2210
	DO 29 I=1,NDIM	RKGS2220
	AUX(1,I)=Y(I)	RKGS2230
	AUX(2,I)=DERY(I)	RKGS2240
	AUX(3,I)=AUX(6,I)	RKGS2250

Y(I)=AUX(5,I)	RK0S2260
29 DERY(I)=AUX(7,I)	RK0S2270
CALL OUTP(X-H,Y,DERY,IHLF,NDIM,PRMT)	RK0S2280
IF(PRMT(5))40,30,40	RK0S2290
30 DO 31 I=1,NDIM	RK0S2300
Y(I)=AUX(1,I)	RK0S2310
31 DERY(I)=AUX(2,I)	RK0S2320
IREC=IHLF	RK0S2330
IF(IEND)32,32,39	RK0S2340
C INCREMENT GETS DOUBLED	RK0S2350
C 32 IHLF=IHLF-1	RK0S2360
ISTEP=ISTEP/2	RK0S2370
H=H+H	RK0S2380
IF(IHLF)4,33,33	RK0S2390
33 IMOD=ISTEP/2	RK0S2400
IF(ISTEP-IMOD-IMOD)4,34,4	RK0S2410
34 IF(DELT-.02=PRMT(4))35,35,4	RK0S2420
35 IHLF=IHLF-1	RK0S2430
ISTEP=ISTEP/2	RK0S2440
H=H+H	RK0S2450
GOTO 4	RK0S2460
C RETURNS TO CALLING PROGRAM	RK0S2470
C 36 INCF=11	RK0S2480
CALL FCT(X,Y,DERY)	RK0S2490
GOTO 39	RK0S2500
37 IHLF=12	RK0S2510
GOTO 39	RK0S2520
38 IHLF=13	RK0S2530
39 CALL OUTP(X,Y,DERY,IHLF,NDIM,PRMT)	RK0S2540
40 RETURN	RK0S2550
END	RK0S2560
	RK0S2570
	RK0S2580
	RK0S2590

REFERENCES

1. Cronkhite, J. D., and Wilson, W. F., "Dynamic Analysis of Two-Per-Rev Vibrations in the Model AH-1J Helicopter", Report No. 299-100-021, Bell Helicopter Company, Fort Worth, Texas February, 1972.
2. Cronkhite, J. D., and Berry, V. L., and Brunken, J. E., "A NASTRAN Vibration Model of the AH-1G Helicopter Airframe", Volumes I and II, Bell Helicopter Company, Fort Worth, Texas April, 1972, AD R-TR-74-045.